ÉCOLE DE TECHNOLOGIE SUPÉRIEURE
UNIVERSITÉ DU QUÉBEC

THÈSE PRÉSENTÉE À
ÉCOLE DE TECHNOLOGIE SUPÉRIEURE

COMME EXIGENCE PARTIELLE
À L'OBTENTION DU
DOCTORAT EN GÉNIE
Ph.D.

PAR
SAID BENAMEUR

RECONSTRUCTION 3D BIPLANAIRE NON SUPERVISÉE DE LA COLONNE VERTÉBRALE ET DE LA CAGE THORACIQUE SCOLIOTIQUES PAR MODÈLES STATISTIQUES

MONTRÉAL, LE 6 AOÛT 2004

CETTE THÈSE A ÉTÉ ÉVALUÉE

PAR UN JURY COMPOSÉ DE :

Dr. Jacques De Guise, directeur de thèse
Département de Génie de la Production Automatisée, École de Technologie Supérieure

Dr. Max Mignotte, codirecteur de thèse
Département d'Informatique et Recherche Opérationnelle,Université de Montréal

Dr. Jacques-André Landry, président du jury
Département de Génie de la Production Automatisée, École de Technologie Supérieure

Dr. Amar Mitiche, examinateur externe
Institut National de Recherche Scientifique, Université du Québec

Dr. Jean Meunier, examinateur
Département d'Informatique et Recherche Opérationnelle,Université de Montréal

Dr. Jean Dansereau, examinateur
Département de Génie Mécanique, École Polytechnique de Montréal

ELLE A FAIT L'OBJET D'UNE SOUTENANCE DEVANT JURY ET PUBLIC

LE 8 JUIN 2004

À ÉCOLE DE TECHNOLOGIE SUPÉRIEURE

RÉSUMÉ

Cette thèse présente trois approches statistiques pour la reconstruction 3D de la colonne vertébrale et de la cage thoracique scoliotiques à partir de deux images radiographiques conventionnelles. Globalement, les méthodes sont basées sur l'utilisation de contours de vertèbres ou des côtes détectées dans deux images radiographiques et une connaissance géométrique *a priori* de nature statistique de chaque élément. La reconstruction est formulée comme un problème de minimisation de fonctions d'énergie résolues par des méthodes d'optimisation. Pour la colonne vertébrale, les méthodes sont validées par comparaison avec des reconstructions de 57 vertèbres scoliotiques reconstruites à partir d'images tomodensitométriques. Plusieurs méthodes ont été proposées afin de raffiner les solutions obtenues et de rendre les méthodes non supervisées.

RECONSTRUCTION 3D BIPLANAIRE NON SUPERVISÉE DE LA COLONNE VERTÉBRALE ET DE LA CAGE THORACIQUE SCOLIOTIQUES PAR MODÈLES STATISTIQUES

Said Benameur

SOMMAIRE

Dans cette thèse, nous présentons trois méthodes statistiques de reconstruction 3D de structures osseuses à partir de deux images radiographiques conventionnelles (postéro-antérieure avec incidence de 0° et latérale) calibrées.

Dans un premier article, une méthode statistique supervisée de reconstruction 3D des vertèbres scoliotiques est présentée. Cette méthode utilise un modèle déformable statistique intégrant, en plus des déformations linéaires, une série de déformations non linéaires modélisées par les premier modes de variation des déformations de l'expansion de Karhunen-Loeve et les contours des vertèbres préalablement segmentées sur les deux images radiographiques. La fonction d'énergie est minimisée par une technique de descente de gradient simplifié.

Dans un second article, nous présentons une méthode biplanaire, non supervisée, hiérarchique et statistique de reconstruction 3D de la colonne vertébrale scoliotique. Cette méthode est basée sur les spécifications de deux modèles 3D statistiques. Le premier, un modèle géométrique sur lequel des déformations linéaires globales admissibles sont définies, est utilisé pour une reconstruction grossière de la colonne vertébrale. Une reconstruction 3D précise est alors réalisée pour chaque niveau vertébral par un deuxième modèle de vertèbre sur lequel des déformations non linéaires admissibles sont définies. Cette reconstruction 3D est formulée comme un double problème de minimisation de fonction d'énergie résolu par un algorithme stochastique d'exploration/sélection.

Dans un troisième article, nous présentons une méthode biplanaire non supervisée de reconstruction 3D de la cage thoracique scoliotique. Cette méthode utilise un modèle statistique déformable basée sur un mélange d'analyse en composantes principales probabilistes qui est appliqué sur une base d'apprentissage de cages thoraciques scoliotiques. Pour chacune des composantes du mélange, un modèle *a priori* paramétrique de forme tridimensionnelle est extrait et utilisé pour contraindre le problème de reconstruction 3D. La reconstruction relative à chacune des composantes consiste à ajuster les projections du modèle 3D de la cage thoracique avec les contours préalablement segmentés sur les deux images. La reconstruction 3D optimale correspond à la composante du mélange de déformation et aux paramètres associés à celle-ci menant à une énergie de fonction minimale. La fonction d'énergie est minimisée par un algorithme stochastique d'exploration/sélection. Les paramètres du mélange sont estimés par l'algorithme Stochastic Expectation Maximization.

UNSUPERVISED 3D BIPLANAR RECONSTRUCTION OF THE SCOLIOTIC SPINE AND RIB CAGES USING STATISTICAL MODELS

Said Benameur

ABSTRACT

In this thesis, we present three statistical 3D reconstruction methods of anatomical shapes from two conventional calibrated radiographic images (postero-anterior with normal incidence and lateral).

In a first article, a supervised statistical 3D reconstruction method of the scoliotic vertebrae is presented. This method uses *a priori* global knowledge of the geometric structure of each vertebra and the contours segmented on the two radiographic images. This geometric knowledge is efficiently captured by a statistical deformable template integrating a set of admissible deformations, expressed by the first modes of variation in Karhunen-Loeve expansion, of the pathological deformations observed on a representative scoliotic vertebra population. The energy function is solved with a gradient descent technique.

In a second article, we present a unsupervised 3D biplanar hierarchical and statistical 3D reconstruction method of the scoliotic spine. This method uses *a priori* hierarchical global knowledge, both on the geometric structure of the whole spine and of each vertebra. It relies on the specification of two 3D statistical templates. The first, a rough geometric template on which rigid admissible deformations are defined, is used to ensure a crude registration of the whole spine. An accurate 3D reconstruction is then performed for each vertebra by a second template on which non-linear admissible global, as well as local deformations, are defined. This unsupervised 3D reconstruction procedure leads to two separate minimization procedures efficiently solved with a Exploration/Selection stochastic algorithm.

In a third article, we present a unsupervised 3D biplanar statistical reconstruction method of the scoliotic rib cages. It uses a deformable statistical model based on a mixture of Probabilistic Principal Component Analysers which is applied on a training base of scoliotic rib cages. The 3D reconstruction for each mixture's component consists of extracting and fitting the projections of the deformable template with the preliminary segmented contours on the postero-anterior radiographic view. The 3D reconstruction is stated as an energy function minimization problem, which is solved with a exploration/selection algorithm. The optimal 3D reconstruction then corresponds to the component of the deformation mixture and parameters leading to the minimal energy function. Parameters of this mixture model are estimated with the Stochastic Expectation Maximization.

REMERCIEMENTS

Cette thèse a été réalisée au sein du laboratoire de recherche en imagerie et orthopédie (LIO) de l'École de technologie supérieure, qui est une constituante du réseau de l'Université du Québec, et le laboratoire de traitement d'images de l'Université de Montréal.

J'adresse tous mes sincères remerciements à Monsieur Jacques de Guise, Professeur à l'École de technologie supérieure à Montréal et directeur de ma thèse, pour la confiance et le soutien qu'il m'a accordés ainsi que les nombreux conseils qu'il m'a prodigués pendant toute la durée de ma thèse. Qu'il en soit ici chaleureusement remercié.

C'est l'occasion pour moi d'exprimer toute ma reconnaissance à Monsieur Max Mignotte, Professeur à l'Université de Montréal et codirecteur de ma thèse, qui m'a dirigé avec patience et constance tout au long de cette thèse, montrant toujours une extrême disponibilité, et s'adaptant de façon permanente à son interlocuteur. Son énergie communicative et ses encouragements m'ont été très précieux. J'ai ainsi pu apprécier sa compétence scientifique. Qu'il trouve ici l'expression de ma plus grande sympathie.

Je remercie Monsieur Jacques-André Landry, Professeur à l'École de technologie supérieure à Montréal d'avoir accepter de présider le jury de cette thèse.

Je remercie Monsieur Amar Mitiche, Professeur à l'Institut national de la recherche scientifique (INRS), qui m'a fait le plaisir de juger mon travail et qui a accepté d'être membre du

jury. Son expérience dans les domaines vision par ordinateur et reconnaissance de formes fait que sa présence dans mon jury est un honneur pour moi.

Je remercie aussi Monsieur Jean Meunier, Professeur à l'Université de Montréal et Monsieur Jean Dansereau, Professeur à l'École polytechnique de Montréal pour leur participation à ce jury, pour leurs conseils avisés, leurs critiques et leurs encouragements.

Je ne voudrais pas oublier de remercier les différents organismes pour leurs bourses et subventions sans lesquelles cette thèse n'aurait pas été possible : École de technologie supérieure (ETS), Centre de recherche de Sainte-Justine, Conseil de recherche en sciences naturelles et en génie du Canada (CRSNG), Valorisation - Recherche Québec et la compagnie française Biospace.

Je tiens à exprimer ma sympathie à toutes les personnes que j'ai pu côtoyer au sein du laboratoire de recherche en imagerie et orthopédie et du laboratoire de traitement d'images pour l'aide qu'elles m'ont toujours prodiguée.

Je tiens également à remercier ma femme qui, par sa patience, ses encouragements et son soutien, m'a permis de mener ce travail à terme.

TABLE DES MATIÈRES

LISTE DES TABLEAUX

Page

LISTE DES FIGURES

Page

LISTE DES ABRÉVIATIONS ET DES SIGLES

2D	Bidimensional
3D	Tridimensional
DLT	Direct Linéaire Transformation
E/S	Exploration Selection
GA	Genetic Algorithm
KL	Karhunen-Loeve
ML	Maximum Likelihood
MPPCA	Mixture of Probabilistic Principal Component Analysers
NSCP	Non Stereo Corresponding Points
PCA	Principal Component Analysis
PDM	Point Distribution Model
PPCA	Probabilistic Principal Component Analyses
RMS	Root Mean Square
SEM	Stochastic Expectation Maximisation

$\mathcal{R}$	Ensemble des nombres réels
I_{PA}	Image postéro-antérieure avec incidence de 0°
$I_{PA-20°}$	Image postéro-antérieure avec incidence de 20°
I_{LAT}	Image latérale
s	Forme d'un modèle
$\bar{s}$	Forme moyenne d'un modèle
C	Matrice de covariance
b	Vecteur associé aux modes de déformation les plus significatifs
b_i	i^{eme} composante du vecteur b

Φ	Matrice de vecteurs propres correspondants aux modes de déformation les plus significatifs
λ_i	i^{eme} valeur propre
$M(k, \alpha)$	Matrice de transformation regroupant la rotation d'angle α et l'homothétie de facteur k
T	Vecteur de translation
R_{α_1}	Matrice de rotation d'un angle α_1 par rapport à l'axe des x
R_{α_2}	Matrice de rotation d'un angle α_2 par rapport à l'axe des y
R_{α_3}	Matrice de rotation d'un angle α_3 par rapport à l'axe des z
$E(\cdot)$	Fonction d'énergie
$E_l(\cdot)$	Énergie de vraisemblance
$E_p(\cdot)$	Énergie *a priori*
$E_r(\cdot)$	Énergie de déformation locale
θ	Vecteur de paramètres de déformation
$\Psi(\cdot)$	Fonction de potentiel
$P(s)$	Probabilité *a priori*
$P(I_{PA}, I_{LAT} \mid s)$	Vraisemblance
$\gamma(x, y)$	Angle entre la tangente au contour rétroprojeté et la tangente au plus proche point du contour extrait de l'image radiographique au point (x, y)
β	Coefficient de rigidité
t^l	Position du niveau vertébrale l
k^l	Vecteur de facteurs d'échelle du niveau vertébrale l
α^l	Vecteur d'angles de rotation du niveau vertébrale l
Δt^l	Pas d'intégration de chaque composante de t du niveau vertébrale l
Δk^l	Pas d'intégration de chaque composante de k du niveau vertébrale l

$\Delta\alpha^l$	Pas d'intégration de chaque composante de α du niveau vertébrale l
$\Delta\theta$	Pas d'intégration de chaque paramètre θ
δ	Vecteur des déformations locales
μ^2	Paramètre de variance du modèle agissant sur la régularité des déformations locales
ν^2	Paramètre de variance du modèle agissant sur la minimisation de l'effet des déformations locales
$\vec{n}$	Vecteur normal
τ	Paramètre de degré de lissage de la fonction d'énergie
(ξ_x, ξ_y)	Distance au plus proche point du contour sur l'image
ν	Forme moyenne d'une classe de déformation
ε	Bruit Gaussien
I_d	Matrice identité $d \times d$
σ^2	Variance
$\mathcal{N}()$	Distribution normale
$\mathcal{N}(s; \nu, \sigma^2 I_d + \Phi\Phi^T)$	Loi normale de paramètres ν (moyenne) et de variance $\sigma^2 I_d + \Phi\Phi^T$
K	Nombre de classes dans MPPCA
e	Erreur de reconstruction
m	Dimension des données réduites
$\mathcal{U}()$	Distribution uniforme
m_c	Dimension des données réduites de la classe c
$var_{\text{Rib}_i^{\text{out}}}$	Variance de l'ensemble des niveaux de gris localisés sur le contour externe de la i^{ieme} côte du modèle déformable avec facteur d'échelle $k + \epsilon$ projetée sur l'image I_{PA}

$var_{\text{Rib}_i^{\text{in}}}$	Variance de l'ensemble des niveaux de gris localisés sur le contour externe de la i^{ieme} côte du modèle déformable avec facteur d'échelle $k - \epsilon$ projetée sur l'image I_{PA}
s_c	Forme d'un modèle de la classe c
P_m	Probabilité de mutation de l'algorithme génétique
P_c	Probabilité de croisement de l'algorithme génétique
$P(\theta_i)$	Probabilité de sélection de l'algorithme génétique
V_T	Somme des valeurs propres
ζ_p	Constante de normalisation pour l'énergie *a priori*
ζ_l	Constante de normalisation pour l'énergie de vraisemblance
ζ	Constante de normalisation pour l'énergie de déformation locale
n_{LAT}	Nombre de points du contour externe du modèle projeté sur l'image latérale
n_{PA}	Nombre de points du contour externe du modèle projeté sur l'image postéro-antérieure avec incidence de 0°

CHAPITRE 1

INTRODUCTION

Contexte

Le terme «scoliose»vient du grec skolios qui veut dire tortueux. Avec l'avènement de la radiographie, les médecins et chirurgiens ont caractérisé la scoliose par une ou plusieurs courbures dans le plan frontal de la colonne vertébrale. En effet la radiographie n'offre qu'une projection plane de la déformation.

Depuis deux décennies les médecins et les chirurgiens qui prennent en charge les scolioses redécouvrent cette torsion du rachis et la scoliose a retrouvé son caractère tridimensionnel. C'est-à-dire que cette déformation de la colonne vertébrale ne se lit plus dans un plan postéro-antérieur uniquement, mais que la déformation est reconnue aussi dans le plan postéro-antérieur et dans un plan latéral (voir figure 1)[1].

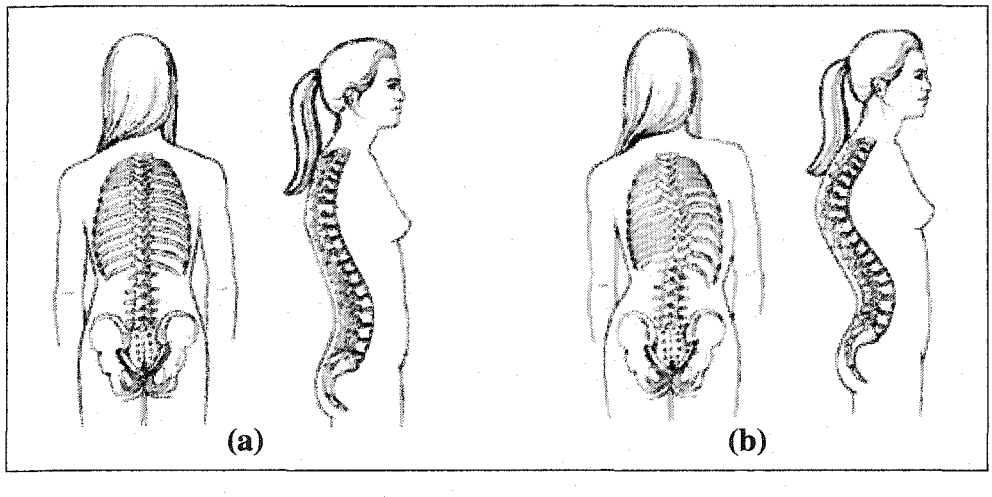

Figure 1 Vues postéro-antérieure et latérale du rachis d'un patient. **(a)** patient sain, **(b)** patient scoliotique

[1] http://www.magnaspine.hpg.ig.com.br/escoliose_lordose_cifose_ingles.htm

Les utilisateurs d'imagerie médicale éprouvent un besoin croissant de disposer des informations tridimensionnelles pour améliorer le diagnostic de pathologies complexes comme la scoliose, afin de mieux évaluer et planifier les méthodes de correction orthopédiques et chirurgicales. Une représentation de la scoliose en modèle géométrique 3D permet l'accès à la déformation complète de la colonne tant au niveau global qu'au niveau local, c'est-à-dire pour chacune des vertèbres. De nombreuses méthodes de reconstruction 3D ont été développées au cours des dernières années pour extraire cette information tridimensionnelle.

Problématique

Les méthodes de reconstruction 3D associées aux systèmes d'imagerie médicale CT-Scan ou IRM permettent d'obtenir des reconstructions tridimensionnelles précises des structures osseuses humaines. Cependant, le système CT-Scan est très irradiant pour le patient, un volume important d'information à traiter est nécessaire, et la position allongée, imposée au patient durant l'examen ne permet pas une étude des déformations auxquelles le clinicien a habituellement accès, c'est-à-dire sous l'influence de la gravité, le patient en position debout. Bien que le système IRM est non irradiant, on retrouve les deux derniers inconvénients du CT-Scan. L'imagerie par ultrasons n'a pas été adaptée à l'analyse de la forme géométrique tridimensionnelle de la structure osseuse car les structures osseuses génèrent trop d'écho et beaucoup de bruit de mesures (échos parasites à la forme géométrique des surfaces des structures denses) [26].

L'imagerie médicale par rayons X des structures osseuses est largement utilisée en clinique. Dans le cas de la scoliose, l'accès à une information tridimensionnelle personnalisée, quantitative et fiable est essentiel afin d'assurer un diagnostic amélioré et un traitement orthopédique ou chirurgical adéquat. La scoliose nécessite un suivi dans le temps, pouvant exposer les patients à des quantités importantes de radiation sans vraiment tenir compte de leur passé radiologique. La scoliose concerne 2 à 4% de la population de l'Amérique du Nord dont 90% sont des jeunes filles en période de croissance, avec pour

corollaire la nécessité de réduire les doses de radiation administrées à chaque examen conformément aux nouvelles recommandations internationales pour les examens médicaux répétitifs. L'utilisation des méthodes de reconstruction 3D multiplanaires pour extraire de l'information 3D devient donc un impératif de plus haute importance pour les patients, les chercheurs et la communauté clinique.

Le problème de reconstruction 3D multiplanaire appartient à la classe des problèmes mal-posés au sens de Hadamard. L'acquisition de deux images radiographiques biplanaires ne fournit qu'un ensemble de données incomplètes qui ne permet pas d'assurer l'unicité de la solution.

Pour pallier à cette limitation, il est nécessaire de régulariser la procédure de reconstruction 3D en introduisant une connaissance *a priori* de l'objet à reconstruire. Des modèles géométriques ont été proposés mais leur grande rigidité ne leur permet pas de prendre en compte les variabilités anatomiques et celles liées aux pathologies.

Au contraire, les méthodes de reconstruction 3D multiplanaires par modélisation statistique, telles que celle que nous proposons dans cette thèse offrent une plus grande souplesse de modélisation et permettent de prendre en compte les variabilités anatomiques et celles liées aux pathologies des structures osseuses à reconstruire.

Objectifs généraux et hypothèses

L'objectif de cette thèse est de développer une méthode de reconstruction 3D de chaque vertèbre, de la colonne vertébrale et de la cage thoracique scoliotiques à partir de deux images radiographiques conventionnelles calibrées (postéro-antérieure avec incidence de $0°$ (I_{PA}) et latérale (I_{LAT})) sous certaines hypothèses[2] par modèles statistiques. Dans le cadre de cette thèse, le problème de reconstruction 3D sera vu comme un problème d'estimation des paramètres de déformation du modèle ou, de manière équivalente, comme

un problème de minimisation d'une fonction d'énergie. Cette minimisation se fera par un algorithme d'optimisation déterministe ou stochastique.

Nous supposons qu'il est possible d'obtenir,

- Une modélisation géométrique 3D des vertèbres scoliotiques, précise, et de manière supervisée en combinant les informations (contours) obtenues des images radiographiques I_{PA} et I_{LAT} et des informations géométriques *a priori* de nature statistique.

- Une modélisation géométrique 3D de la colonne vertébrale scoliotique, précise, et de manière non supervisée en combinant les informations (contours) obtenues des images radiographiques I_{PA} et I_{LAT} et des informations géométriques *a priori* de nature statistique.

- Une modélisation géométrique 3D de la cage thoracique scoliotique, précise, et de manière non supervisée en combinant les informations (contours et régions) obtenues de l'image radiographique I_{PA} et l'image I_{LAT} comme contrainte et des informations géométriques *a priori* de nature statistique.

---

[2]Toutes les images radiographiques conventionnelles I_{PA} et I_{LAT} utilisées dans la reconstruction 3D de la colonne vertébrale et de la cage thoracique scoliotiques sont issues du système Fuji FCR 7501S disponible à l'hôpital Sainte-Justine de Montréal. L'environnement radiographique est calibré par la technique de calibration utilisée au laboratoire d'informatique de scoliose 3D (LIS-3D) de l'hôpital Sainte-Justine de Montréal.
Nous disposons de:

- Une base d'apprentissage de vertèbres (500 normales et 500 scoliotiques) issue de la numérisation de plus de 200 repères anatomiques sur des vertèbres secs par le système Fastrack© dont la précision est 0.2 mm [82].

- Une base d'apprentissage de 532 cages thoraciques scoliotiques issue de la reconstruction 3D stéréoradiographique dont l'erreur moyenne est évaluée à 1.1 mm avec un écart-type de 0.72 mm [24].

- Un échantillon de 57 vertèbres lombaires et thoraciques (13 patients scoliotiques) qui ont été reconstruites par la méthode CT-Scan pour fin de validation.

À cette fin, nous avons construit trois modèles statistiques permettant la reconstruction 3D de chaque vertèbre, de la colonne vertébrale et de la cage thoracique scoliotiques à partir de deux images radiographiques conventionnelles calibrées I_{PA} et I_{LAT}.

Dans un premier article, nous présentons une méthode statistique supervisée de reconstruction 3D des vertèbres scoliotiques à partir de deux images radiographiques conventionnelles calibrées I_{PA} et I_{LAT} utilisant les contours de vertèbres détectés sur deux images radiographiques conventionnelles calibrées et une connaissance géométrique *a priori* de nature statistique de chaque vertèbre obtenue par une analyse en composantes principales appliquée à une base d'apprentissage d'environ 1000 vertèbres (30 vertèbres saines et 30 vertèbres scoliotiques par niveau vertébral). La minimisation de la fonction d'énergie se fera par un algorithme de descente de gradient [7]. Cette méthode sera validée sur un échantillon de 57 vertèbres scoliotiques issues de reconstructions CT-Scan.

Dans un second article, nous présentons une méthode statistique non supervisée de reconstruction 3D de la colonne vertébrale scoliotique à partir de deux images radiographiques conventionnelles calibrées I_{PA} et I_{LAT} utilisant les contours de vertèbres détectés sur I_{PA} et I_{LAT} et une connaissance globale hiérarchique *a priori* de la structure géométrique de la colonne puis de chaque niveau vertébral. La structure géométrique de chaque niveau vertébral sera obtenue de la même manière que dans le premier article. La minimisation de la fonction d'énergie se fera par un algorithme stochastique d'Exploration/Sélection [33]. Cette méthode sera validée sur un échantillon de 57 vertèbres scoliotiques issues de reconstructions CT-Scan.

Dans un troisième article, nous présentons une méthode statistique non supervisée de reconstruction 3D de la cage thoracique scoliotique à partir de deux images radiographiques conventionnelles calibrées I_{PA} et I_{LAT} utilisant d'une part les contours de la cage thoracique détectés sur la radiographie I_{PA} et d'autre part une connaissance géométrique *a priori* de nature statistique de la cage thoracique obtenue par un mélange d'analyse en composantes principales probabiliste [92, 93]. Cette connaissance géométrique *a pri-*

ori est extraite d'une base d'apprentissage de 532 cages thoraciques scoliotiques et les paramètres de celle ci seront estimés par l'algorithme Stochastic Expectation Maximization [33]. La minimisation de la fonction d'énergie se fera par un algorithme stochastique d'Exploration/Sélection [79]. Cette méthode sera validée sur un échantillon de 20 cages thoraciques scoliotiques issues de reconstructions stéréo-radiographique [24].

Plan de la thèse

Dans le chapitre 2, nous présentons une revue de littérature pour illustrer la contribution des travaux précédents à l'élaboration de notre thèse, ainsi que l'originalité de nos principales contributions.

Les trois chapitres suivants correspondent à trois articles. Ils constituent une contribution originale de l'auteur de cette thèse au domaine de la vision 3D en imagerie médicale. Nos idées originales ont été exposées dans des actes de conférences internationales [6] [8] [5].

«3D/2D Registration and Segmentation of Scoliotic Vertebrae Using Statistical Models, dans Computerized Medical Imaging and Graphics », publié dans le journal *Computerized Medical Imaging and Graphics*, 27(5):321-327, 2003.

«A Hierarchical Statistical Modeling Approach for the Unsupervised 3D Biplanar Reconstruction of the Scoliotic Spine », soumis au journal *IEEE Transactions on BioMedical Engineering*, 2004.

«Unsupervised 3D Biplanar Reconstruction of Scoliotic Rib Cage using the Estimation of a Mixture of Probabilistic Prior Models », soumis au journal *IEEE Transactions on BioMedical Engineering*, 2004.

Nous terminons par une discussion générale au chapitre 6, une conclusion et nos recommandations au chapitre 7.

CHAPITRE 2

REVUE DE LITTÉRATURE

Nous présentons dans ce chapitre l'état de l'art sur la reconstruction 3D des structures osseuses antérieures à nos travaux. Ces méthodes sont classées suivant la nature de la connaissance *a priori* utilisée pour contraindre le problème mal-posé de reconstruction 3D. Les méthodes présentées sont supervisées et ne disposent pas d'une base d'apprentissage de la structure osseuse à reconstruire. Nous nous sommes inspirés de plusieurs idées générales sous-jacentes à ces méthodes pour développer nos méthodes de reconstruction 3D.

2.1 Méthodes de reconstruction 3D des structures osseuses : état de l'art

À notre connaissance, il n'existe pas dans la littérature de critères de classification de méthodes multiplanaires de reconstruction 3D. Nous avons distingué trois classes de méthodes multiplanaires de reconstruction 3D.

2.1.1 Méthodes de reconstruction 3D sans connaissance a priori

Plusieurs auteurs ont proposé des techniques de reconstruction 3D des vertèbres à partir de deux vues radiographiques conventionnelles (postéro-antérieure avec incidence de 0° (I_{PA}) et latérale (I_{LAT})) [89][83][85][40]. Ces techniques sont basées sur l'identification de quelques repères anatomiques dans I_{PA} et I_{LAT}. Les vertèbres sont alors modélisées par des quadrilatères 3D.

Dansereau et Stokes ont proposé une méthode de reconstruction 3D de la cage thoracique à partir de deux vues radiographiques conventionnelles (postéro-antérieure avec incidence de 0° et postéro-antérieure avec incidence de 20° ($I_{PA-20°}$)) [24]. Seules les lignes médianes des côtes sont reconstruites par une méthode itérative combinant l'algorithme DLT

[71] et des courbes splines. Les points postérieurs des côtes sont déduits d'une reconstruction 3D des vertèbres de la colonne vertébrale. La position du sternum et les points antérieurs des côtes sont déterminés par des marqueurs radio opaques placés sur la peau. Ces méthodes sont supervisées et imprécises à cause du fait qu'une erreur d'identification d'un repère anatomique de 2 mm peut engendrer des erreurs de reconstruction 3D de 5 mm [1]. Martin et Aggarwal ont proposé une méthode de reconstruction 3D à partir des silhouettes [70] permettant de reconstruire des objets 3D polygonaux par rétroprojection des silhouettes. Une méthode d'extraction de la géométrie 3D des structures osseuses à partir de deux vues radiographiques est proposée par Caponetti et Fanelli [14] dans laquelle le positionnement initial de la structure osseuse 3D issue de la rétroprojection est ensuite raffiné par une interpolation B-spline.

En raison de la nature du problème mal-posé de reconstruction 3D, une bonne et précise reconstruction de la structure géométrique 3D ne peut être estimée sans contraintes. Des méthodes de reconstruction 3D utilisant une connaissance *a priori* sur la structure géométrique de l'objet à reconstruire ont donc été proposées dans la littérature.

2.1.2 Méthodes de reconstruction 3D avec connaissance géométrique a priori

Pour contraindre le problème inverse mal-posé de reconstruction 3D, il faut introduire une information sur l'objet à reconstruire. De nombreuses méthodes ont été proposées dans la littérature permettant une reconstruction 3D des structures osseuses avec connaissance géométrique *a priori*. Terzopoulos *et al.* ont proposé une méthode permettant de récupérer la forme 3D des profils d'un objet utilisant comme contrainte géométrique *a priori* une combinaison de tubes et colonne vertébrale déformables [90]. La déformation est contrôlée par des forces physiques internes et externes. Bardinet *et al.* ont proposé une méthode permettant de recaler un modèle de superquadriques déformable localement à un ensemble de points en utilisant des déformations de forme libre [4]. Nikkhade *et al.* ont présenté une méthode de reconstruction 3D des fémurs à partir de deux vues radiographiques conventionnelles orthogonales [78]. Cette méthode consiste à recaler des surfaces paramétriques

cubiques aux trois parties du fémur puis à les rassembler en un seul modèle complet. Kita a présenté un modèle déformable 3D permettant d'analyser les images radiographiques de l'estomac [57]. Le modèle *a priori* est un tube dont l'initialisation est réalisée avec une seule image radiographique. Le modèle est ensuite déformé en utilisant les autres images. Une méthode multiplanaire de reconstruction 3D à partir de deux vues radiographiques conventionnelles est présentée par Dansereau et Stokes [24]. Elle est basée sur la numérisation de six repères anatomiques stéréo-correspondants par vertèbre (centroïdes des plateaux vertébraux, sommets des pédicules) sur les deux images radiographiques. Ces repères anatomiques seront ensuite reconstruits en 3D par l'algorithme DLT [71]. Un modèle surfacique est ensuite déformé par krigeage dual [94] pour s'ajuster aux repères anatomiques reconstruits. Mitton *et al.* ont amélioré cette méthode en tenant compte des repères anatomiques stéréo-correspondants et non stéréo-correspondants [75]. Les points du modèle de vertèbre reconstruit, reliés entre eux par des ressorts linéaires, sont contraints à se déplacer le long des lignes épipolaires. Le modèle est ensuite déformé vers un état mécanique stable. Ces deux méthodes sont tout d'abord supervisées, imprécises et n'exploitent pas toute l'information contenue dans les deux images radiographiques (par exemple, les contours de chaque vertèbre). Huynh *et al.* ont modélisé la cunéiformisation vertébrale[1] par des modèles d'ellipses [52]. Cette modélisation est basée sur la numérisation d'une suite de points sur les contours des plateaux vertébraux sur les deux images radiographiques. Les points stéréo-correspondants de cette suite sont reconstruits par l'algorithme DLT [71]. Le contour reconstruit des plateaux vertébraux est modélisé par une ellipse dont la forme et la position sont optimisées par un processus itératif. Pour réaliser la mise en correspondance des courbes sur les deux images radiographiques, un ensemble de points est généré mathématiquement sur l'ellipse, puis réprojetés sur les deux images. Ces points sont alors déplacés pour se superposer sur les points correspondants des contours déjà mo-

[1]Disparition de l'aspect parallèle des plateaux vertébraux d'une ou plusieurs vertèbres sur une projection frontale ou sagittale.

délisés par des courbes splines. Delorme *et al.* ont adopté cette technique de modélisation de la cunéiformisation vertébrale par des modèles d'ellipses dans [27].

Lötjönen *et al.* ont proposé une méthode de reconstruction 3D d'un thorax à partir de deux vues radiographiques conventionnelles [64]. Cette méthode consiste à simuler les images radiographiques du modèle, et de construire ensuite les champs des déformations élastiques 3D nécessaires pour recaler les images simulées avec les images réelles. Veisterä *et al.* ont appliqué cette méthode à la reconstruction 3D du coeur [95].

Toutes ces méthodes soulèvent deux problèmes. D'une part, elles proposent des modèles géométriques dont la rigidité ne leur permet pas de prendre en compte les variabilités anatomiques et les pathologies (cas de la scoliose). D'autre part, elles n'exploitent pas la connaissance statistique des déformations possibles de l'objet à reconstruire. Par conséquent, la forme 3D reconstruite ne correspond pas nécessairement à la réalité. Ces inconvénients peuvent être surmontés par une approche statistique.

2.1.3 Méthodes de reconstruction 3D avec connaissance statistique a priori

L'approche statistique permet la prise en compte des connaissances *a priori* sur la structure des objets et leurs déformations, ce qui introduit une robustesse appréciable dans les techniques de recalage ou de reconstruction 3D.

Les deux approches que nous présentons dans cette thèse s'inspirent de travaux qu'il nous a semblé nécessaire de décrire. La première approche (approche modale), qui a été présentée à l'origine par Cootes *et al.* [20][22], est adaptée spécifiquement pour notre problème de reconstruction 3D des vertèbres et de la colonne vertébrale scoliotiques. La seconde approche (approche de mélange de modèles de forme *a priori*), qui a été présentée à l'origine par Tipping et Bishop [92][93], est retenue pour la reconstruction 3D de la cage thoracique scoliotique.

2.1.3.1 Travaux de Cootes

Les modèles statistiques linéaires ont été popularisé par les travaux de Cootes [22][20] et ont permis la création et l'utilisation de modèles de formes et d'apparence en 2D, après apprentissage supervisé. Au sein de ces modèles, la variabilité est prise en considération dans un cadre linéaire et modélise ainsi les déformations statistiquement admissibles par le modèle.

Ce modèle a essentiellement été utilisé en segmentation d'images fixes et pour le suivi temporel d'images d'organes humains. Kervrann et Heitz [55] ont proposé quelques améliorations à ce modèle. Tout d'abord, les déformations sont estimées dans un cadre bayésien. Ensuite, une description hiérarchique permet de distinguer nettement les déformations globales des modes de déformations obtenus dans la base d'apprentissage. L'estimation des paramètres qui décrivent la forme globale de l'objet d'intérêt est effectuée préliminairement à l'estimation des déplacements locaux.

De nombreux auteurs [37] [47] ont adapté les modèles statistiques linéaires de Cootes aux problèmes 3D. En imagerie médicale, la modélisation des déformations permet la caractérisation et l'interprétation des pathologies des structures osseuses. Fleute et Lavallée ont proposé une méthode de reconstruction 3D à partir de multi acquisitions radiologiques calibrées basée sur l'identification des contours dans les images radiographiques [39]. Un modèle statistique est créé à partir de plusieurs modèles surfaciques obtenus par reconstruction CT-Scan supervisée et une analyse en composante principale (ACP ou transformé de Karhunen-Loeve) sur cet ensemble de géométries. La reconstruction 3D est obtenue par déformation du modèle statistique de sorte que les contours projetés du modèle reconstruit s'adaptent au mieux aux contours identifiés dans les radiographies. Lorenz et Krahnstöver ont proposé un modèle 3D de vertèbre lombaire à partir d'un ensemble de vertèbres représentatives préalablement numérisées par tomographie [62]. Mouren a proposé dans [77] une méthode de reconstruction 3D de la cage thoracique scoliotique à partir de I_{PA} et I_{LAT}, semblable à celle proposé précédemment dans nos travaux [7] pour la reconstruc-

tion de vertèbres scoliotiques. Cette méthode consiste à reconstruire la cage thoracique côte par côte. La reconstruction de côte consiste à déformer un modèle de forme statistique de côte afin de recaler les projections (postéro-antérieure et latérale) du contour externe de ce modèle *a priori* 3D de côte avec les contours de la côte correspondante préalablement segmentés sur les deux vues radiographiques I_{PA} et I_{LAT}. Le positionnement initial du modèle déformable de chaque côte est réalisé par l'utilisation de quelques points numérisés manuellement dans la vue radiographique I_{LAT}. Cette méthode est supervisée et l'ACP n'est pas toujours la bonne solution pour la caractérisation des modes de déformation d'une structure osseuse (cf. Chap. 4).

2.1.3.2 Travaux de Tipping et Bishop

L'approche de mélange de modèles *a priori*[2] pourrait être qualifiée d'approche "linéaire par morceaux". Elle a été proposée initialement par Tipping et Bishop [92][93]. Cette approche considère le modèle global non linéaire comme un mélange de modèles localement linéaires qui fournissent des "clusters" ou "classes" de formes. Chacun de ces sous-modèles peut alors être analysé par une analyse en composantes principales probabiliste qui fournit une réduction de dimension pour chacun d'entre eux. Les paramètres de ces sous-modèles sont estimés par des algorithmes de type EM (Expectation Maximisation) au sens du ML (Maximum Likelihood).

Dans ce type d'approches, se pose notamment la question du choix du nombre de composantes du mélange, à laquelle il n'est pas forcément évident de répondre, ainsi que celle du choix du nombre de composantes principales à retenir pour la définition de l'espace de travail de dimension réduite. En plus, l'algorithme itératif EM est sensible à l'initialisation, il converge extrêmement lentement et la convergence vers un bon maximum n'est pas assurée.

[2]Cette approche est connue sous le nom de mélange d'analyses en composantes principales probabilistes.

Mentionnons que l'analyse en composantes principales probabiliste a été déjà utilisée dans la localisation de forme dans une image [32], la classification d'objets [35] et l'inférence 3D de la structure [41]. Il a été seulement exploité dans la compression d'images [92] mais, à notre connaissance, il n'a pas été utilisé pour la modélisation 3D en imagerie médicale.

RECALAGE 3D/2D ET SEGMENTATION DES VERTÈBRES SCOLIOTIQUES PAR MODÈLES STATISTIQUES

Article : 3D/2D Registration and Segmentation of Scoliotic Vertebrae Using Statistical Models

Cet article a été publié comme l'indique la référence bibliographique

S. Benameur, M. Mignotte, S. Parent, H. Labelle, W. Skalli, J. De Guise. 3D/2D registration and segmentation of scoliotic vertebrae using statistical models. *Computerized Medical Imaging and Graphics*, 27(5) :321-327, Septembre 2003.

Cet article est présenté ici dans sa version originale.

Résumé

La scoliose est une déformation tridimensionnelle de la courbe naturelle de la colonne vertébrale, incluant des rotations et des déformations vertébrales. Afin d'étudier et d'analyser des caractéristiques 3D de cette déformation, différentes méthodes de reconstruction 3D de la colonne vertébrale scoliotique à partir d'images multiplanaires ont été développées. Ces caractéristiques servent pour la conception, l'évaluation et l'amélioration des méthodes de correction orthopédiques ou chirurgicales de la colonne vertébrale scoliotiques. La majorité des méthodes existantes dans la littérature utilisent un nombre restreint de repères anatomiques numérisés sur les images radiographiques et n'exploitent pas tout le potentiel d'information (notamment les contours) dans les deux images radiographiques [75] [43] [76].

Nous présentons dans cet article une méthode statistique supervisée de reconstruction 3D des vertèbres scoliotiques à partir de deux images radiographiques conventionnelles (postéro-antérieure avec incidence de 0° et latérale) calibrées. Cette méthode est basée sur une connaissance *a priori* globale de la structure géométrique de la vertèbre. Cette

connaissance est issue d'une base d'apprentissage d'environ 1000 vertèbres (30 vertèbres saines et 30 vertèbres scoliotiques par niveau vertébral) et représentée par un modèle déformable statistique intégrant, en plus des déformations linéaires, une série de déformations non linéaires modélisées par les premier modes de variation des déformations de l'expansion de Karhunen-Loeve. Cette première étape nous permettra d'établir un modèle *a priori* paramétrique concis de forme tridimensionnelle qui sera ensuite utilisé pour contraindre notre problème de reconstruction 3D. Le positionnement initial du modèle déformable statistique dans l'espace radiographique est réalisé à l'aide de six repères anatomiques (centroïdes des plateaux vertébraux, sommets des pédicules). La méthode de reconstruction présentée consistera alors à ajuster les projections (postéro-antérieure et latérale) de ce modèle 3D de la vertèbre avec les contours préalablement segmentés de la vertèbre correspondante sur les deux images radiographiques. Le problème de reconstruction 3D est vu comme un problème d'estimation des paramètres de déformation de ce modèle ou, de façon équivalente, comme un problème de minimisation d'une fonction d'énergie. Cette minimisation est réalisée par une technique de descente de gradient simplifiée. La méthode présentée est validée sur une base de 57 vertèbres lombaires et thoraciques de 13 patients scoliotiques qui ont aussi été reconstruites par CT-scan pour des fins de comparaison. Une erreur moyenne de (0.71 ± 0.06) mm pour les vertèbres lombaires et de (1.48 ± 0.27) mm pour les vertèbres thoraciques est obtenue sur les distances point-surface entre le modèle reconstruit avec notre méthode et le modèle issu de la reconstruction CT-scan.

CHAPITRE 3

3D/2D REGISTRATION AND SEGMENTATION OF SCOLIOTIC VERTEBRAE USING STATISTICAL MODELS

Abstract

We propose a new 3D/2D registration method for vertebrae of the scoliotic spine, using two conventional radiographic views (postero-anterior and lateral), and a priori global knowledge of the geometric structure of each vertebra. This geometric knowledge is efficiently captured by a statistical deformable template integrating a set of admissible deformations, expressed by the first modes of variation in Karhunen-Loeve expansion, of the pathological deformations observed on a representative scoliotic vertebra population. The proposed registration method consists of fitting the projections of this deformable template with the preliminary segmented contours of the corresponding vertebra on the two radiographic views. The 3D/2D registration problem is stated as the minimization of a cost function for each vertebra and solved with a gradient descent technique. Registration of the spine is then done vertebra by vertebra. The proposed method efficiently provides accurate 3D reconstruction of each scoliotic vertebra and, consequently, it also provides accurate knowledge of the 3D structure of the whole scoliotic spine. This registration method has been successfully tested on several biplanar radiographic images and validated on 57 scoliotic vertebrae. The validation results reported in this paper demonstrate that the proposed statistical scheme performs better than other conventional 3D reconstruction methods.

Key words: 3D/2D registration, 3D reconstruction model, statistical deformable model, shape model, biplanar radiographies, scoliosis, medical imaging, energy function optimization.

3.1 Introduction

Registration, an important problem in computer vision, is still incompletely solved. It primarily consists of establishing a geometric relation between the objects represented by two images. Many methods of image registration have been proposed in the literature (see, for example, a good survey of image registration methods proposed by Brown in [12], and the excellent review of existing registration techniques proposed by Van den Elsen et al in [30], Lavallée in [59], or Maintz and Viergever in [67], specific to the medical image registration problem). A comparison between several registration approaches has been also undertaken by West in [97]. Registration is a problem common to many tasks in medical imagery. Among these tasks, we can cite the 3D reconstruction of anatomical structures, the fusion of information coming from several methods, the construction of anatomical and functional atlases in medical imaging (allowing the detection of local and/or anatomical or functional abnormalities), the voluminal and dynamic visualization of images, etc.

In our application, we use a 3D/2D statistical registration model from biplanar radiographic images for the 3D reconstruction of scoliotic vertebrae of a spine. Scoliosis is a 3D deformation of the natural curve of the spinal column, including rotations and vertebral deformations. To analyze the 3D characteristics of these deformations, which can be useful for the design, evaluation and improvement of orthopedic or surgical correction, several 3D reconstruction methods have been developed. The 3D reconstruction methods of tomodensitometric imagery modalities (e.g., X-rays, magnetic resonance) provide accurate 3D information of the human anatomy. However, the high level of radiation received by the patient, the large quantity of information to be acquired and processed, and the cost of these methods make them less functional [43]. 3D reconstruction methods using a limited number of projections and some simple a priori knowledge of the geometry of the object to be reconstructed are interesting but are widely supervised; for example they may require manual identification (by an operator) of a set of 19 different points of interest (landmarks) on two different radiographic images (postero-anterior with normal incidence

(I_{PA}) and lateral (I_{LAT})) of 17 lumbar and thoracic vertebrae [43][75][76]. Besides, these afore-mentioned methods may not be very accurate, especially because they do not exploit all the information contained in the two radiographic images (e.g., the contours of each vertebra or a priori global geometrical knowledge of the object to be reconstructed), and because they are highly operator-dependent. To this end, Bayesian inference or statistical modeling is a convenient way of taking a priori information into consideration. The statistical approach is quite popular and has been successfully applied in medical imagery [21][19][68], in image analysis for extracting 2D objects in an image [22] or in an image sequence [56], for the 3D representation of vertebra [62], nonrigid 3D/2D registration of the knee [39][38], segmentation of 2D anatomical structures [23][49][46][48], localization and classification [36], etc.

In this way, we propose a new 3D/2D registration modeling approach for scoliotic vertebrae from biplanar radiographic images which can be viewed as a new statistical 3D reconstruction method. Our approach relies on the description of each vertebra by a deformable 3D template which incorporates (statistical) knowledge about its geometrical structure and its pathological variability. The deformations of this template are expressed by the first modes of variation in Karhunen-Loeve (KL) expansion of the pathological deformations observed on a representative scoliotic vertebra population. This prototype template, along with the set of admissible deformations, constitutes our global a priori model that will be used to rightly constraint the ill-posed nature of our 3D/2D registration problem [44]. In our application, the proposed method consists of fitting this template with the segmented contours of the corresponding vertebra on two calibrated radiographic views. This matching problem leads to an optimization problem of a cost function, efficiently solved in our application by a gradient descent algorithm initialized by a rough and rigid 3D/2D registration method estimated in the least square sense.

This paper is organized as follows. Section 3.2 presents the statistical deformable model. Section 3.3 describes the proposed 3D/2D registration method. Section 3.4 discusses the

validation protocol of our method. The experimental results of our 3D/2D registration or 3D reconstruction method are presented in Section 3.5. Finally, we conclude the paper in Section 3.6 with a discussion and perspectives.

3.2 Statistical Deformable Model

The shape s of each vertebra is defined by a set of l control points or landmarks, which approximate the geometric shape of each vertebra in $\mathcal{R}^3$ [22]. Each vertebra, in the training set, is thus represented by the following $3l$ dimensional vector,

$$s = (x_1, y_1, z_1, ..., x_l, y_l, z_l)^t ,$$

where $(x_i, y_i, z_i)^t$ are the Cartesian coordinates of each surface point. In the following, we will assume that s is the realization of a random vector that follows a normal law of mean vector $\bar{s}$ and covariance matrix C, as suggested in [22]. After alignment of the N training shapes [22], the mean shape and the covariance matrix are defined as,

$$\bar{s} = \frac{1}{N}\sum_{i=1}^{N} s_i , \qquad C = \frac{1}{N}\sum_{i=1}^{N}(s_i - \bar{s})(s_i - \bar{s})^T .$$

The variabilities within the training set are characterized by the displacement vector $\tilde{s} = s - \bar{s}$ of the different surface points with respect to the mean model. Statistical analysis of this random vector makes it possible to deduce the deformation modes relative to the mean shape. The eigenvectors of the covariance matrix C of this random vector describe the variation modes in the deformation parameter space or information on the variability of scoliotic deformations in the vertebra database. The associated eigenvalues λ_i are the amplitudes of these variation modes. An accurate description of the main variation modes may be obtained by retaining only the m eigenvectors associated with the t largest eigen-

values[1]. [22]. The model allows the generation of new instance of the shape by adding linear combinations of the m most significant variation vectors to the mean shape,

$$s = \Phi\, b + \bar{s}, \tag{3.1}$$

where Φ represents an orthogonal base of variation modes of scoliotic vertebrae contained in the training base, and b is the global deformation parameter vector setting the amplitudes of each deformation mode b_i. By ensuring,

$$-3\sqrt{\lambda_i} \leq b_i \leq +3\sqrt{\lambda_i}, \tag{3.2}$$

where λ_i is the eigenvalue associated with the deformation mode b_i, only the important deformations are extracted, discarding training data noise [22]. This low parametric representation of a vertebra constitutes to our global a priori model that will be used in our 3D reconstruction method (cf. Figures 2 and 3).

In theory, the ratio of an eigenvalue to the total sum of the other eigenvalues expresses the percentage of error introduced if the eigenvector associated with the corresponding eigenvalue is not selected [22]. One must thus specify a threshold f_v ($f_v \in [0, 1]$) for the eigenvalues above which the error is considered to be sufficiently small to generate a good approximation of the initial vector. Hence, if V_T is the sum of the eigenvalues, then the number m of eigenvalues to be selected is such that,

$$\sum_{i=1}^{m} \lambda_i \geq f_v V_T, \tag{3.3}$$

[1] As C is symmetric ($C^T = C$), its eigenvalues are real and the associated eigenvectors are orthogonal. As C is positive definite, its eigenvalues are positive or null.

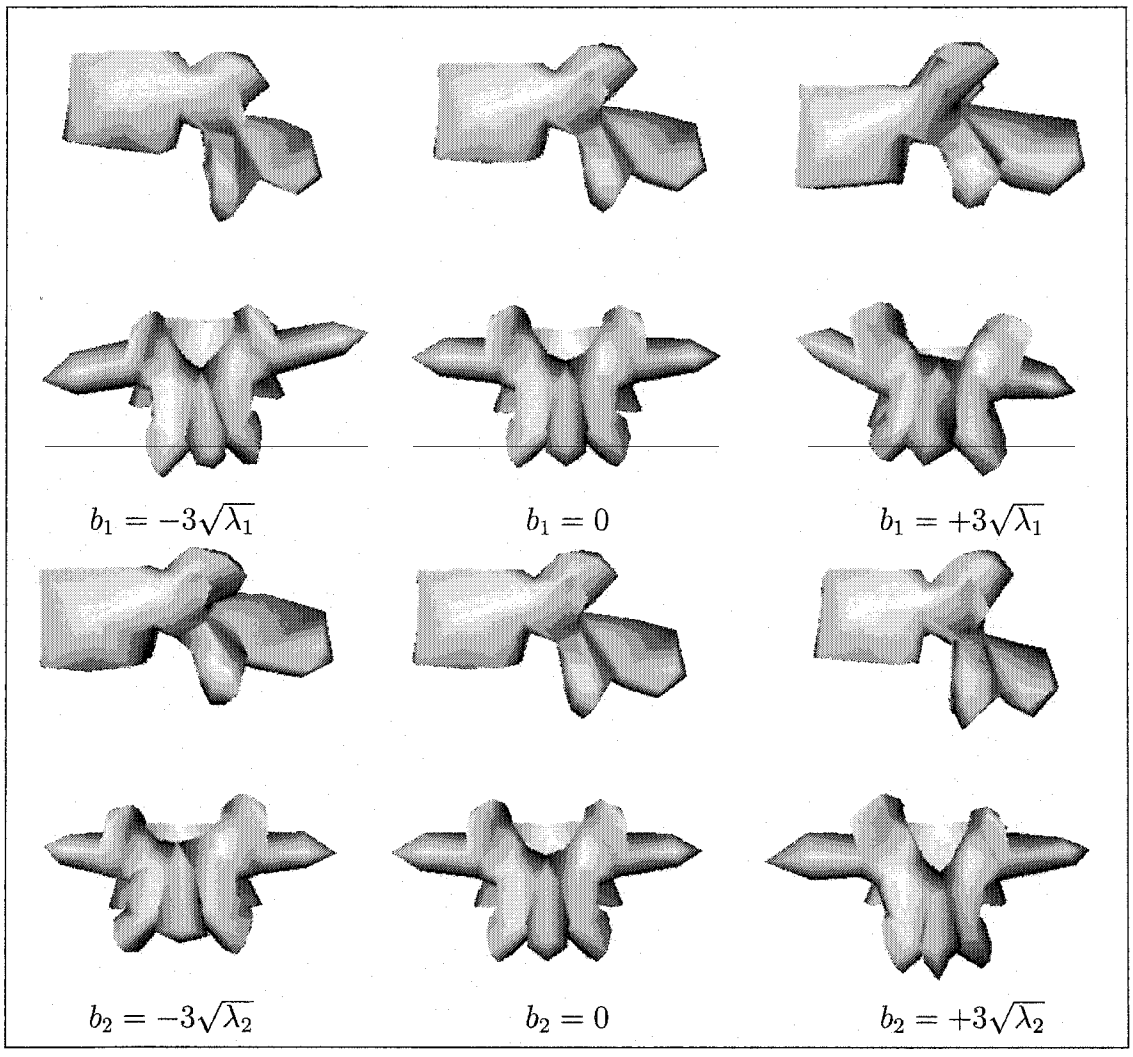

Figure 2 Visualization of mean shape (middle row) from the sagittal (top row) and coronal views (bottom row), and two deformed shapes obtained by applying (± 3 standard deviations of the first and second deformation modes to the mean shape for the L3 vertebra

By doing so, we ensure that the selected deformation modes allow us to represent $100 f_v\%$ of the existing scoliotic deformations in the training base[2].

[2]Each vector can also be characterized by the Mahalanobis distance $(s-\bar{s})^T C^{-1}(s-\bar{s})$ directly related to a normal distribution. From relation 3.2, we deduce that [22],

$$\sum_{i=1}^{m} \frac{b_i^2}{\lambda_i} \leq 9m. \tag{3.4}$$

A random vector s which does not check this condition could be considered to be not representative with respect to statistical training. In practice, the criterion expressed by Eq. 3.4 could be used to validate certain configurations of shapes [23].

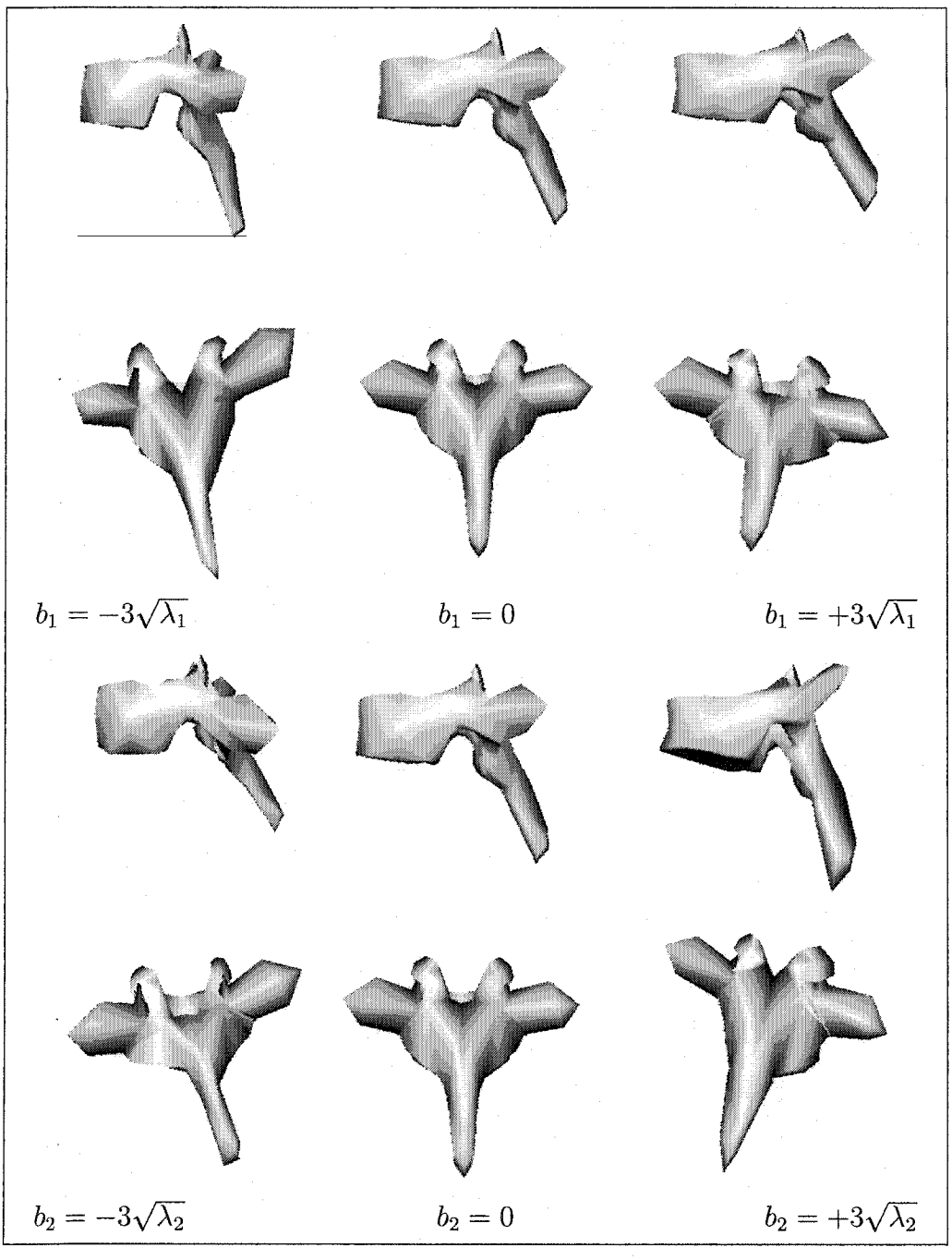

Figure 3 Visualization of mean shape (middle row) from the sagittal (top row) and coronal views (bottom row), and two deformed shapes obtained by applying (± 3 standard deviations of the first and second deformation modes to the mean shape for the T6 vertebra

3.3 3D/2D Registration Method

Besides the above-mentioned global deformation parameters, we also consider 3D global transformations from the similarity group which finally lead to the following model for global deformations,

$$s = M(k, \alpha)[\Phi b + \bar{s}] + T,$$

with $k(k \geq 0)$ and α being, respectively, the scale and the rotation vector, and T, a global translation vector. The rotation matrix R can be represented by a product of three separate rotation matrices R_{α_1}, R_{α_2}, and R_{α_3} which correspond to rotations around the x, y, and z axes respectively α_1, α_2, $\alpha_3 \in [0,2\pi]$. The rotation matrix R and the scale k are regrouped in the $3n \times 3n$ dimensional transformation matrix $M(k, \alpha)$ as follows,

$$\mathbf{M}(\mathbf{k}, \alpha) = \begin{pmatrix} M(k,\alpha) & 0 & \dots & 0 \\ 0 & M(k,\alpha) & \dots & 0 \\ \vdots & \vdots & \ddots & \vdots \\ 0 & 0 & \dots & M(k,\alpha) \end{pmatrix},$$

where $M(k, \alpha) = k\, R_{\alpha_3}\, R_{\alpha_2}\, R_{\alpha_1}$, $T = (T_x, T_y, T_z)^T$, and,

$$\mathbf{R}_{\alpha_1} = \begin{pmatrix} 1 & 0 & 0 \\ 0 & \cos(\alpha_1) & -\sin(\alpha_1) \\ 0 & \sin(\alpha_1) & \cos(\alpha_1) \end{pmatrix}, \mathbf{R}_{\alpha_2} = \begin{pmatrix} \cos(\alpha_2) & 0 & \sin(\alpha_2) \\ 0 & 1 & 0 \\ -\sin(\alpha_2) & 0 & \cos(\alpha_2) \end{pmatrix},$$

$$\mathbf{R}_{\alpha_3} = \begin{pmatrix} \cos(\alpha_3) & -\sin(\alpha_3) & 0 \\ \sin(\alpha_3) & \cos(\alpha_3) & 0 \\ 0 & 0 & 1 \end{pmatrix},$$

3.3.1 Crude and Rigid Initial Registration

To ensure a first crude and rigid reconstruction of each vertebra, we use the technique proposed in [54]. This technique identifies, in a preliminary step, a sequence of eight points along the centerline of the spine from the C1 cervical vertebra to the L5 lumbar vertebra on the two radiographic views of the spine. These points are then exploited to determine the position of six anatomical points (namely, the center of the superior and inferior end-plates, the upper and lower extremities of both pedicles) for each vertebra of the spine (cf. Figure 4). The corresponding points on the shape of the mean vertebra being known, we can obtain, in the least square sense [51], an initial estimate of the parameter vector (α, T). This leads us to crude and rigid registration for each vertebra that will then be refined by our 3D reconstruction model.

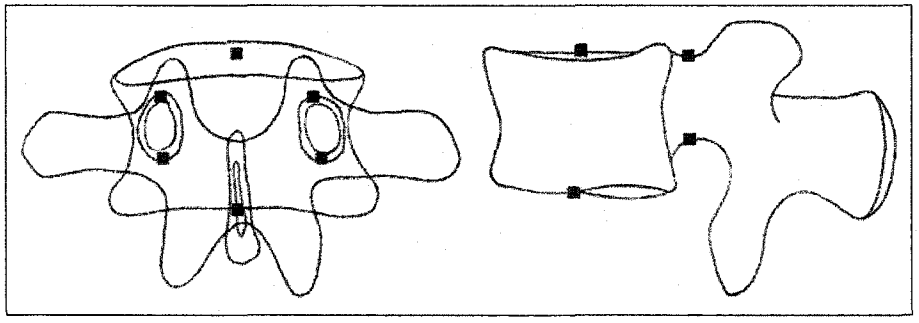

Figure 4 Anatomical stereo-corresponding landmarks

3.3.2 3D/2D Model Registration

Our reconstruction model from two radiographic views is stated as the minimization of the following cost function,

$$E(s(\theta)) = E_l(s(\theta), I_{\text{PA}}, I_{\text{LAT}}) + \beta E_p(s(\theta)), \tag{3.5}$$

where $E_l(s(\theta), I_{\text{PA}}, I_{\text{LAT}})$ is the likelihood energy term, and $E_p(s(\theta))$ is the prior energy term (or the regularization term), used to constrain the ill-posed nature of this optimization

problem. β is a factor that provides relative weighting between the two penalty terms and allows us to control the rigidity of the statistical template [53]. $\theta = (M(k, \alpha), T, b)$ is the deformation parameter vector of the model to be estimated. It should be noted that this optimization problem can also be formulated as the search for the maximum a posteriori (MAP) of θ, the deformation parameters of the deformed template s,

$$\theta^* = \arg\max_{\theta} P(I_{PA}, I_{LAT} \mid s(\theta))P(s(\theta)), \tag{3.6}$$

where $P(I_{PA}, I_{LAT} \mid s(\theta)) = \frac{1}{\zeta_l} \exp\left(-E_l(s(\theta), I_{\text{PA}}, I_{\text{LAT}})\right)$ is the likelihood of the observations (i.e., the segmented contours on the two radiographic views) given by a deformed template, and $P(s(\theta)) = \frac{1}{\zeta_p} \exp\left(-E_p(s(\theta))\right)$ is the prior probability of the deformed template (or the prior probability of a scoliotic deformation for a given vertebra). ζ_l and ζ_p are two constants of normalization.

3.3.3 Likelihood Energy Term

In our application, our likelihood model is expressed by a measure of similarity between the external contour of the lateral and the postero-anterior perspective projections of the deformed template and an *edge potential field* estimated on the two radiographic views. First, this edge potential field requires the preliminary detection of edges in the two radiographic images. To do so, we use a Canny edge detector [13]. Second, this field is determined by the positions of the detected edges in the radiographic images. For a pixel (x, y) in the postero-anterior or lateral image, we define its edge potential by,

$$\Psi(x, y) = \exp\left(-\frac{\sqrt{\xi_x^2 + \xi_y^2}}{\tau}\right),$$

where (ξ_x, ξ_y) is the displacement to the nearest edge point in the image, and τ is a smoothing factor which controls the degree of smoothness of this potential field[3]. This edge potential induces an energy function that relates a deformed template s to the edges in the two radiographic images I_{PA} and I_{LAT} (cf. Figure 11)

$$E_l(s(\theta), I_{\text{PA}}, I_{\text{LAT}}) = -\frac{1}{n_{\text{PA}}} \sum_{\Gamma_{\text{PA}}} \Psi_{\text{PA}}(x, y) - \frac{1}{n_{\text{LAT}}} \sum_{\Gamma_{\text{LAT}}} \Psi_{\text{LAT}}(x, y), \tag{3.7}$$

where the summation of the first and second term of $E_l(s(\theta), I_{\text{PA}}, I_{\text{LAT}})$ is overall the n_{PA} and n_{LAT} points of the external contour of the, respectively, lateral and postero-anterior perspective projections of the deformed template on the two pre-computed edge potential fields of each radiographic image. This energy function attains its maximum value when there is an exact correspondence between the projected contours (of the deformed template) and the preliminary segmented contours of the two radiographic views.

3.3.4 Prior Energy Term

Due to Karhunen-Loeve transformation, the random variables b_i are independent and follow a normal law of a null mean and variance λ_i [22]. Thus, the law of probability of $s(\theta)$, the deformed template, can be written as [56],

$$P(s(\theta)) = \prod_{i=1}^{m} \frac{1}{\sqrt{2\lambda_i \pi}} \exp\left(-\frac{b_i^2}{2\lambda_i}\right),$$

[3]We can easily complete this edge potential field $\Psi(x, y)$ by adding to it a directional component to obtain a directional edge potential field,

$$\Psi'(x, y) = \Psi(x, y) \mid \cos(\gamma(x, y)) \mid,$$

where $\gamma(x, y)$ is the angle between the tangent of the nearest edge and the tangent direction of the contour at (x, y). This potential field is similar to the one proposed in [53] for a template-based localization approach.

This probability expresses the fact that the shape to be reconstructed is likely close to the mean shape. By considering that $P(s(\theta)) = \frac{1}{\zeta_p} \exp\left(-E_p(s(\theta))\right)$ the prior energy term can be written as,

$$E_p(s(\theta)) = \frac{1}{2} \sum_{i=1}^{m} \frac{b_i^2}{\lambda_i}, \tag{3.8}$$

This energy term penalizes the deviation of the deformed template from the mean shape. This term does not penalize affine transformations. Eq. 3.8 closely resembles the Mahalanobis distance. It defines an ellipsoid centered in $\mathcal{R}^m$ whose principal axes are identified by $\sqrt{\lambda_i}$ when $E_p(s(\theta))$ is a constant.

3.3.5 Silhouette Extraction of the 3D Model

The 3D model of vertebrae is represented in the form of a triangulated mesh (cf. Figure 6). Silhouette detection is based on estimation of the normal at each vertex of the mesh. The normal in each vertex is computed by the average of the normal of all facets to which the vertex belongs (cf. Figure 7). For two neighbours V_1 and V_2 of facet F_i whose product of the weights is negative, we interpolate linearly along the edge (V_1, V_2) (cf. Table 1). The line joining two interpolated vertices of F_i is called the external edge (cf. Figure 8). On a surface Γ, the external edges of the vertebra shape are lines where the direction of projection is tangent on the surface [16][86]. The external edges are saved in a list. As in the case of a not-convex object, the external edges can be hidden by other parts of the surface. We keep all the external edges, including those that are occluded (i.e., those that are hidden by another part of the vertebra). Let us recall that we use semi-transparent radiographic images (i.e., superposition of the various structures on the same plane). In our application, occluded edges are also exploited in our 3D/2D registration method. Let us put all the external edges having a joint vertex in a list. Each one of these lists constitutes an external contour of the vertebra. The set of these external contours constitutes the silhouette of the vertebra (cf. Figure 9). We summarize the whole procedure in Table 1.

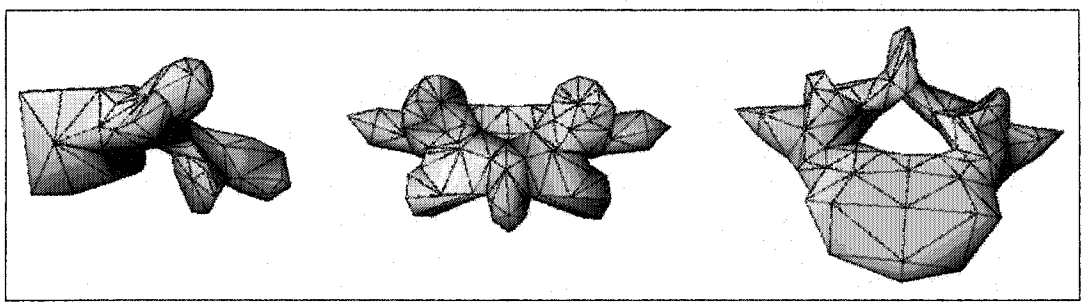

Figure 5 Visualization of the shape model: sagittal, coronal and axial views

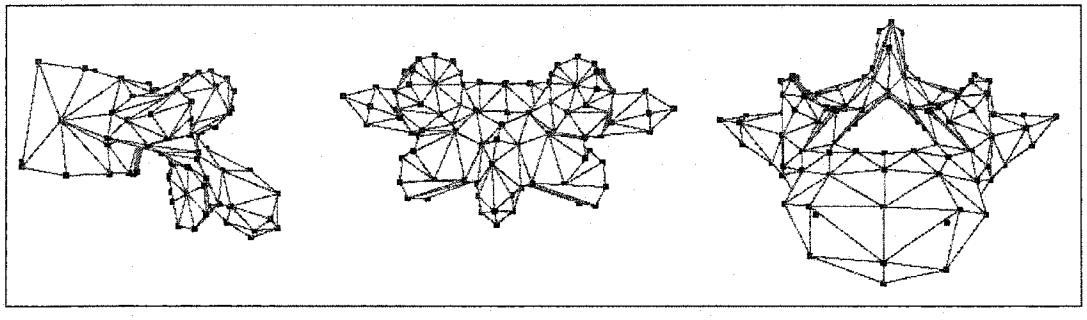

Figure 6 Model of vertebra: triangulated mesh (187 vertices and 378 triangles)

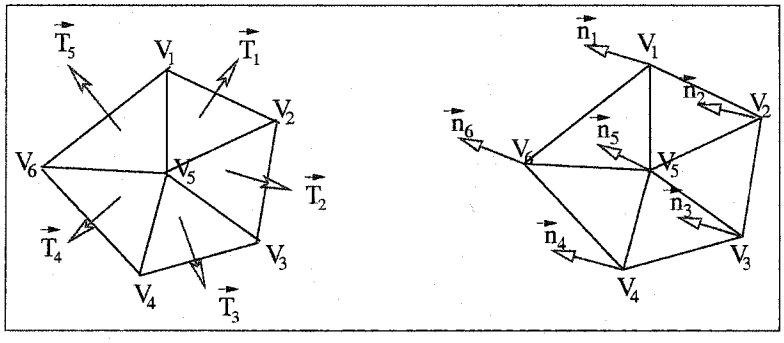

Figure 7 Normal at the triangles, normal at the points

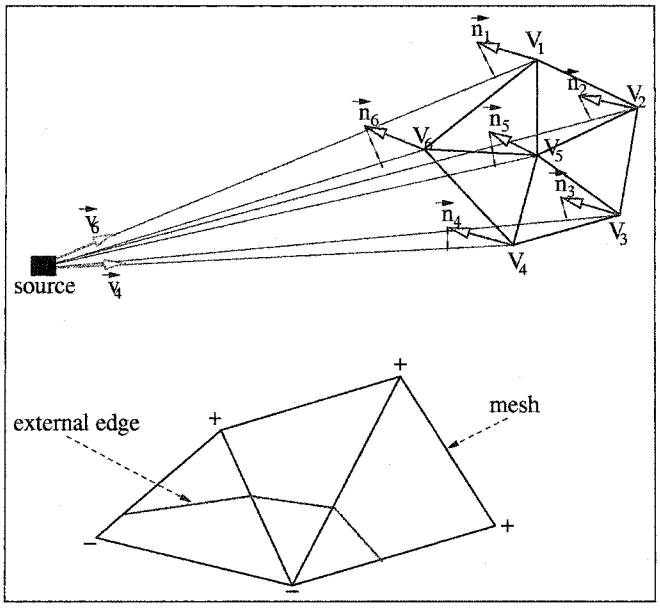

Figure 8 Example of an external edge, the + and − signs on the vertices indicate the signs of its weights

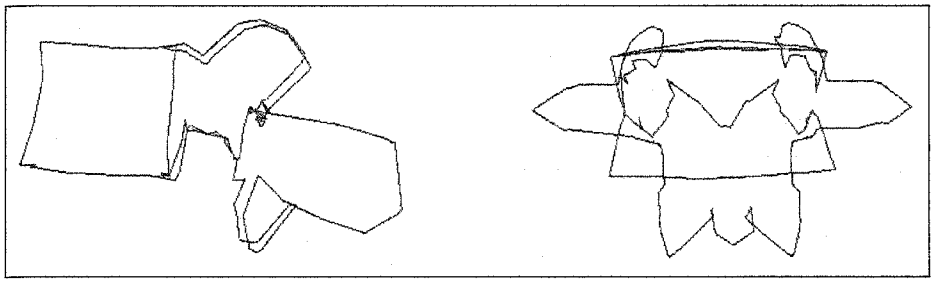

Figure 9 Example of lateral and postero-anterior silhouettes of a vertebra given by the silhouette extraction algorithm

3.3.6 Optimization of the Energy Function

The energy function to be minimized, namely,

$$E(s(\theta)) = -\frac{1}{n_{\text{PA}}}\sum_{\Gamma_{\text{PA}}} \Psi_{\text{PA}}(x,y) - \frac{1}{n_{\text{LAT}}}\sum_{\Gamma_{\text{LAT}}} \Psi_{\text{LAT}}(x,y) + \beta\frac{1}{2}\sum_{i=1}^{m}\frac{b_i^2}{\lambda_i}, \tag{3.9}$$

is a complex function with several local minima over the deformation parameter space. A global search is impossible due to the size of the configuration space. In our application,

Table 1

Algorithm used for silhouette extraction

Silhouette extraction algorithm

$M = (V, F)$	Mesh such that
V:	$V = \{V_1, \ldots, V_n\} \subset R^3$ Set of vertices
F:	$F = \{F_1, \ldots, F_f\}$ set of facets
L	Empty list
$\vec{n}_i$	Normal in vertex V_i of facet F_i
$\vec{v}_i$	Unit vector line joining the projection source and vertex V_i

for *each facet* F_i *of* F **do**
  Compute the normal at facet F_i

for *each vertex* V_i *of* V **do**
  Compute the normal at vertex V_i and its weight $\vec{n}_i \cdot \vec{v}_i$

for *each facet* F_i *of* F **do**
  for *each pair of vertex* (V_i, V_j) *of* F_i **do**
    if $(\vec{n}_i \cdot \vec{v}_i) \times (\vec{n}_j \cdot \vec{v}_j) < 0$ **then**
      - Interpolate linearly along the edge (V_i, V_j)
      - Add the edge joining two interpolated points to L

Gather all the edges of L having a joint vertex in list L_i ($L = L_i / i \geq 0$)

experiments have shown that the initial crude and rigid reconstruction technique described in Section 3.3.1 (i.e., the estimation of rigid deformation parameters) can be efficiently exploited to initialize a gradient descent technique.

Various types of gradient descent have been used for rigid registration [66][91][99][100]. For our application, we combine the gradient descent technique with the strategy described in [53], which consists of sampling, out of θ, function $E(s(\theta))$ and using various samples obtained to initialize a local gradient descent technique. In our case, we sample out function $E(s(\theta))$ around estimations given by the crude and rigid reconstruction technique

presented in Section 3.3.1. The final adopted solution is the one associated with the lowest energy. However, the sampling of these template positions and transformation parameters must be chosen judiciously. It should be fine enough not to miss the significant local minima of the energy function, and large enough to avoid high computational requirements. In our application, we also use a simplified version of the traditional gradient descent technique, which does not require an analytical expression of the gradient of $E(s(\theta))$ (clearly unavailable in our case), and similar to the one proposed in [73]. We have summarized the whole procedure in Table 2. This gradient descent technique, combined with the above-mentioned sampling strategy, is deployed to simultaneously refine the estimation of rigid parameters and to estimate nonrigid parameters.

3.4 Validation of 3D/2D Registration

In our application, our 3D/2D registration technique is validated by comparing the reconstructed model obtained by our method and by reconstruction from CT-scan slices [34] by SliceOmatic© (TomoVision. http://www.tomovision.com/) software. 3D reconstruction models of the vertebrae contain up to $7,000$ points per vertebra and will constitute the ground truth for our validation procedure. First, the validation procedure consists of fitting the model of 200 points of our 3D/2D registration method on the scanned vertebra. To this end, we manually extract some easily identifiable anatomical landmarks on the reconstructed model resulting from CT-scan whose position is known, and we estimate the rigid transformation allowing us to pass from the set of anatomical landmarks of our reconstructed model to the set of corresponding anatomical landmarks on the scanned model. Then, we apply this rigid transformation to all points of the reconstructed vertebra. Once this is done, we optimize the rigid transformation, which enables us to readjust the two models of vertebra. Optimization consists of finding neighbours on the scanned vertebra to each point of the reconstructed vertebra and then of estimating and re-applying the rigid deformation, allowing us to pass from the set of points of the reconstructed vertebra to the set of points closes to the scanned vertebra.

Table 2

Deterministic algorithm used for optimization of the energy function

Gradient descent algorithm

E	Energy function
θ	The deformation parameter vector
$\Delta\theta_i$	Step of each parameter

Sampling in θ of function $E(s(\theta))$ around the estimation given by the rigid reconstruction technique (Section 3.3.1)

for *each configuration or sample obtained* **do**
  for *each parameter* $\theta_i (1 < i < t)$ **do**
    - Evaluate:
    $E(\theta_1, \ldots, \theta_i - \Delta\theta_i, \ldots, \theta_t)$
    $E(\theta_1, \ldots, \theta_i, \ldots, \theta_t)$
    $E(\theta_1, \ldots, \theta_i + \Delta\theta_i, \ldots, \theta_t)$
    - Retain the configuration θ associated with the lowest energy

  We stop the algorithm for this sample when $E(s(\theta))$ is stable and the estimate obtained is memorized if the computed energy is lower than the last better estimate.

The variation of error between the two sets of points is also computed[4]. This procedure is repeated until the difference in variation of error between two successive stages is lower than a given threshold. The whole procedure is summarized in Table 3. We can exploit this 3D/2D registration method to estimate the mean and the maximum error distance between the 3D reconstructed model from our method and the 3D model resulting from CT-scan.

[4]many methods have been proposed in the litterature to estimate the rigid transformations R and T. In [63], Lorusso compared the quaternion method [51], polar decomposition [50], the method of decomposition in singular values (SVD) [2], and the duaux quaternion method [96]. This study concludes that the difference in precision is not significant, the computational times are comparable, and that the only substantial difference is the sensitivity of the algorithms when the points used approach a degenerated configuration. In our case, we use the quaternion method.

Table 3

Algorithm used for fitting two 3D meshes

Fitting algorithm of two 3D mesh points

V_{scan_vert}	Set of vertex of scanned vertebra
V_{reco_vert}	Set of vertex of reconstructed vertebra
$V_{scan\_vert}^{corresp}$	Set of corresponding vertex of scanned vertebra
$V_{reco\_vert}^{corresp}$	Set of corresponding vertex of reconstructed vertebra
$V_{scan\_vert}^{nearest}$	Empty set
ϵ	Threshold
R	Rotation
T	Translation
$Quaternions$	Quaternions algorithm

1. Initialization

- $[R, T]$ = Quaternions($V_{reco\_vert}^{corresp}$,$V_{scan\_vert}^{corresp}$)
- T apply the rigid transformation (rotation R and translation T) to V_{reco_vert}

2. Optimization

j=0; Σ_0=0;
while $\mid \Sigma_{j+1} - \Sigma_j \mid > \epsilon$ **do**
- **for** *each vertex* V_i *of* V_{reco_vert} **do**
  - Compute the nearest point N_i of V_i in V_{scan_vert} and add N_i to $V_{scan\_vert}^{nearest}$
- $[R, T]$ = Quaternions($V_{reco\_vert}^{corresp}$,$V_{scan\_vert}^{nearest}$)
- Apply the rigid transformation (rotation R and translation T) to V_{reco_vert}
- Compute $\Sigma_j^2 = \sum_{i=1}^{n} \parallel V_{scan\_vert_i}^{nearest} - V_{reco\_vert_i} \parallel$

Retain the rigid transformation (rotation R and translation T) corresponding at the last step

3.5 Experimental Results

3.5.1 Vertebra Database

The vertebra database consists of $1,020$ thoracic and lumbar vertebrae (510 normal and 510 scoliotic). These data were obtained by digitization of the anatomical points on anatomical specimens. These anatomical specimens have been selected from the Hamann-Todd osteology collection of over $1,800$ complete specimens in Cleveland, USA, and from the Robert J. Terry anatomical skeletal collection of over $1,700$ specimens at the Smithsonian Institution in Washington, D. C., USA[5]. [82].

Fastrack© (POLHEMUS, A Rockwell Collins Company) is the name of the electromagnetic device used to digitize each vertebra by means of a pointer. The accuracy of this device is evaluated at ± 0.2 mm [11]. The 3D coordinates of the pointer were recorded in a specific reference system. The digitizing protocol consisted of measuring specific anatomical landmarks on each vertebra, thus creating a set of approximately 200 points depending on the level measured with regard to its particular geometry [88]. Different points were acquired in a specific order and recorded in this sequence. After the measurements were done, each vertebra was then reconstructed using computer graphics software. Each set of points was then re-localized in a local coordinate system[6] .

3.5.2 Radiographic Images

In our application, we used two radiographic images (i.e., postero-anterior and lateral) acquired with a Fuji FCR 7501S radiographic imaging system. Radiography is the image in 2D projection of a 3D object whose X-rays are the source of illumination. The intensity transmitted through a specific zone of an object varies according to the nature and thickness of the material through which radiation passes. Thus, air, soft tissue (muscles, cartilage, etc.) and bones present different attenuation coefficients for X-rays and can, in

[5] Age, sex, race, height, weight, cause of death and peculiar dissection findings of each scoliotic specimen are available.

[6] To our knowledge, the vertebrae base is the largest database available in the literature [82].

this way, become theoretically localized in radiological images. Thus, the radiographic image illustrates the superposition of various structures on a same plane and gives place to semi-transparent images.

3.5.3 Calibration

Calibration is a necessary step to compute the geometrical parameters of the radiological environment. The images are calibrated by a calibration object which is composed of two acrylic sheets parallel to the X-ray film plane. The two sheets contain embedded radiopaque spherical markers (55 steel balls) which are easily detectable on the radiographic images. The scene is calibrated using the 3D coordinates $(X, Y, Z)^T$ of each steel ball previously measured and their corresponding 2D observations $(x, y)^T$ to solve the following equation,

$$(x, y, \mu)^T = D(\vartheta, \kappa) \times (X, Y, Z)^T,$$

where μ is the x-ray tube distance, ϑ and κ being respectively the scale and rotation vector [71]. The rotation vector ϑ and the scale κ are regrouped in the 3×3 dimensional matrix $D(\vartheta, \kappa)$.

3.5.4 Comparison Protocol

We have validated our 3D/2D registration method on 57 scoliotic vertebrae (6 lumbar vertebrae and 51 thoracic vertebrae) from 13 patients (13 pairs of radiographic images (postero-anterior and lateral views) of scoliotic spines). This comparison was made using the distance (mean, root mean square (RMS), and maximum) between a point from the reconstructed vertebra and the surface of the corresponding vertebra obtained with CT-scan, which was considered as the ground truth and whose accuracy is ± 1 mm [3].

We also considered five morphometric parameters related mostly to the dimensions of the pedicles and the spinal canal (cf. Figure 10). These measures can be useful for the surgeon

because the pedicles are significant places for the installation of fastenings and hooks to allow rectification of the spinal column.

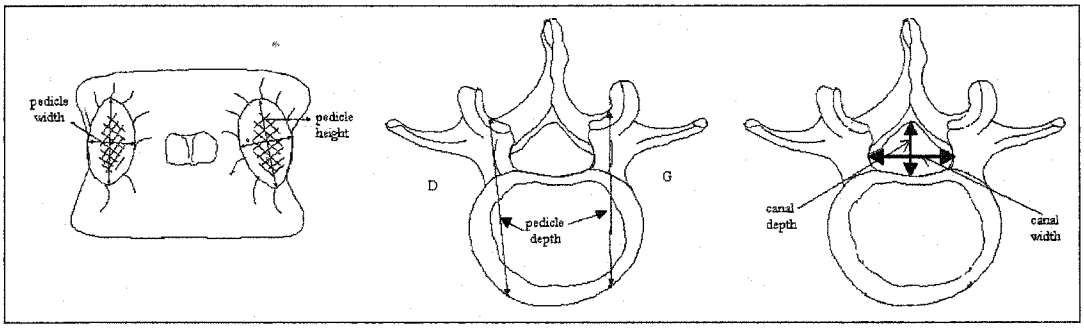

Figure 10 Morphometric parameters used in our validation protocol

3.5.5 Experimental Results

The mean vertebra shape of each vertebral level is computed from a sample of 30 normal vertebrae. The deformation modes of each vertebral level is computed on a sample of 30 scoliotic vertebrae.

We used the Canny edge detector to estimate the edge map which is then employed to estimate the edge potential field on the two radiographic views (cf. Figure 11). In our application, sigma=1, mask size is 5×5, and the lower and upper thresholds are given by the unsupervised estimation technique proposed in [13]. In our application, we have chosen to take the number of deformation modes that allows representation of at least 90% of the admissible deformations for each type of vertebra. Table 4 shows that, for the L3 vertebra, the first 10 deformation modes integrate 90.90% of the deformations considered to be statistically admissible. For the T6 vertebra, the first eight deformation modes represent 92.49% of the deformations.

Besides, experiments have shown that the crude and rigid reconstruction procedure is not always a good initialization for the gradient-based optimization technique. As already

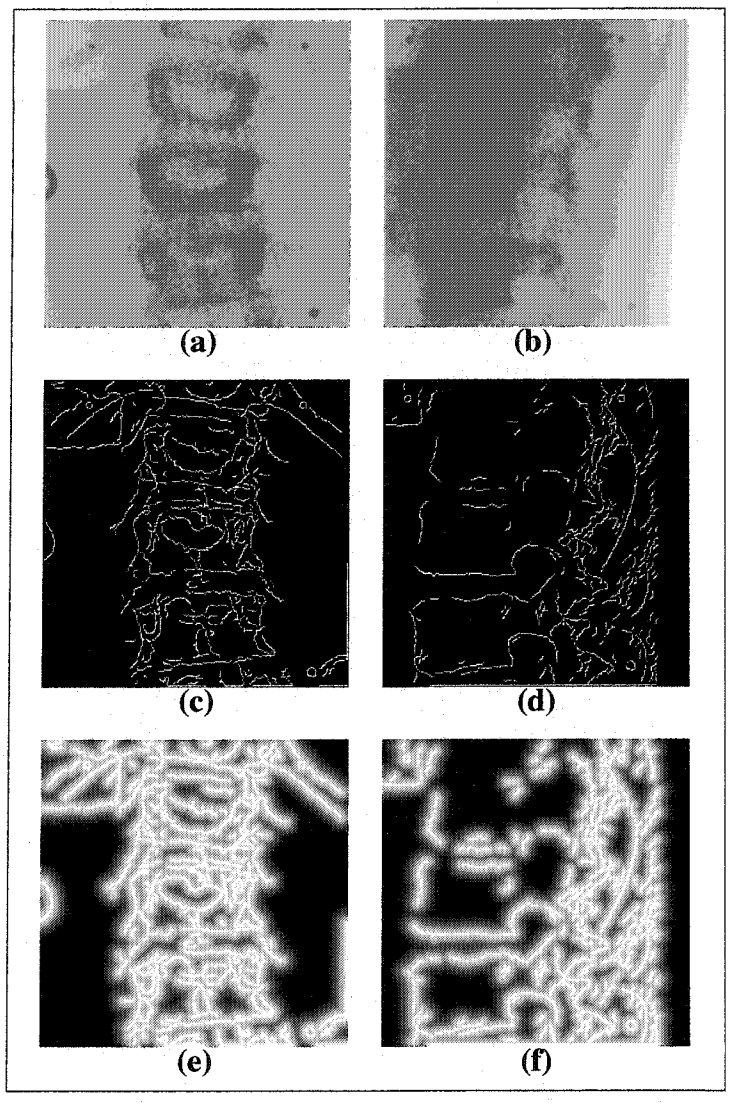

Figure 11 Preprocessing: **(a)** Postero-anterior, **(b)** Lateral image (256×256 pixels, **(c)** and **(d)** Edge map using a Canny edge detector, **(e)** and **(f)** Edge potential field

stated in Section 3.3.5 and, in order to overcome this problem, our solution consists of placing the template at evenly-spaced positions and in deforming it according to a discretized set of translation orientations or scales (corresponding to rigid parameters) within a range of values around the initial estimate obtained by the rigid reconstruction procedure. These deformed template configurations can then be used to initialize a deterministic gradient descent algorithm. However, spacing between the template positions and the sampling of the transformations must be chosen judiciously: not too spaced out to cover

Table 4

Normalized eigenvalues computed on a training set of 178 point models of 30 vertebrae obtained from the covariance matrix

L3 vertebra		T6 vertebra	
$\frac{\lambda_i}{V_T}$ (%)	$\frac{\lambda_i}{V_T}$ cumulated (%)	$\frac{\lambda_i}{V_T}$ (%)	$\frac{\lambda_i}{V_T}$ cumulated (%)
26.46	26.46	27.62	27.62
19.44	45.90	24.06	51.68
8.95	54.85	12.37	64.04
7.95	62.80	9.55	73.59
6.89	69.69	6.49	80.09
6.22	75.91	5.42	85.50
4.88	80.80	4.19	89.69
3.88	84.68	2.80	92.49
3.45	88.12		
2.78	90.90		

all the significant local minima of the energy surface, and not too little spacing to avoid high computational requirements.

For the experiments, we have chosen $\beta = 1$ for the weighting factor penalizing the prior energy term with respect to external energy. The proposed method allows good registration of the vertebra. An example of projections of the shape of a L3 vertebra on postero-anterior and lateral radiographic images for a scoliotic patient is presented in Figure 12. The mean and the maximum error distance between the reconstructed model resulting from our 3D/2D registration method and the model resulting from CT-scan are, respectively, (0.71 ± 0.06) mm, and (3.67 ± 0.80) mm for the lumbar vertebrae and (1.48 ± 0.27) mm, and (6.44 ± 1.76) mm for the thoracic vertebrae. The results of comparison for 11 vertebral levels are given in Table 9. Pedicle width, pedicle height, pedicle depth, canal depth and canal width difference between the reconstructed model resulting from our 3D/2D registration method and the model resulting from CT-scan are of the same order. The results of comparison for 11 vertebral levels are given in Table 10. Visual comparison

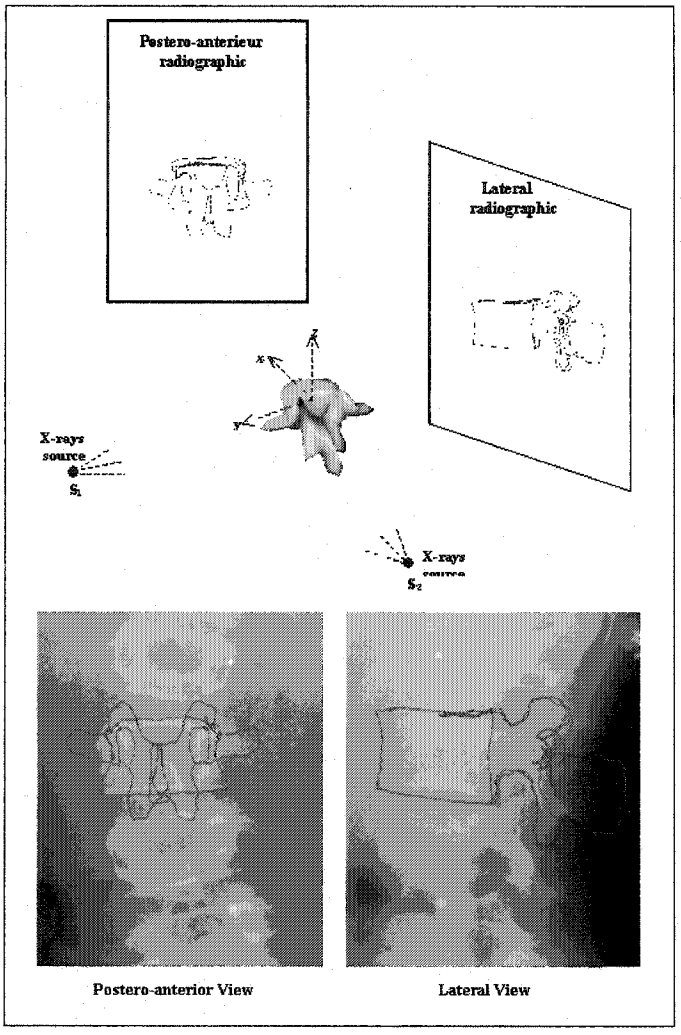

Figure 12 Initial estimate of the mean shape of the vertebra on the two radiographic views by the proposed crude and rigid initial reconstruction method

between the reconstructed model resulting from our 3D/2D registration method and the model resulting from CT-scan for the L3 and T6 vertebrae is presented respectively in Figures 13 and 14.

3.6 Discussion and Conclusion

We have presented an original statistical method of 3D/2D registration of scoliotic vertebrae using both the contours extracted from biplanar radiographic images and a priori knowledge of the geometric structure of each vertebra. This technique can also be viewed

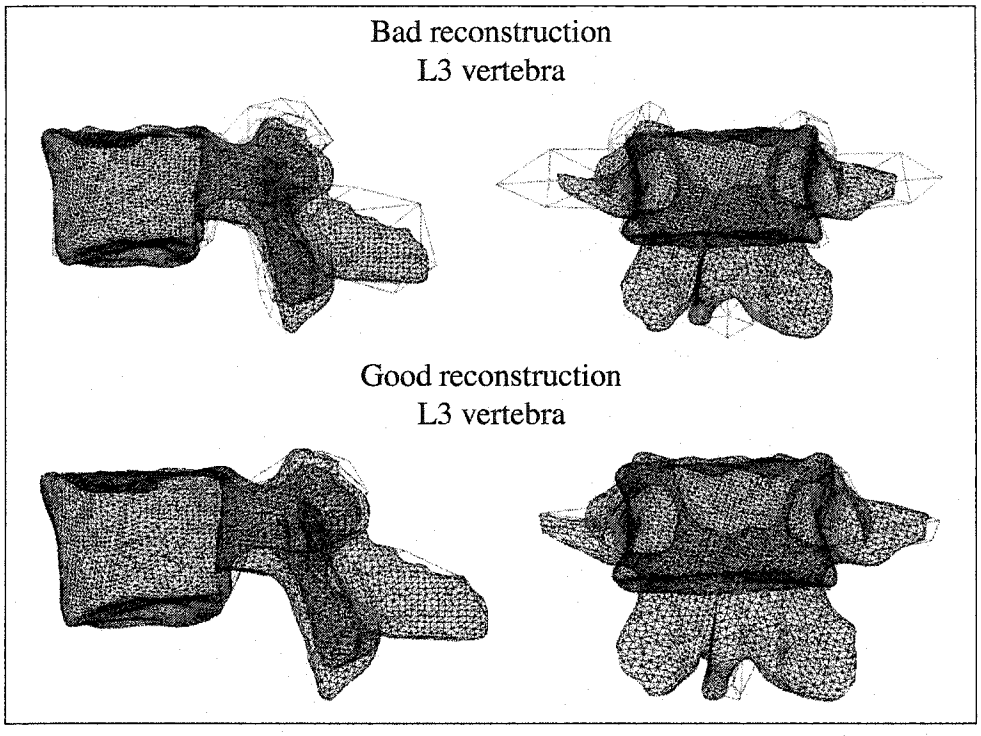

Figure 13 Visual comparison between 3D reconstruction using our 3D/2D registration method (red lines) and reference CT-scan (black lines) for the L3 vertebra

as an original 3D/2D reconstruction or segmentation model. The 3D/2D registration problem is stated as the minimization of a cost function for each vertebra and is solved with a gradient descent technique combined with a sampling strategy.

The results of validation presented above show that the reconstruction of lumbar vertebrae obtained by our 3D/2D registration method is more accurate than the 3D biplanar reconstruction method using non-stereo-corresponding points (NSCP) [75] and the 3D biplanar reconstruction method using corresponding points (DLT) [43][76]. The mean error is 0.7 mm for our method, 1.4 mm for NSCP, and 2.4 mm for DLT in [76], and 2.6 mm for DLT in [3]. Some maximum errors obtained on spinous processes are still high (i.e., maximum error is 3.9 mm for lumbar vertebra and 7.9 mm for thoracic vertebra) (cf. Figures 15 and 16). Even though these maxima correspond to points with no significant role in surgery planning, the accuracy of reconstruction is relatively acceptable with the results obtained by CT-scan which is considered as the more accurate reconstruction technique.

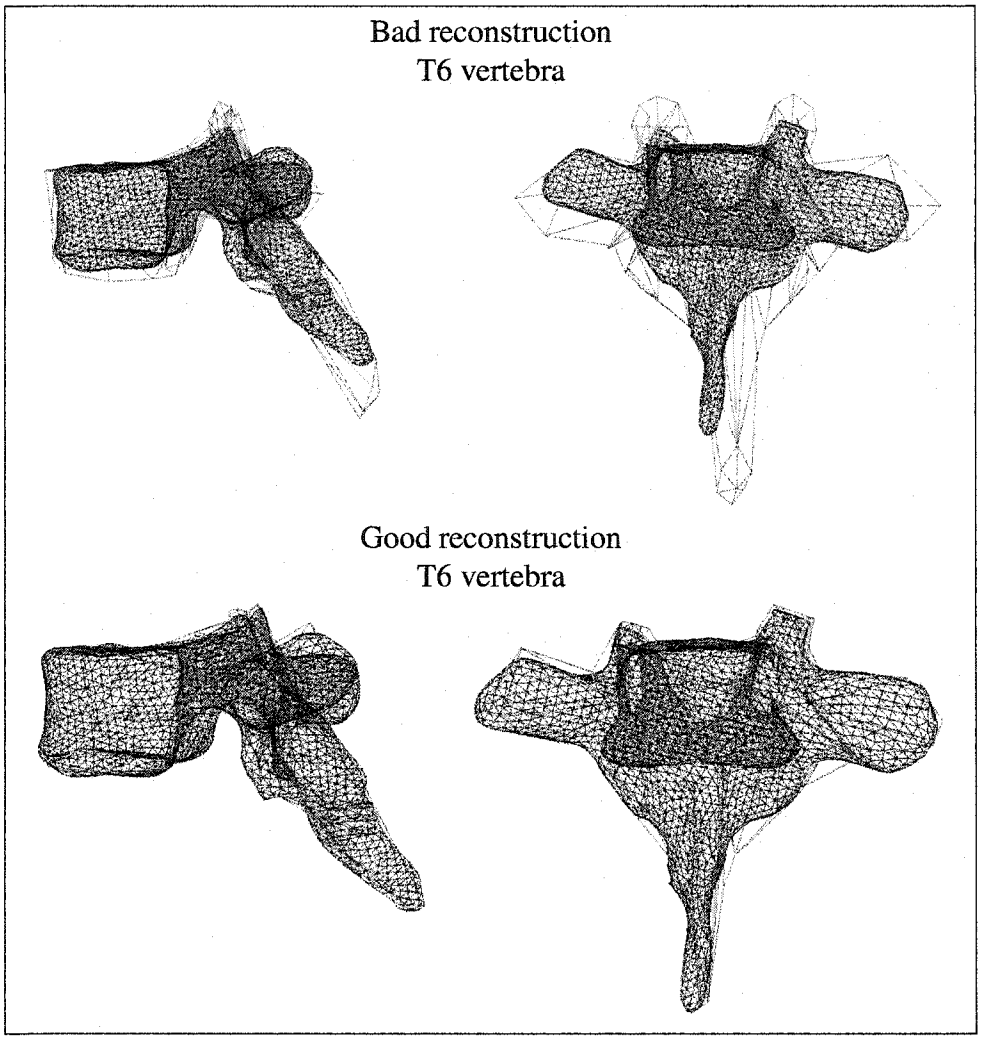

Figure 14 Visual comparison between 3D reconstruction using our 3D/2D registration method (red lines) and reference CT-scan (black lines) for the T6 vertebra

We note that the results are better for the lumbar vertebrae. For the thoracic vertebrae, the segmented contours are difficult to detect due to the presence of the ribs. Let us add that the size of the vertebra database, on which we performed a principal component analysis (PCA) to extract the deformations (considered to be statistically admissible), remains insufficient and does not certainly contain all the scoliotic deformations. Consequently, a large part of our reconstruction error results from the fact that some scoliotic deformations have not been modeled by PCA. Another part of our reconstruction error is due to the reconstruction error of the CT-scan technique considered as null in our validation protocol.

Table 5

Results on point-to-surface comparisons of 57 scoliotic vertebrae. All data are shown as mean ± standard deviation

Vertebral level	N	Mean error (mm)	Root mean square (mm)	Maximum error (mm)
Thoracic				
T6	3	1.16±0.07	0.20±0.06	5.30±1.04
T7	6	1.70±0.29	0.22±0.06	6.01±0.57
T8	9	1.79±0.18	0.25±0.10	7.28±4.00
T9	10	1.46±0.32	0.24±0.07	6.89±1.61
T10	9	1.24±0.31	0.23±0.07	6.59±0.61
T11	9	1.62±0.52	0.21±0.07	6.63±1.28
T12	5	1.37±0.21	0.16±0.03	6.38±1.17
Lumbar				
L1	2	0.49±0.03	0.04±0.01	3.84±0.21
L2	1	0.76±0.12	0.05±0.01	3.85±0.90
L3	2	0.80±0.02	0.06±0.01	4.91±0.15
L5	1	0.70±0.06	0.04±0.01	2.07±1.26

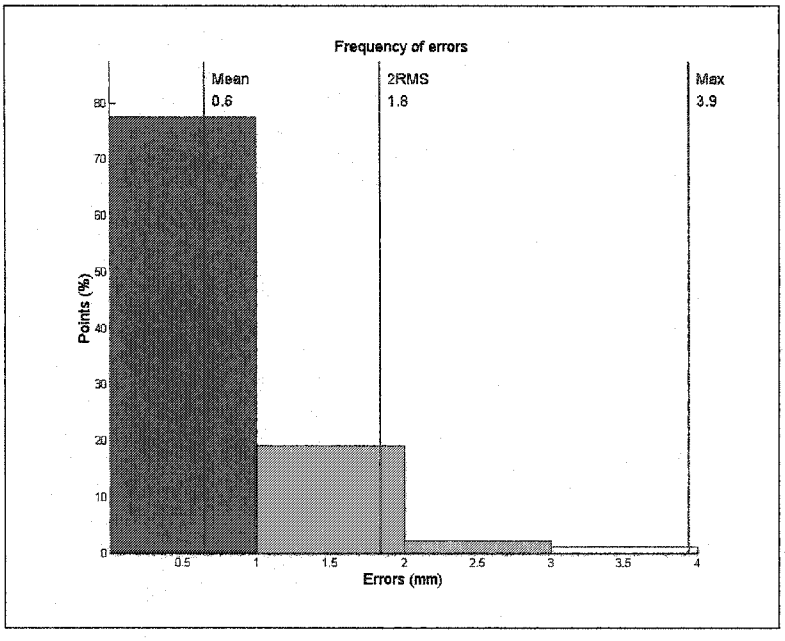

Figure 15 Maximum and mean errors for reconstructed L3 vertebra

Table 6

Results on comparisons of 57 scoliotic vertebrae. All data are shown as mean ± standard deviation

Vertebral level	N	Pedicle			Canal	
		width (mm)	height (mm)	depth (mm)	depth (mm)	width (mm)
Thoracic						
T6	3	0.43±0.28	0.68±0.22	0.71±0.14	0.36±0.45	0.53±0.47
T7	6	1.03±0.46	1.03±0.55	1.33±0.52	0.97±0.64	1.42±0.44
T8	9	1.34±0.94	1.14±0.63	1.44±0.37	0.91±0.50	0.59±0.44
T9	10	1.15±0.63	0.99±0.81	1.59±0.40	0.95±0.72	1.00±0.63
T10	9	1.04±0.61	1.05±0.66	1.28±0.48	1.32±0.59	1.36±0.88
T11	9	1.06±0.68	1.22±0.71	1.30±0.63	1.40±0.52	0.96±0.65
T12	5	1.12±0.46	0.88±0.63	1.12±0.59	1.23±0.71	1.06±0.36
Lumbar						
L1	2	0.26±0.06	0.18±0.08	0.22±0.19	0.11±0.05	0.02±0.01
L2	1	0.27±0.05	0.50±0.09	0.17±0.09	0.41±0.11	0.14±0.10
L3	2	0.22±0.25	0.30±0.17	0.31±0.18	0.38±0.34	0.21±0.25
L5	1	0.25±0.15	0.03±0.01	0.29±0.15	0.04±0.02	0.61±0.31

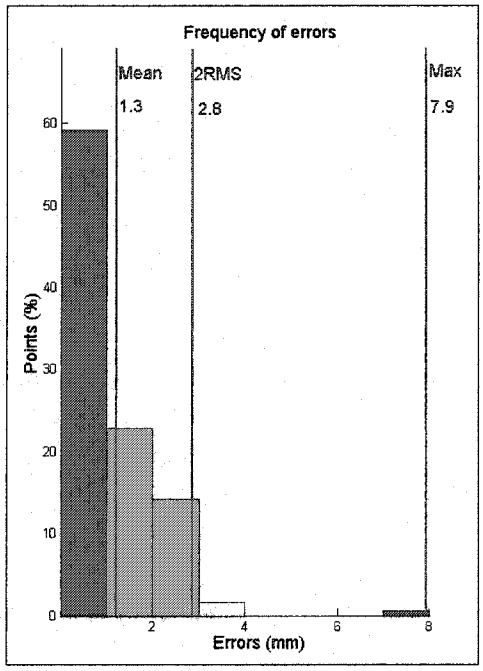

Figure 16 Maximum and mean errors for reconstructed T6 vertebra

Nevertheless, we can observe that the results obtained for morphometric parameters are nearly comparable with those obtained by CT-scan. Let us mention that these parameters are important for the surgical correction of scoliosis.

Let us recall that the surgical correction of scoliosis consists of correcting the scoliotic deformation by rotations and translations practiced at the level of the vertebrae and/or the level of the spine until a more normal alignment of the vertebrae is obtained. Correction consists of fixing the spine in this configuration using a metal rod supported by hooks and screws installed in the pedicles. Knowledge of the accurate sizes and geometry of these pedicles is thus crucial.

Let us note that the estimated global deformation parameters after reconstruction (i.e., parameter vector b, setting the amplitude of each deformation mode of the scoliotic deformations) and the measures of morphometric parameters can also be used to quantify the scoliosis, its nature or to analyze the improvement of orthopedic or surgical corrections.

To conclude, this method has demonstrated its efficiency and robustness. We strongly believe that a method which gives results almost equal to those obtained by using more than 500 CT images for a whole spine but based on only two standard X-ray images is quite original, important, and interesting. It is interesting for the quantity of data to be acquired, processed and managed. For example, two plain digital Fuji X-rays require 15 Mbytes ($1,760 \times 2,140 \times 2$ bytes) of storage in comparison to 260 Mbytes ($512 \times 512 \times 2$ bytes $\times 500$ slices). It is important for the quantity of radiation received by the patient. With the generalization of multi-detector spiral CT, patients will be more and more exposed to radiation and a method that can keep this amount of radiation as low as possible is also quite important and has to be considered. It becomes especially important when we deal with young scoliotic patients who will be exposed to multiple diagnostic radiographic examinations during their childhood and adolescence. In [34], a retrospective study confirmed that multiple radiographic examinations may increase the risk of breast cancer among women with scoliosis. Another important point is that scoliosis must be

evaluated when the patient is in a standing position, which is impossible with standard CT scanners.

The proposed method remains sufficiently general to be applied to other medical reconstruction problems (i.e., rib cage, pelvis, knee, etc.) for which the database of this anatomical structure is available (with two or several radiographic views). We now intend to improve the proposed method by integrating a region homogeneity term in the energy function related to this statistical reconstruction approach, to refine the statistical model by local deformations, and to use a more efficient global optimization technique.

RECONSTRUCTION 3D BIPLANAIRE NON SUPERVISÉE DE LA COLONNE VERTÉBRALE SCOLIOTIQUE PAR APPROCHE STATISTIQUE HIÉRARCHIQUE

Article : A hierarchical statistical modeling approach for the unsupervised 3D biplanar reconstruction of the scoliotique spine.

Cet article a été soumis au journal *IEEE Transactions on Biomedical Engineering* comme l'indique la référence bibliographique

S. Benameur, M. Mignotte, H. Labelle, J. A. De Guise. A hierarchical statistical modeling approache for the unsupervised 3D biplanar reconstruction of the scoliotic spine. *IEEE Transactions on BioMedical Engineering*, soumis, 2004.

Cet article est présenté ici dans sa version originale.

Résumé

La reconstruction 3D des structures osseuses à partir d'un nombre limité d'images radiographiques conventionnelles est l'un des axes importants de recherche en vision et imagerie médicale. La majorité des méthodes existantes dans la littérature sont supervisées et/ou ne s'appliquent pas aux cas pathologiques (cas de la scoliose) [7] [39]. Nous présentons dans cet article une méthode non supervisée, hiérarchique et statistique de reconstruction 3D de la colonne vertébrale scoliotique à partir de deux vues radiographiques conventionnelles (postéro-antérieure avec incidence de 0° et latérale) calibrées. La méthode présentée utilise les contours des vertèbres segmentées dans les deux vues radiographiques et une connaissance globale hiérarchique *a priori* comprenant la structure géométrique de la colonne vertébrale et de chaque niveau vertébral. La méthode proposée est basée sur les spécifications de deux modèles 3D statistiques. Le premier, un modèle géométrique sur lequel des déformations linéaires globales admissibles sont définies, est utilisé pour une reconstruction grossière de la colonne vertébrale. Une reconstruction 3D précise est

alors réalisée pour chaque niveau vertébral par un deuxième modèle de vertèbre sur lequel des déformations non linéaires admissibles et des déformations locales sont définies à partir d'une base d'apprentissage d'environ $1,000$ vertèbres (30 vertèbres saines et 30 vertèbres scoliotiques par niveau vertébral). Cette reconstruction 3D est formulée comme un double problème de minimisation de fonction d'énergie. Cette minimisation est réalisée par un algorithme stochastique d'exploration/sélection [79]. La méthode proposée est validée sur une base de 57 vertèbres lombaires et thoraciques de 13 patients scoliotiques qui ont aussi été reconstruites par CT-scan pour des fins de comparaison. Une erreur moyenne de (1.45 ± 1.46) mm pour les vertèbres lombaires et de (1.27 ± 1.29) mm pour les vertèbres thoraciques obtenue sur les distances point-surface entre le modèle reconstruit avec notre méthode et le modèle issu de la reconstruction CT-scan. La reconstruction 3D nécessite un temps de calcul de l'ordre de 28 secondes pour une vertèbre (sur un PC/Linux à 2.0 GHz).

CHAPITRE 4

A HIERARCHICAL STATISTICAL MODELING APPROACH FOR THE UNSUPERVISED 3D BIPLANAR RECONSTRUCTION OF THE SCOLIOTIC SPINE

Abstract This paper presents a new and accurate 3D reconstruction technique for the scoliotic spine from a pair of planar and conventional (postero-anterior with normal incidence and lateral) calibrated radiographic images. The proposed model uses *a priori* hierarchical global knowledge, both on the geometric structure of the whole spine and of each vertebra. More precisely, it relies on the specification of two 3D statistical templates. The first, a rough geometric template on which rigid admissible deformations are defined, is used to ensure a crude registration of the whole spine. An accurate 3D reconstruction is then performed for each vertebra by a second template on which non-linear admissible global, as well as local deformations, are defined. Global deformations are modeled using a statistical modal analysis of the pathological deformations observed on a representative scoliotic vertebra population. Local deformations are represented by a first order Markov process. This unsupervised coarse-to-fine 3D reconstruction procedure leads to two separate minimization procedures efficiently solved in our application with evolutionary stochastic optimization algorithms. In this context, we compare the results obtained with a classical Genetic Algorithm (GA) and a recent Exploration Selection (ES) technique. This latter optimization method with the proposed 3D reconstruction model, is tested on several pairs of biplanar radiographic images with scoliotic deformities. The experiments reported in this paper demonstrate that the discussed method is comparable in terms of accuracy with the classical CT-scan technique while being unsupervised and while requiring only two radiographic images and a lower amount of radiation for the patient.

Key words: 3D reconstruction model, 3D/2D registration, hierarchical statistical modeling, shape model, biplanar radiographies, scoliosis, medical imaging, energy function minimization, stochastic optimization.

4.1 Introduction

In the past few years, there has been a great deal of research in reconstructing three-dimensional (3D) shapes of anatomical structures from radiographic images. In medical imagery, this 3D reconstruction problem remains a necessary step to obtain qualitative information, such as the detection of pathological deformations, as well as for quantitative measurements needed for surgical planing and follow-up evaluation. In this paper, we are concerned with computer vision methods for 3D reconstruction of scoliotic spine, from two X-ray radiographic images.

Scoliosis is a complex 3D deformity of the natural curve of the spinal column, including rotations and vertebral deformations. The classical evaluation obtained by the spinal projections on the two-dimensional (2D) radiographic planar images does not give a full and accurate interpretation of scoliotic deformities [15]. To analyze the 3D characteristics of these deformations, several 3D reconstruction methods have been developed. Among these methods, the 3D reconstruction methods of tomodensitometric imagery modalities (e.g., computerized tomography [61][62], or magnetic resonance [65][87]) provide accurate 3D information of the human anatomy or 4D information including time as one more degree of freedom. However, few hospitals can afford a magnetic resonance system. Efficient and affordable tomodensitometric imagery systems can now be found in every hospital and many clinics but for ethical reasons hazardous X-ray dosages cannot be used extensively enough to provide full 3D data or large bone structures as the spine or rib cage. Also, these medical imaging techniques require that the patient be in a lying position, which is incompatible with many diagnostic protocols evaluating scoliosis.

For these above-mentioned reasons, a 3D reconstruction method of shapes using a limited number of X-ray radiographic projections and thus ensuring a lower amount of radiation

for the patient, is really interesting. Surprisingly, this problem has not been widely studied in the statistical framework, and few references exist in the computer vision and medical imagery literature. Among the proposed algorithmic technique, we can cite the 3D reconstruction method from silhouettes, proposed by Martin and Aggarwal in [70]. Their method allows to reconstruct polygonal 3D objects by back-projecting the silhouettes. A method for extracting 3D geometry of bones from two orthogonal X-ray radiographic projections is also proposed by Caponetti and Fanelli in [14]. The initial estimation of the 3D bone structure, produced by back-projecting profile points, is then refined by using a B-spline interpolation. In [9], Benjamin generates surface information using common points, present in different projections, and the tracks between the points, extracted from about ten projection images.

Due to the ill-posed nature of this reconstruction problem, a right and accurate estimation of the 3D geometrical structure of the shape cannot be found without constraints. In this way, methods using simple *a priori* knowledge on the geometrical structure of the object to be reconstructed, and thus expressed as the solution of a regularized inverse problem, have been proposed. Terzopoulos *et al.* propose in [90] a method allowing to recover the 3D shape from the 3D profiles of an object using, as geometric prior constraint, a deformable tube coupled to a deformable spine. The deformation is controlled by physically-based internal and external forces. Bardinet *et al.* present in [4] a method that consists in matching a parametric deformable model to unstructured 3D data. More precisely, a super-quadric model is fitted to a given point set, and the generated super-quadric model is deformed locally using free-form deformations. In [78], Nikkhade *et al.* present 3D reconstruction method of femurs from two orthogonal X-ray radiographic projections. They separate the femur into three subparts; each of them assumed to be round. They fit cubic parametric surface patches to the subparts and then assemble them to a complete model. Kit develops in [57] a method allowing to analyze X-ray radiographic projections of the stomach using a deformable 3D model. Their *a priori* model is a tube which is first initialized using only one projection. Afterward, the model is deformed using the other projections.

Nevertheless, in these methods, the geometric *a priori* constraint does not model the set of admissible deformation (or in the case of scoliosis, the pathological variability) of the anatomical structure to be reconstructed. Consequently, the 3D reconstructed shape estimation does not necessarily correspond to the reality.

In order to rightly constraint the ill-posed nature of this problem, a solution consists in supervising the 3D reconstruction technique. In this sense, a 3D multiplanar radiography reconstruction method using a direct linear transformation (DLT) [71] is presented by Dansereau and Stokes in [24]. They rely on manual stereo-digitization of six anatomical landmarks (on each X-ray radiographic image) of the vertebrae to produce 3D coordinates. Adding the kriging technique using the 3D reconstructed points as control points yields good visualization of the vertebral geometry [28]. There is a need for more landmarks to obtain a better description of all the vertebrae. In the same way, a non-stereo corresponding points technique is also described by Mitton et *al.* in [75] to improve the accuracy of the 3D reconstruction by identifying more anatomical landmarks on the X-ray projections. This method is then based on deformation of an elastic deformable mesh that respects stereo corresponding and non-stereo corresponding points available in different X-ray radiographic projections. In addition to the supervision, the methods proposed by Dansereau *et al.*, Mitton *et al.* and Delorme *et al.* are limited due to the inherent inaccuracy produced in identifying anatomical landmarks (leading to reconstruction errors). Besides, they do not exploit all information contained in the two X-ray radiographic projections (e.g., the contours of each vertebra) or the statistical knowledge of the possible deformation of the object to be reconstructed.

Methods using statistical *a priori* knowledge of the geometric shapes of the objects of interest lead to better constrain the reconstruction problem. In [39], Fleute and Lavallée propose a method allowing to reconstruct the 3D geometry of the femur using a few orthogonal X-ray radiographic projections. They apply point distribution models (PDM) [18] to reconstruct a geometric prior model representing mean shapes and containing the

typical deformation modes in statistical sense. Thereafter, they deform the model non-rigidly, according to the rays back-projected from the contour points of the projections taken from a patient. Benameur *et al.* proposed in [7] a 3D statistical reconstruction method, for each individual vertebra, using a pair of planar and conventional (postero-anterior with normal incidence and lateral) radiographic images for a patient in standing position, and a prior global knowledge of the geometric structure of each vertebra. The method consists of fitting the projections of this deformable template with the preliminary segmented contours of the corresponding vertebra on the two X-ray radiographic projections. Nevertheless the above-mentioned technique remains widely supervised and requires the knowledge of the position of six anatomical points (namely, the center of the superior and inferior end-plates, the upper and lower extremities of both pedicles) to initialize 3D reconstruction process of each vertebra of the spine.

To overcome this problem of supervision and improve the 3D reconstruction and the optimizer related to the energy-based model presented in [7], we propose in this paper a 3D statistical reconstruction method based on the likelihood introduced in [7] but using hierarchical global *a priori* knowledge on the geometric structure of both the whole spine and each vertebra[1]. More precisely, the hierarchical model we propose relies on the specification of two 3D templates. The first, a rough and cubic approximation geometric template on which rigid admissible deformations are defined, is used to fit its (postero-anterior and lateral) projections with the preliminary segmented contours of each vertebra body of the spine on the two calibrated radiographic views. It ensures crude registration of the whole spine and gives a rough position and orientation of each vertebra. 3D reconstruction is then refined by a second template which takes into account *a priori* global knowledge on the geometric structure of each vertebra. This geometric knowledge is efficiently captured by a statistical deformable template integrating a set of admissible deformations, expressed

[1]Hierarchical statistical models have been applied in fusion of multiresolution image data [58], segmentation [55], restoration [60], in active shape models using the wavelet transform [25]. To our knowledge, no hierarchical statistical model for 3D reconstruction methods have been described in the literature.

by the first modes of variation in Karhunen-Loeve (KL) expansion, of the pathological deformations observed on a representative scoliotic vertebra population. A local deformation process, which assumed to follow a first-order Markovian process, is then used to refine the global deformation applied to the model. This unsupervised coarse-to-fine 3D reconstruction procedure leads to two optimization problems related to two (coarse and fine) energy-based models. These two optimization problems are efficiently solved in our application with a recent stochastic optimization technique based on an Exploration Selection procedure. Finally, we propose a complete validation of the proposed reconstruction technique.

This paper is organized as follows. Section 4.2 presents the hierarchical prior model used in our coarse-to-fine reconstruction method. Section 4.3 briefly recalls the likelihood model and the 3D/2D registration strategy introduced in [7]. Section 4.4 describes silhouette extraction of the 3D model. Section 4.5 presents energy function minimization related to the coarse-to-fine registrations and the stochastic optimization procedure used to estimate optimal reconstruction. Section 4.6 presents the validation protocol of 3D reconstruction method. In Section 4.7, we show some 3D reconstruction results and validate the proposed model.

4.2 Coarse-to-fine Prior Model

4.2.1 Crude prior model of the spine

To ensure crude registration of the whole spine and to estimate a rough position $t = (t_x, t_y, t_z)$, scale k and orientation α of each vertebra, we first consider a crude *a priori* geometric model for the whole spine [8].

This model relies on a set of cubic templates, roughly representing each vertebral body and stacked on top of one another to form the spinal column (cf. Fig. 17). Each cubic template (defined by a set of control point vectors of the cubic representation) associated with each vertebral level has its scale, orientation and position constrained within a restricted

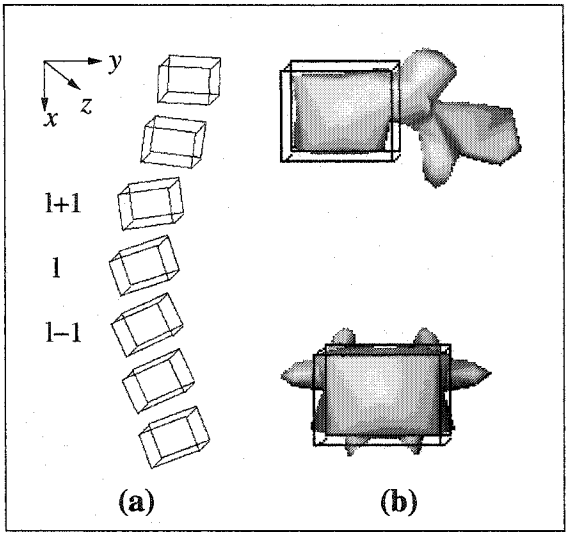

Figure 17 Crude prior model of the spine. **(a)** Deformable model of the whole spine, **(b)** cubic template representation associated with each vertebra

domain whose center is given by knowledge of the (previously) estimated parameters of the cubic template which is located below. For example, if the registration of the whole crude spine is made from bottom to top, then the position $t^l = (t^l_x, t^l_y, t^l_z)$, scale vector $k^l = (k^l_x, k^l_y, k^l_z)$ and orientation $\alpha^l = (\alpha^l_x, \alpha^l_y, \alpha^l_z)$ at (vertebral) level l, given the rough parameter estimation of vertebra below the level l (i.e., $l-1$), are restrained within the domain defined by,

$$
\begin{aligned}
t^{l-1}_x + k^{l-1}_x - \Delta t^l_x \leq t^l_x \leq t^{l-1}_x + k^{l-1}_x + \Delta t^l_x,\\
t^{l-1}_y - \Delta t^l_y \leq t^l_y \leq t^{l-1}_y + \Delta t^l_y,\\
t^{l-1}_z - \Delta t^l_z \leq t^l_z \leq t^{l-1}_z + \Delta t^l_z,\\
k^{l-1} - \Delta k^l \leq k^l \leq k^{l-1} + \Delta k^l,\\
\alpha^{l-1} - \Delta \alpha^l \leq \alpha^l \leq \alpha^{l-1} + \Delta \alpha^l,
\end{aligned}
$$

where α is the rotation vector (ensuring rotation around x, y or z axes). Δt_x, Δt_y, Δt_z, Δk and $\Delta \alpha$ are given by statistical knowledge on the scoliotic deformation of the spine [81][80]. A global configuration of the deformable spine model is thus described by 9 rigid transformation parameters for each cubic template associated with each vertebral level.

4.2.2 Fine prior model of each vertebra

Our *a priori* knowledge model relies also on the description of each vertebra by a 3D deformable template (i.e., a vector $s \in \mathcal{R}^{3n}$ of n control points) which incorporates statistical knowledge about its geometrical structure and its pathological variability. The deformations of this template are expressed by the first modes of variation in KL expansion of pathological deformations observed on a representative training scoliotic vertebra population [7]. This can be done by using principal component analysis (PCA), i.e., by computing the covariance matrix C of shapes $\{s_i\}$. The main deformation modes of the template model s are then described by the eigenvectors ϕ of C, with the largest eigenvalues λ (cf. Fig. 18).

4.2.2.1 Deformable template representation

The shape s is represented as a template, that is a set of points

$$s = (p_1, p_2, \cdots p_i, \cdots, p_n)^T,$$

where $p_i = (x_i, y_i, z_i)^T$ are the Cartesian coordinates of each surface point.

Given a sample s_1,$\cdots$,s_n of shapes with the same number of points, we resort to the procedure proposed in [50] to align this training set. We then apply the PCA to reduce the dimension to $m \ll 3n$. This gives us non-linear deformations of the mean shape $\bar{s}$ and terminates the training phase.

4.2.2.2 Global deformations

The globally deformed template is defined by,

$$s = M(k, \alpha)[\bar{s} + \Phi b] + T, \tag{4.1}$$

where,

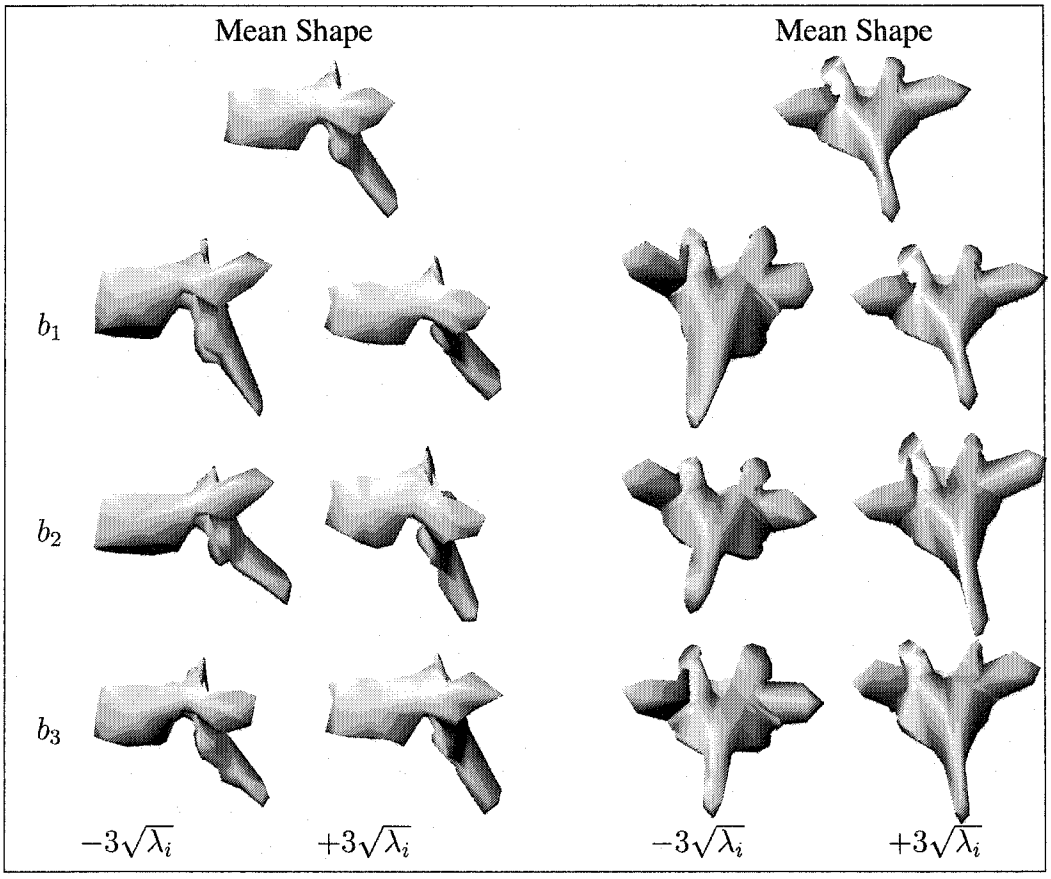

Figure 18 Fine prior model of each vertebra. Two deformed shapes obtained by applying ± 3 standard deviations of the first 3 deformation modes to the mean shape of $T8$ vertebra and from the sagital and coronal views

- T and $M(k, \alpha)$ account for rigid deformations of the template, (T is a global translation vector, and $M(k, \alpha)$ performs a rotation (in the x, y or z axes) and a scaling by k).

- $\Phi = (\phi_1, \ldots, \phi_m)$ is the matrix of the first m eigenvectors of C associated with the m largest eigenvalues and $\mathbf{b} = (b_1, \ldots, b_m)^T$ is a vector containing the weights for these m deformation modes.

A global configuration of the deformable vertebra template is thus described by $7 + m$ parameters corresponding to rigid transformations and m modal weights b_j. Due to the Karhunen-Loeve transform, the random variables b_i are independent and follow a normal

law of a null mean and variance λ_i. Thus, the law of probability of $s(\theta)$, the deformed template, can be written as [7],

$$P(s(\theta)) = \mathcal{U}(T,k,\alpha)\prod_{i=1}^{m}\frac{1}{\sqrt{2\lambda_i\pi}}\exp\left(-\frac{b_i^2}{2\lambda_i}\right), \tag{4.2}$$

where $\mathcal{U}$ denotes the uniform distribution. This low parametric representation for each vertebra level, along with the crude parametric representation of the whole spinal column constitutes our global hierarchical *a priori* model that will be used to rightly constrain the ill-posed nature of our proposed coarse-to-fine 3D reconstruction method.

The *a priori* energy term related to the prior distribution (Eq. 4.2), can be written as,

$$E_p(s(\theta)) = \frac{1}{2}\sum_{i=1}^{m}\frac{b_i^2}{\lambda_i}, \tag{4.3}$$

which is close to the Mahalonobis distance. This prior energy term penalizes the deviation of the deformed template from the mean shape (but not the affine transformations).

4.2.2.3 Local deformations

Inspired by the work of Grenander and Keenan on stochastic pattern representation [42], a statistical local deformations process δ is now applied to the n control points or "landmarks" which approximate the geometrical shape of each vertebra.

These local deformations are modeled as local random perturbations of the shape and can be considered as a refinement of the global deformations applied to the deformed mean shape, since the main deformation modes have already been captured by the preliminary global statistical prior knowledge of each vertebra. The local deformation vector $\delta = (\delta_1, \delta_2, \ldots, \delta_n)^T$ with $\delta_i = (\delta_{x_i}, \delta_{y_i}, \delta_{z_i})$ is described by a first order Gauss-Markov process defined on the graph corresponding to the n control points of the deformable template of each vertebra. If we represent these local deformations by local random translations (that

are superimposed on the globally deformed shape), the complete (i.e., globally and locally) deformable model of each vertebra can be defined by,

$$\hat{s} = M(k, \alpha)[\overline{s} + \Phi b] + T + \delta. \tag{4.4}$$

In our application, this local deformation process allows to take into account firstly, the fact that our PCA does not model 100% of the scoliotic deformations of our vertebra database (the first m deformation modes are chosen in order to get a reasonably low parametric representation model) and secondly the fact that our vertebra database could not be big or representative enough and consequently could not certainly contain all the possible scoliotic deformations. Assuming a first-order neighborhood structure on the graph associated to the n control points of the deformable template, the probability distribution of the random field δ can be written as,

$$P(\delta) = \frac{1}{\zeta} \exp\left(-E_r(\delta)\right),$$

where ζ is a normalization constant, and $E_r(\delta)$ is the local deformation energy term which can be written as,

$$E_r(\delta) = \frac{1}{2} \sum_{i=1}^{n} \left(\frac{1}{\mu_i^2} \sum_{j \in \mathcal{N}(i)} \|\delta_i - \delta_j\|^2 + \frac{1}{\nu_i^2} \|\delta_i\|^2 \right), \tag{4.5}$$

where $\mathcal{N}(i)$ is the set of first-order neighborhood of point i, μ_i^2 and ν_i^2 are the variance parameters of this local deformation model. μ_i^2 weight the interactions between neighboring points. ν_i^2 control the amplitude of the local deformations compared to the globally deformed model. In our application, we consider $\mu_i = \mu$ and $\nu_i = \nu, \forall i$, since the different control points of our 3D vertebra template are approximatively equally spaced.

4.3 Likelihood Model

As proposed in [7], the likelihood model is expressed by a measure of similarity between the external contour of the (postero-anterior and the lateral) projections of the 3D deformed template and a directional edge potential field estimated on the two radiographic views. This likelihood energy term is defined by,

$$E_l(s(\theta), I_{\text{PA}}, I_{\text{LAT}}) = -\frac{1}{n_{\text{PA}}\Gamma_{\text{PA}}}\sum \Psi_{\text{PA}}(x,y) - \frac{1}{n_{\text{LAT}}\Gamma_{\text{LAT}}}\sum \Psi_{\text{LAT}}(x,y), \tag{4.6}$$

where the summation of the first and second term of E_l is overall the n_{PA} and n_{LAT} points of the external contour of the respectively lateral (I_{LAT}) and postero-anterior (I_{PA}) perspective projections of the deformed template on the two pre-computed edge potential fields of each radiographic image. The 2D perspective projections of the 3D deformed template, i.e., the lateral and postero-anterior outline is computed with the silhouette extraction algorithm.

To compute the edge potential field Ψ associated with each radiographic view, we first use a Canny edge detector with the unsupervised technique proposed in [13]. Then, Ψ is defined as in [53] by,

$$\Psi(x,y) = \exp\left(-\frac{\sqrt{\xi_x^2 + \xi_y^2}}{\tau}\right)\left|\cos(\gamma(x,y))\right|, \tag{4.7}$$

where $\xi = (\xi_x, \xi_y)$ is the displacement to the nearest edge point in the image, and τ is a smoothing factor which controls the degree of smoothness of this potential field. $\gamma(x,y)$ is the angle between the tangent of the nearest edge and the tangent direction of the contour at (x,y) (cf. Fig. 19). This likelihood energy term, as expressed in Eq. (4.4), is exploited for the 3D reconstruction of the fine prior model of each vertebra (see subsection 4.2.2). In order to ensure a good reconstruction of each cube template of the crude prior model

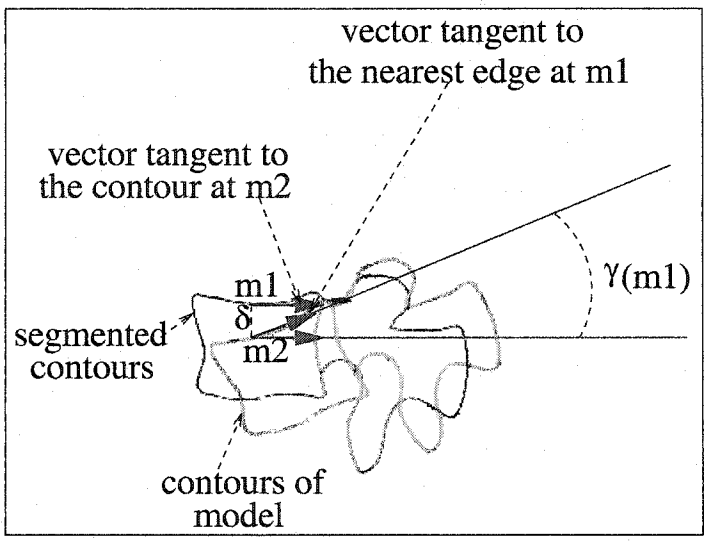

Figure 19 Directional component used in the directional edge potential field Ψ

of the spine (see subsection 4.2.1), which will be used to initialize this latter fine 3D reconstruction, we propose to improve this likelihood measure with the following heuristic; let s_0 and s_1 denote the shape of one cube template with scale k and a slightly larger scale $k + \epsilon$ respectively. The considered likelihood energy term is expressed as,

$$E_l(s(\theta), I_{\text{PA}}, I_{\text{LAT}}) = E_l(s_0(\theta), I_{\text{PA}}, I_{\text{LAT}}) - E_l(s_1(\theta), I_{\text{PA}}, I_{\text{LAT}}). \tag{4.8}$$

This measure attains its minimum value when there is an exact correspondence between the (postero-anterior and lateral) projected contours of the inner cube template s_0 and the preliminary segmented contours of the two radiographic views (expressed by $E_l(s_0, I_{\text{PA}}, I_{\text{LAT}})$) and no correspondence between the projected contours of the outer cube template s_1 and the pre-segmented contour map ($E_l(s_1, I_{\text{PA}}, I_{\text{LAT}})$). Experiments have shown that this heuristic allows to obtain a better matching when the crude registration is used on low resolution, low contrast and low signal-to-noise ratio radiographic images (cf. Fig. 20).

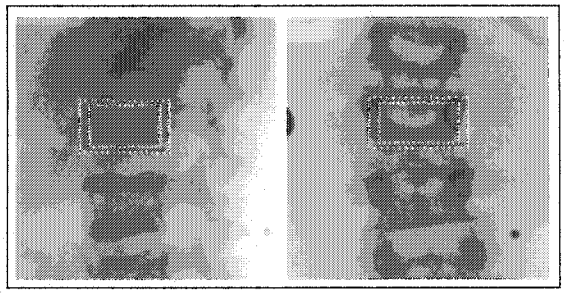

Figure 20 The two projected contours of the shape of cube templates with scale k and a slightly larger scale $k + \epsilon$ on the corresponding vertebral body on postero-anterior and lateral views

4.4 Silhouette Extraction of the 3D model

The 3D model of vertebrae is represented in the form of a triangulated mesh. Silhouette occurs when a triangle faces towards the projection source and a neighbor triangle across an edge faces away from the source. So for two triangles T_i and T_j with normals $\vec{n}_i$ and $\vec{n}_j$ and a view vector $\vec{v}$, a shared edge is a silhouette edge if

$$(\vec{n}_i \cdot \vec{v}) \times (\vec{n}_j \cdot \vec{v}) \leq 0.$$

On a surface, the silhouette edge of the vertebra shape are lines where the direction of projection is tangent to the surface. As in the case of a not-convex object, the silhouette edges can be hidden by other parts of the surface. We keep all the edges, including those that are occluded. Let us recall that we use semi-transparent radiographic images [7]. Fig. 21 shows an example of silhouette from 3D model.

4.5 Coarse-to-fine optimization strategy

This unsupervised coarse-to-fine 3D reconstruction procedure is stated as a double energy function minimization problems, namely,

$$E(s(\theta), \delta) = E_l(s(\theta), I_{\text{PA}}, I_{\text{LAT}}) + \beta\Big(E_p(s(\theta)) + E_r(\delta)\Big), \tag{4.9}$$

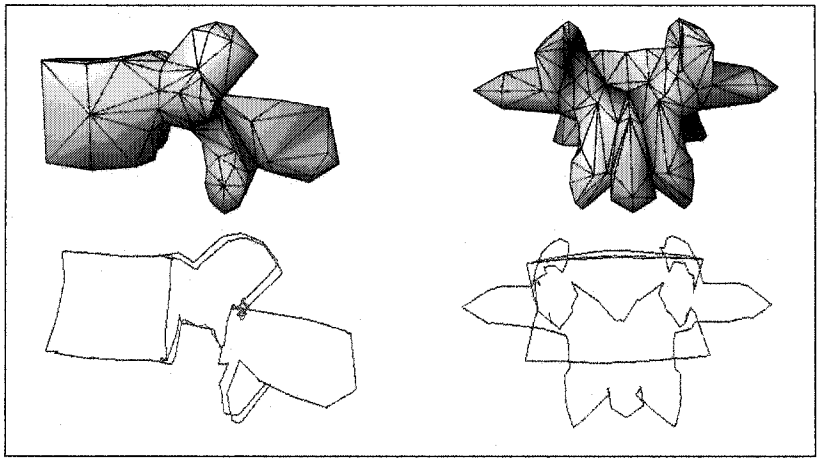

Figure 21 Example of lateral and postero-anterior outlines from 3D model

where E_l is the likelihood energy term enforcing data closeness, $(E_p + E_r)$ is the prior energy term enforcing regularity in the Tikhonov sense. β is a factor allowing to control the balance between the two energy components and the rigidity of the deformable template.

1. This energy-based model is first used for the registration of the whole spine with the set of cubic template presented in Subsection 4.2.1 and the likelihood measure presented in Eq. (4.8). In this crude reconstruction step, there is no prior energy term ($E_p = 0$ and $E_r = 0$) since we do not use non-linear and local deformations. The ill-posed reconstruction problem is nevertheless constrained by the low parametric representation of the whole spine and the restricted search space defined for each cubic templates (see Subsection 4.2.1). This step only requires to identify the center of the superior and inferior end-plate of the lowest vertebra of the spine on the two radiographic views. User interaction is limited to simply placing these points on the two radiographic images (thanks to a graphical user interface). The 3D coordinates of these landmarks are obtained by direct linear transformation (DLT) [71][7] (the corresponding points on the cubic template being known). After optimization, this crude registration allows to estimate the rough position $T = (T_x, T_y, T_z)$, scale k and orientation $\alpha = (\alpha_x, \alpha_y, \alpha_z)$ of each vertebra.

2. This optimization problem is then used with the fine prior template of each vertebra (see Subsection 4.2.2) and the likelihood measure proposed in Eq. (4.4) in two steps.

   (a) Optimization is made within a range of values around the rigid parameters roughly estimated by the first crude reconstruction given in step 1. In this step, we consider the local deformations as negligible ($\delta_i = 0, \ \forall i$) and we have to estimate $\theta = (k, \alpha, T, b)$, i.e., $7 + m$ parameters corresponding to rigid transformations and m modal weights b_j.

   (b) Finally, a last minimization procedure is made with θ previously estimated and now fixed to find the optimal local deformation parameters of the complete model.

The energy functions to be minimized in Step 1 and 2 are complex with several local minima over the deformation parameter space. A global search is impossible due to the size of the configuration space. Let us also add that the quality of the reconstruction is closely related to the good estimation of the deformation parameters and consequently to the performance of the optimization procedure. In our application, we use the stochastic optimization algorithm recently proposed by O. François in [79]. We use this algorithm because the adjustment of all internal parameters does not depend on the function to be minimized. Moreover, the convergence is asymptotically ensured [79]. Let us add that this optimization algorithm is also especially well suited to minimize complex (i.e., non-convex) energy functions [32]. We compare the performance of this algorithm, in Section 4.7.3, with a classical genetic algorithm [74].

4.5.1 Exploration/Selection Algorithm

The E/S algorithm belongs to the class of Evolutionary algorithms. This class of algorithm has been successfully applied in diverse areas such as medical imaging [74], localization of shapes [32] to minimize complex energy functions [32]. This success has initiated the development of various evolutionary algorithm variants and stimulated the theoretical

research about convergence properties of these algorithms (see [84] for a good review of evolutionary algorithm in medical imagery).

The E/S algorithm can be summarized as follows (more details are given in [79]); Let F be a finite discrete subset of the Cartesian product of k compact intervals $[m_i, M_i]$, for $1 \leq i \leq k$, and $\theta = \{\theta_1, \ldots, \theta_n\}$ a set of n potential solutions randomly chosen. We define $\hat{\theta}$ as the optimal element θ_i of θ such that $E(s(\theta_j)) > E(s(\theta_i))$, for $1 \leq j < i$, and $E(s(\theta_j)) \geq E(s(\theta_i))$, for $1 < j \leq n$. We consider a graph G defined on F called the *exploration graph*. The exploration graph is assumed to be non-oriented and connected. We denote by $\mathcal{N}(a)$ the neighborhood of the element $a \in F$ in the graph G defined by $\{b \in F$: for some j, $|b_j - a_j| \leq r(M_j - m_j)$, $b_i = a_i$, $i \neq j\}$ where r is a real number in the interval [0,1] called the radius of exploration.

Each solution of θ is regarded as an individual that attempts a random search on the exploration graph [79]. For $b \in F$, we fix a positive distribution a_b on $\mathcal{N}(b)$. The exploration process acts independently on each individual, and consists of choosing a random N according to the binomial distribution $bin(n, p)$ where n is the size of the population and p is the probability of exploration. We replace θ_i by $\vartheta_i \in \mathcal{N}(\theta_i) \setminus \{\hat{\theta}\}$ according to a uniform distribution, for $i \leq N$ otherwise, we change θ_i by $\hat{\theta}$. This process is runs until a criterion is met (see Table 7).

Finally, the energy function to be minimized in Step 2.2 is just a final refinement of the global deformations applied to the mean shape, since the main deformation modes have been captured by the PCA-based global prior knowledge of each vertebra. For this step, we use the following deterministic procedure,

- For each points p_i of the vertebra shape model s ($s = (p_1, p_2, \ldots p_i, \ldots, p_n)^T$ with $p_i = (x_i\, y_i\, z_i)^T$), and until $E\left(\hat{s}(\theta)\right)$ is stable,
- The model energy $E\left(\hat{s}(\theta)\right)$, expressed by Eq. (4.9) is evaluated for different positions of p_i (namely; $p_i + \delta p_i$, p_i, and $p_i - \delta p_i$) along its normal. The normal is

Table 7

E/S optimization algorithm

E/S Algorithm

$E(.)$	A real-valued l-variable function, defined on F, to be minimized
F	A finite discrete subset of the Cartesian product $\Pi_{j=1}^{l}[m_j, M_j]$ of l compact intervals
n	The size of the population (greater than D)
r	A real number $\in [0, 1]$ called the radius of exploration (with r greater than the ϵ machine)
$\mathcal{N}(a)$	The neighborhood of an element $a \in F$ defined by $\{b \in F$: for some $j \in [1, l]$, $\lvert b_j - a_j \rvert \leq r(M_j - m_j)$, $b_i = a_i$, $i \neq j\}$
$D = l/r$	The diameter of the exploration graph endowed with the system of neighborhood $\{\mathcal{N}(a)\}_{a \in F}$
θ	$\theta = \{\theta_1, \ldots, \theta_n\}$, an element of F^n
$\hat{\theta} \in F$	$\hat{\theta} = \arg\min_{\theta_i \in \theta} E(\theta_i)$, i.e., the minimal point in θ with the lowest label
p	The probability of exploration
k	The iteration step

1. Initialization
Random initialization of $\theta = \{\theta_1, \ldots, \theta_n\} \in F^n$
$k \leftarrow 2$

2. Exploration/Selection
repeat

1. Compute $\hat{\theta}$; $\hat{\theta} = \arg\min_{\theta_i \in \theta} E(\theta_i)$
2. Draw m according to the binomial law $b(n, p)$
   - For $i \leq m$, replace θ_i by $\vartheta_i \in \mathcal{N}(\theta_i) \setminus \{\hat{\theta}\}$ according to the uniform distribution (Exploration step)
   - For $i > m$, replace θ_i by $\hat{\theta}$ (Selection step)
3. $k \leftarrow k + 1$ and $p = k^{-1/D}$

until *a criterion is met*;

estimated by computing the average of the normal of all facets to which the vertex belongs.

- We retain the configuration associated with the lowest energy.

In order to speed up this local deterministic optimization procedure, we start with a given over-estimated value for δp_i until $E(\hat{s}, \theta)$ become stable and we run the procedure successively with decreasing values of δp_i (cf. Fig. 22).

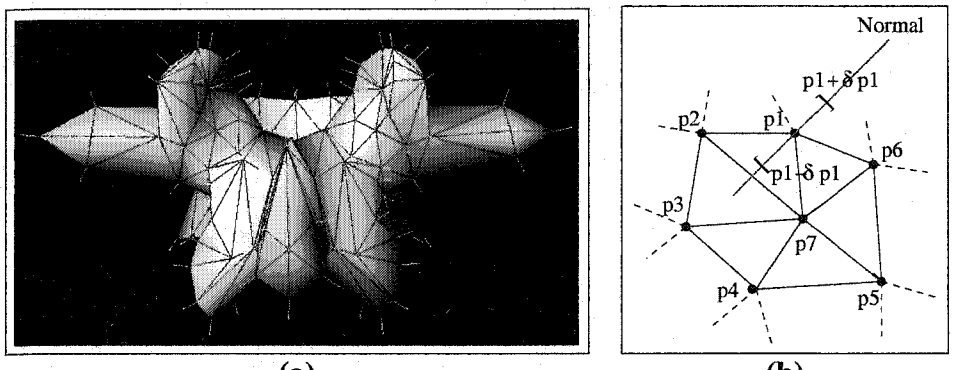

Figure 22 Local deformations. **(a)** normal at the control points, **(b)** movement of point p1 along its normal

4.5.2 Genetic Algorithm

The GA is a stochastic search method inspired by the principle of natural evolution in the biological world. GA starts with an initial set of random solutions called population. Each individual in the population is called a chromosome, representing a solution to the problem at hand. The chromosomes evolve through successive iterations, called generations. During each generation, the chromosomes are evaluated, and new chromosomes are formed using genetic operator (selection, crossover, mutation). Chromosomes that have higher fitness value have higher probabilities of being selected. After several generations, GA converges to the best chromosome, which represents the optimum or suboptimal solution to the problem [84].

In our application, the population used by a GA consists of a L-tuple (L corresponding to the 9+m parameters) of feasible solutions θ_i to the problem. The value $E(s(\theta_i))$ is said to be the fitness of the solution. Let $\{\theta_1^k, \ldots, \theta_n^k\}$ be the set of n solutions of population at iteration k. Each of the L parameters is quantified on q bits. Therefore, the ith chromosome θ_i is a string of $q \times L$ bits length:

$$\theta_i = (\underbrace{c_{11}^i, c_{12}^i, \cdots, c_{1q}^i}_{\theta_1}; \underbrace{c_{21}^i, c_{22}^i, \cdots, c_{2q}^i}_{\theta_2}; \cdots; \underbrace{c_{L1}^i, c_{L2}^i \cdots, c_{Lq}^i}_{\theta_L}).$$

4.5.2.1 Energy and Fitness Value

The energy function $E(s(\theta_i))$ (to be minimized) of the 3D reconstruction problem is a main source to provide the mechanism for evaluating the status of each chromosome. It takes chromosome as input and produces a number as a measure of the chromosome's performance. The following is the detail of the selection, crossover, and mutation operators.

4.5.2.2 Selection

The selection probability $P(\theta_i)$ of a solution (chromosome) θ_i with a fitness value of $E(s(\theta_i))$ can be computed as,

$$P(\theta_i) = \frac{E(s(\theta_i))}{\sum_{\theta_i \in C_p} E(s(\theta_i))},$$

where C_p is the current population.

4.5.2.3 Crossover

Crossover is performed with fixed crossover probability $P_c$between two randomly selected individuals by exchanging parts of their string to form two new individuals.

4.5.2.4 Mutation

The mutation operator is carried out by flipping bits at random, with some probability P_m

4.6 Validation of 3D reconstruction

Validation of 3D reconstruction accuracy is a difficult task because scanned spine database is generally not available. Visual examination is the most obvious method for evaluation of the 3D reconstruction accuracy but can be considered as an informal and insufficient approach. We have 57 scanned vertebrae (6 lumbar vertebrae, 51 thoracic vertebrae, 13 vertebrae segments). The validation technique consists of fitting the model of our 3D reconstruction method to the corresponding scanned vertebra. This 3D reconstruction method is used to estimate the mean and the maximum error distance between the 3D reconstructed model and the corresponding scanned model.

We also considered four morphometric parameters related to the dimensions of the pedicles and the spinal canal[2], and one parameter called the Cobb angle[3], related to the curve of the spinal column (Fig. 23).

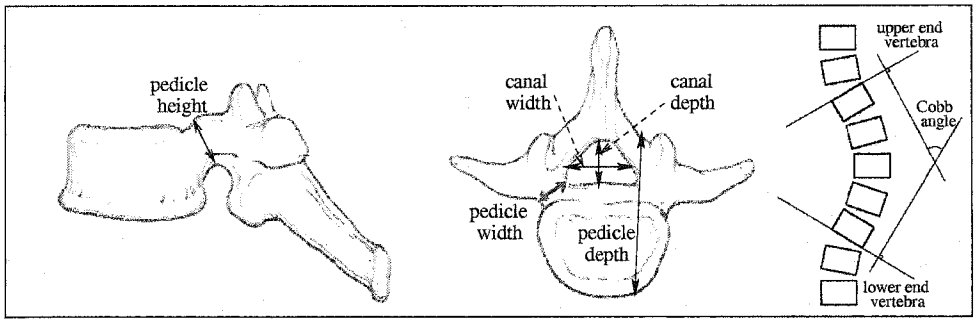

Figure 23 Morphometric parameters used in our validation protocol

4.7 Experimental results

4.7.1 Vertebra database

The vertebra database, used in our application, includes 1,020 thoracic and lumbar vertebrae (510 normal and 510 scoliotic). These data were obtained by digitization of the

[2]The estimation of these morphometric parameters are usefull for the pedicle insertion during a typical surgical intervention of scoliosis.

[3]Cobb angle is used to quantify the scoliosis deformation by evaluating the spinal curve relatively to the postero-anterior radiographic view.

anatomical points on anatomical specimens selected in the Hamann Todd osteology collection, Cleveland, USA, and Smithsonian Institution in Washington, DC, USA [82]. The digitizing protocol consisted of measuring specific anatomical landmarks on each vertebra, thus creating a set of approximately 200 points depending on the level measured with regard to its particular geometry. Different points were acquired in a specific order and recorder in this sequence. After the measurements were done, each vertebra was then reconstructed using computer graphics.

4.7.2 Comparison protocol

In our application, we use the comparison protocol described in [7]. This comparison was made using the distance (mean, root mean square (RMS), and maximum between a point from the reconsructed vertebra and the surface of the corresponding vertebra obtained with CT-scan, which was considered as the ground truth and whose accuracy is $\pm 1mm$ [3].

4.7.3 Experimental results

We have validated our 3D reconstruction method on 13 thoracic spine segments and 57 scoliotic vertebrae (6 lumbar vertebrae and 51 thoracic vertebrae) from 13 pairs of calibrated radiographic images (postero-anterior and lateral) of scoliotic spines. We use an efficient way of calculating the eigenvectors associated with non zero eigenvalues as given in [18]. The first m eigenmodes $\{(\lambda_1, \phi_1), \ldots, (\lambda_m, \phi_m)\}$ are chosen to cover at least 90% of the population's variability. For the experiments, we have chosen $\beta = 0.02$ for the weighting factor penalizing the prior energy term with respect to external energy, $\mu = 90$ and $\nu = 8$ for the variance parameters of the local deformation model. These different threshold values have been chosen empirically after a set of experiments from a database of 30 pairs of calibrated radiographic images and with an optimization procedure ensuring the global minimum (i.e., with E/S algorithm). We used the Canny edge detector to estimate the edge map which are then used for estimation of the edge *potential field* on the two radiographic views (used in the likelihood energy term). In our application, $\sigma = 1$,

the mask size is 5×5, and the lower and upper thresholds are given by the unsupervised estimation technique proposed in [13].

We have implemented the E/S and Genetic algorithms in C++ and compared the execution times of these algorithms (Figs 24 and 25). In our application, parameters of GA are the following; population size=100, crossover rate = 0.80, mutation rate = 0.01, maximum number of generations = 100. Each of $7 + m$ parametres θ_i is quantified on 8 bits. Parameters of E/S algorithm are the following; population size=100, diameter of the exploration graph = 32, maximum number of generations = 100.

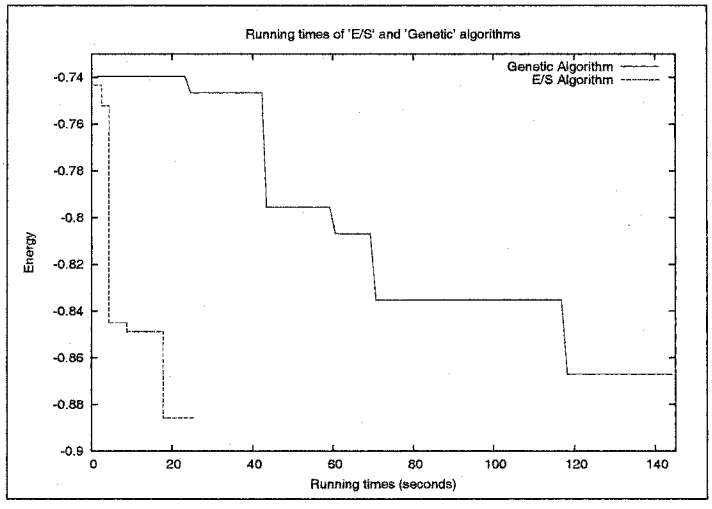

Figure 24 Running times of E/S and Genetic algorithms as a function of energy

Figs 24 and 25 shows that the E/S and Genetic algorithms takes about 55 and 80 generations (or 28 and 120 seconds) respectively to converge to a good estimate for a given vertebral level (with Linux running on a 2.0 GHz PC). In fact, the convergence rate can vary significantly depending on the complexity of the energy function $E(s, \theta)$ to be minimized (or the quality of the input radiographic images). Nevertheless, in all tested cases, we obtain better minima and convergence with the E/S comparatively to the Genetic algorithm (see Table 8).

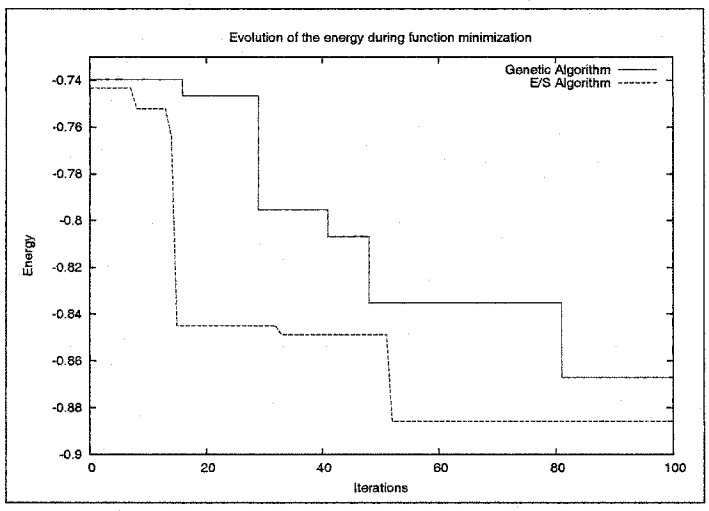

Figure 25 Evolution of energy during function minimization for E/S and Genetic algorithms

Table 8

Example of minima obtained with E/S and Genetic algorithms for lumbar and thoracic vertebrae

Optimization	Vertebral level	
	Lumbar	Thoracic
E/S	$E = -0.89$	$E = -0.87$
Genetic	$E = -0.87$	$E = -0.82$

Fig. 26 shows the projection of the cube template on corresponding vertebral body on postero-anterior and lateral views obtained for the extreme values of position t, scale vector k and orientation α of the restricted search space initially defined for the cube template (see Subsection 4.2.1) and its final reconstruction after E/S optimization.

Fig. 27 shows the projection of the vertebra template on corresponding vertebra on postero-anterior and lateral views obtained for the extreme values of position t, scale vector k and orientation α and the final reconstructed vertebra after GA and E/S optimization.

Fig. 28 shows the estimated reconstructed L2 vertebra when local deformations are taken into acount to refine the reconstruction obtained in Fig. 27. The local deformation process can efficiently adjust the deformable template to the pre-segmented contours of each radiographic image leading to a better 3D reconstruction result.

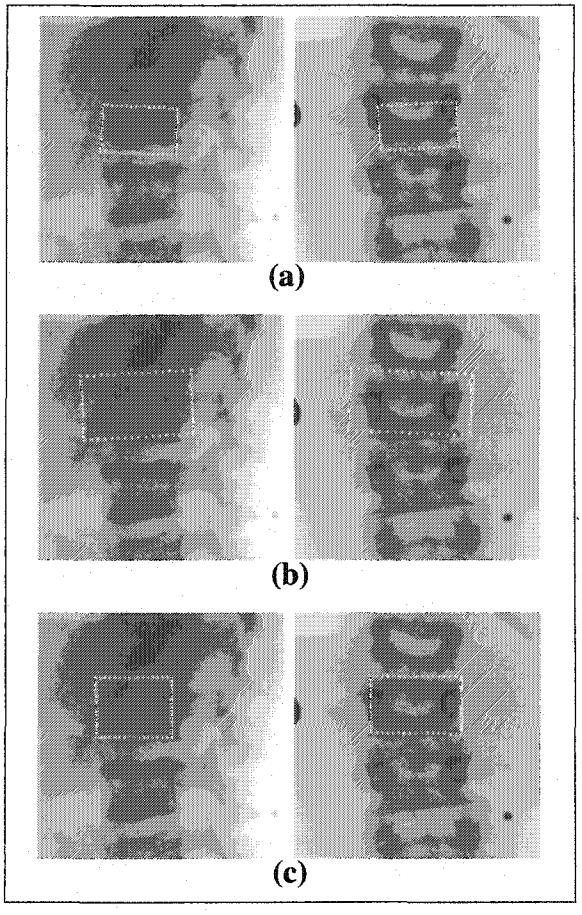

Figure 26 Projection of the cube template on corresponding vertebral body on postero-anterior and lateral views obtained for the extreme values of position t, scale vector k and orientation α. **(a)** $k = (0.8, 0.8, 0.8)$, $\alpha = (-3, -3, -3)$, and $t = (-2, -2, -2)$, **(b)** $k = (1.3, 1.3, 1.3)$, $\alpha = (3, 3, 3)$, and $t = (2, 2, 2)$, **(c)** final reconstruction of the cube, $k = (0.90, 0.98, 1.22)$, $\alpha = (0.80, 0.17, -1.42)$, and $t = (1.72, 0.13, 2.28)$

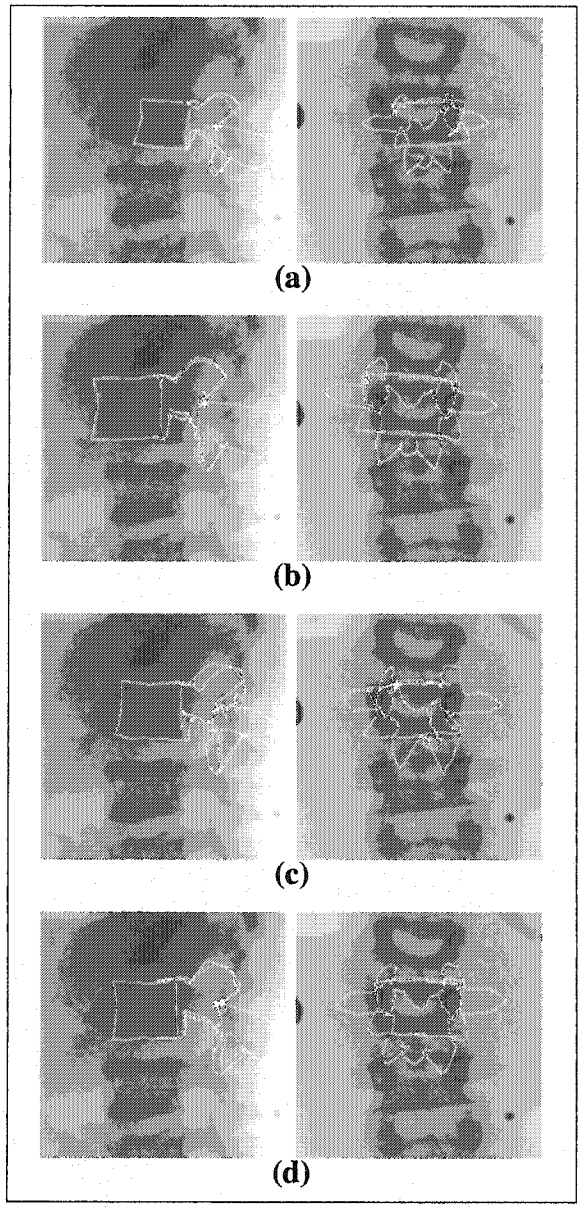

Figure 27 Projection of the L2 vertebra template on corresponding vertebra postero-anterior and lateral views when position t, scale k and orientation α take the least and the greatest values in a corresponding search interval. **(a)** $k = 0.86$,$\alpha = (-4, -4, -4)$, and $t = (-3, -3, -3)$, **(b)** $k = 1.30$,$\alpha = (4, 4, 4)$, and $t = (3, 3, 3)$ **(c)** final reconstruction of the vertebra, $b = (-5, 10, 15, -5, -5, 0, 0, 0, 0, 5)$, $k = 0.96$, $\alpha = (0.5, -2.5, 0.5)$, $t = (1.1, -1.5, 1.0)$, and with GA optimization **(d)** final reconstruction of the vertebra, $k = 0.97$,$\alpha = (0.50, -1.05, 0.49)$, $t = (1.03, -1.49, 1.00)$, and $b = (-5.35, 8.45, 14.69, -7.06, -5.05, 11.08, 5.43, -0.87, 4.10, -6.64)$

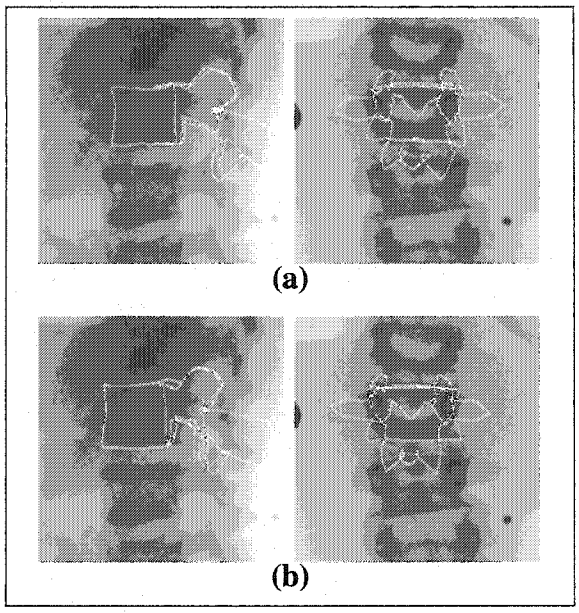

Figure 28 Global and local deformations on L2 vertebra template. **(a)** globally deformed shape $E = -0.79$, **(b)** globally and locally deformed shape $E = -0.88$

Table 9 presents (mean, root mean square (RMS), and maximum) errors between points from the reconstructed vertebra and the surface of the corresponding scanned vertebra for different vertebral levels. These errors are, respectively, (1.46 ± 1.47), (5.35 ± 0.93), and (1.87 ± 0.23) mm for lumbar vertebrae, and (1.30 ± 1.32), (4.64 ± 0.84), and (1.66 ± 0.25) mm for thoracic vertebrae.

Table 10 presents width, height, and depth of spinal pedicles and canal differences between the reconstructed model resulting from our 3D reconstruction method and the model resulting from CT-scan. The elements of the table denote the mean of N absolute values of the difference between the measure of morphometric parameter on reconstructed vertebra and the corresponding measure on scanned vertebra. Table 11 presents the Cobb angle of projections of vertebral end-plates of these reconstructed vertebra segments with the corresponding end-plates of these reconstructed vertebra manually calculated by an expert from Sainte-Justine Hospital (Montréal, Canada) on a postero-anterior X-ray image.

Table 9

Results on point-to-surface comparisons of 57 scoliotic vertebrae. N denotes the total number of vertebrae at different vertebral levels. All data are shown as mean ± standard deviation

Vertebral level	N	Mean error (mm)	Root mean square (mm)	Maximum error (mm)
Thoracic				
T6	3	1.17±1.22	1.48±0.13	4.27±0.55
T7	6	1.32±1.38	1.68±0.33	5.00±1.06
T8	9	1.28±1.28	1.64±0.23	4.66±0.60
T9	10	1.33±1.34	1.70±0.23	4.79±0.75
T10	9	1.23±1.28	1.59±0.14	4.41±0.80
T11	9	1.30±1.31	1.63±0.31	4.43±0.95
T12	5	1.30±1.25	1.66±0.41	4.20±1.04
Lumbar				
L1	2	1.33±1.27	1.67±0.33	4.57±0.84
L2	1	1.70±1.60	2.15±0.00	5.70±0.00
L3	2	1.30±1.30	1.75±0.35	5.20±1.70
L5	1	1.50±1.70	1.93±0.25	5.95±1.20

Figs 29, 33, 31 show a few examples of 3D reconstruction of vertebra segments of some scoliotic spines. To compare these results with those presented in [8], we note that the precision of the 3D/2D registration method presented in [8] remains better than the precision of the 3D reconstruction method described in this paper (see Table 12). This is due to the fact that the method presented in [8] is widely supervised and requires the knowledge of the position of six anatomical points (namely, the center of the superior and inferior endplates, the upper and lower extremities of both pedicles) to initialize the 3D reconstruction process of each vertebra of the spine i.e., the knowledge of the position of 102 anatomical points for the 3D reconstruction of the vertebra segment (L5/.../T1) while the proposed 3D reconstruction method only requires two points, namely the superior and inferior endplates, of the vertebra segment to be defined. The validation results presented above show that the accuracy of our 3D hierarchical reconstruction method is comparable to CT-scan 3D reconstruction.

Table 10

Results on comparisons of 57 scoliotic vertebrae. N denotes the total number of vertebrae at different vertebral levels. All data are shown as mean $\pm$ standard deviation

Vertebral level	N	Pedicle			Canal	
		width (mm)	height (mm)	depth (mm)	depth (mm)	width (mm)
Thoracic						
T6	3	1.90±0.96	2.37±0.74	0.36±0.26	1.55±0.65	1.15±0.79
T7	6	1.74±1.09	1.41±1.00	0.76±0.71	2.87±1.17	0.56±0.78
T8	9	1.58±0.88	1.45±1.03	0.65±0.46	1.45±0.78	1.55±1.23
T9	10	1.55±0.83	1.44±0.91	0.69±0.76	1.62±1.11	1.66±1.28
T10	9	1.32±0.91	0.63±0.66	0.49±0.50	1.07±0.76	1.96±1.25
T11	9	1.39±0.51	1.03±0.93	0.57±0.43	1.22±0.97	1.52±1.14
T12	5	2.05±1.69	0.61±0.36	1.07±1.11	1.51±0.88	1.98±1.35
Lumbar						
L1	2	1.88±1.02	1.50±1.32	1.11±0.58	1.06±0.88	2.43±1.45
L2	1	0.76±0.00	1.33±0.00	1.34±0.00	1.91±0.00	1.55±0.00
L3	2	2.09±0.63	0.78±0.88	1.48±0.70	0.57±0.15	1.78±1.02
L5	1	2.34±0.17	1.78±0.79	0.32±0.30	0.98±0.78	1.79±0.21

Let us note that the estimated global deformation parameters after 3D reconstruction (i.e., parameter vector b, setting the amplitude of each deformation mode of the scoliotic deformation) and the measures of morphometric parameters can also be used to quantify the scoliosis, its nature or to analyse the improvement of orthopedic or surgical corrections. Let us also note that the resulting 3D reconstructed spine can also be efficiently exploited as prior knowledge and geometric constraints for the problem of the rib cage reconstruction. This will be the topic of our futur research.

4.8 Discussion and Conclusion

We have presented an original coarse-to-fine approach for the 3D reconstruction of the scoliotic spine using contours extracted from biplanar radiographic images and *a priori* hierarchical global knowledge both of the geometrical structure of the whole spine and of the statistical structure of each vertebra. From an algorithmic point of view, the reconstruction problem is decomposed in two optimization problems of reduced complexity

Table 11

Cobb angle of projections of vertebral end-plates of these reconstructed vertebra segment with the corresponding end-plates of these reconstructed vertebra manually calculated by an expert from Sainte-Justine Hospital (Montréal, Canada) on a postero-anterior X-ray image

Vertebra segment	No Patient	Cobb angle	
		Projections of vertebra segment (deg)	Postero-anterior X-ray image (deg)
T10 - T12	1	3	3
T10 - T12	2	11	13
T11 - T12	3	15	14
T6 - T11	4	45	43
T6 - T11	5	40	42
T7 - T12	6	46	43
T7 - T10	7	39	42
T7 - T11	8	50	52
T8 - T11	9	38	36
T6 - T9	10	33	32
T7 - T9	11	40	42
T7 - T9	12	34	32
T8 - T9	13	31	29

Table 12

Mean and maximum error distances obtained from the supervised method described in [8] and the proposed method (described in this paper) for the lumbar and thoracic vertebrae

	Mean error (mm)		Maximum error (mm)	
	Lumbar	Thoracic	Lumbar	Thoracic
Supervised method [8]	0.71 ± 0.06	1.48 ± 0.27	3.67 ± 0.80	6.44 ± 1.76
Proposed method	1.46 ± 1.47	1.30 ± 1.32	5.35 ± 0.93	4.64 ± 0.84

allowing us to drastically save computational effort and/or provide accelerated convergence toward an improved estimate. In our application, these two optimization problems are efficiently solved with a stochastic optimization procedure (i.e., with E/S algorithm).

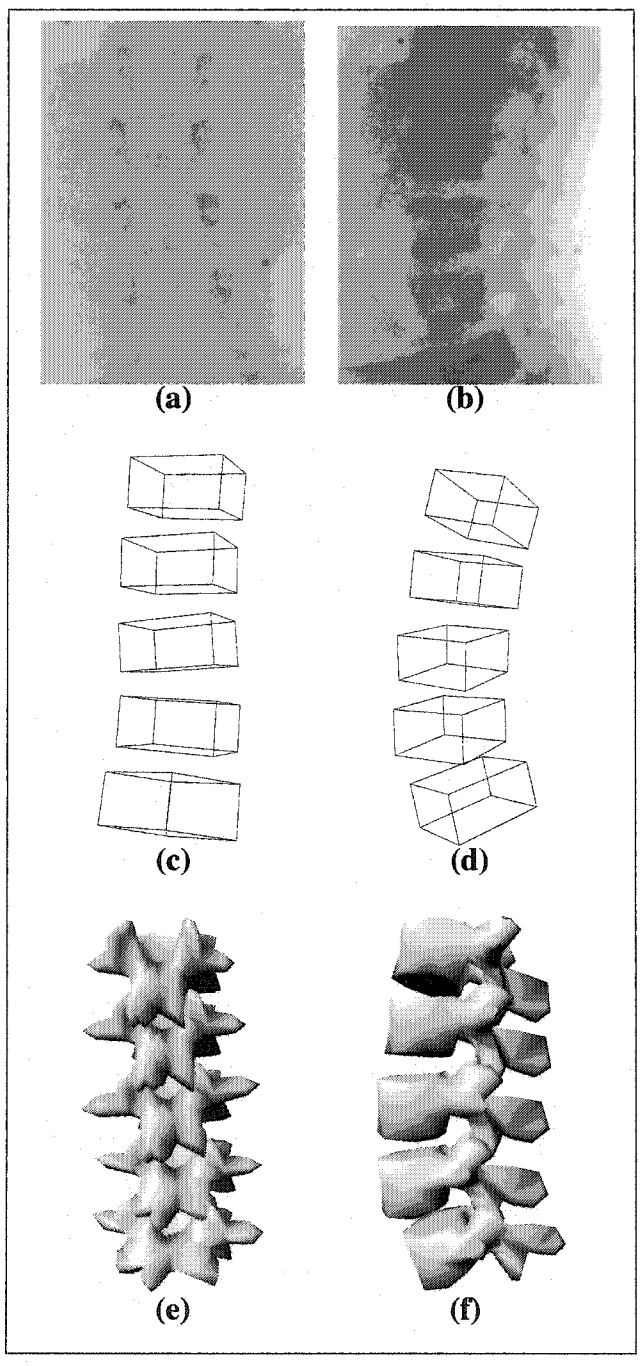

Figure 29 3D reconstruction of vertebra segment (L1/L2/L3/L4/L5) of a given scoliotic spine. **(a)** Postero-anterior image, **(b)** Lateral image, **(c)** and **(d)** Visualization of the reconstructed cube segment (L1/L2/L3/L4/L5) from the coronal and sagittal views. **(e)** and **(f)** Visualization of reconstructed vertebra segment (L1/L2/L3/L4/L5) from the coronal and sagittal views

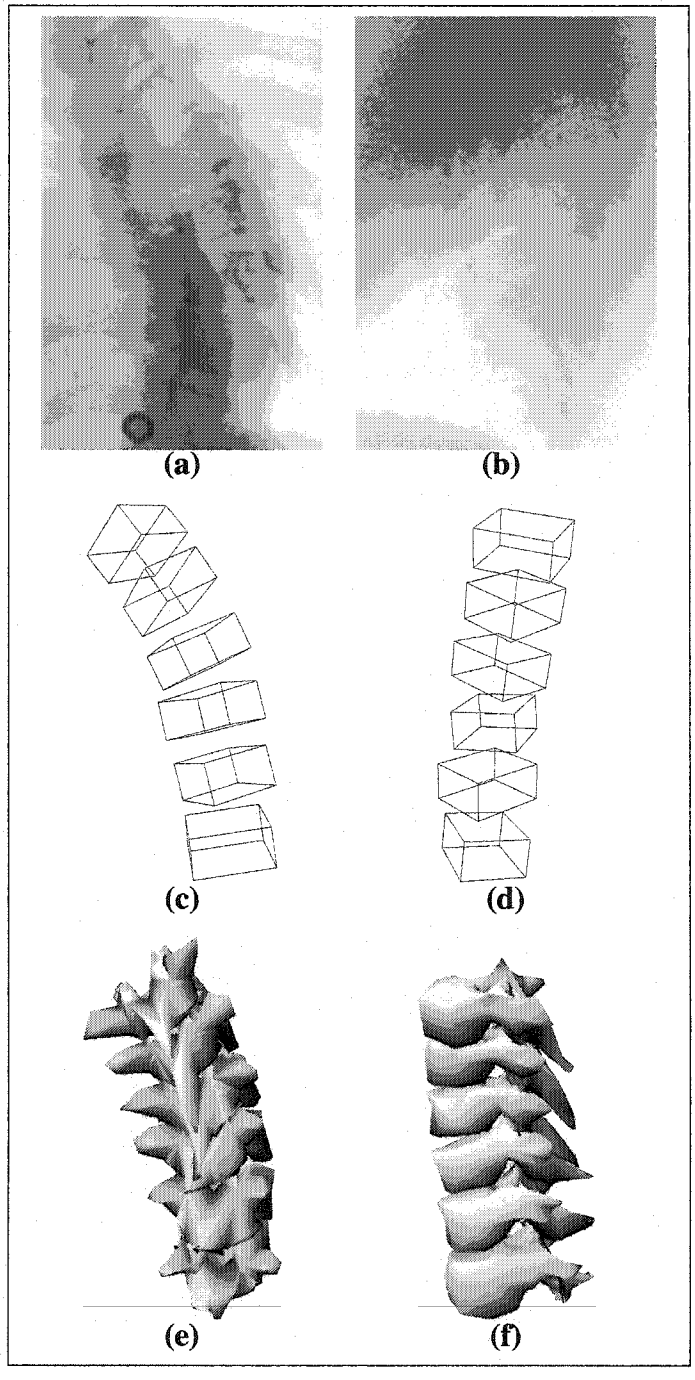

Figure 30 3D reconstruction of vertebra segment (T6/T7/T8/T9/T10/T11) of a given scoliotic spine. **(a)** Postero-anterior image, **(b)** Lateral image, **(c)** and **(d)** Visualization of the reconstructed cube segment (T6/T7/T8/T9/T10/T11) from the coronal and sagittal views. **(c)** and **(d)** Visualization of reconstructed vertebra segment (T6/T7/T8/T9/T10/T11) from the coronal and sagittal views

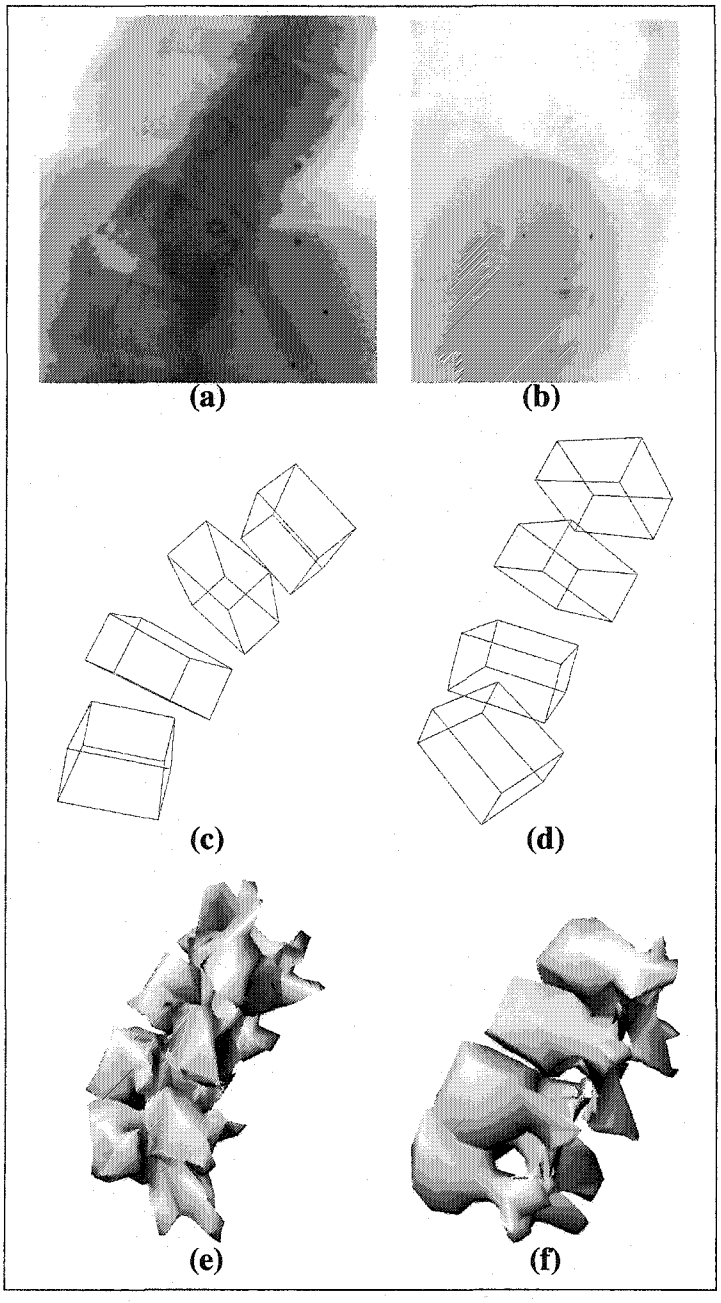

Figure 31 3D reconstruction of vertebra segment (T10/T11/T12/L1) of a given scoliotic spine. **(a)** Postero-anterior image, **(b)** Lateral image, **(c)** and **(d)** Visualization of the reconstructed cube segment (T10/T11/T12/L1) from the coronal and sagittal views. **(c)** and **(d)** Visualization of reconstructed vertebra segment (T10/T11/T12/L1) from the coronal and sagittal views

This optimization procedure is fast compared to other minimization techniques such as the gradient-based method and genetic algorithm. This method has been tested on a number of pairs of radiographic images demonstrating its efficiency and robustness.

The mean error is (1.45 ± 1.46)mm for lumbar vertebra and (1.27 ± 1.29)mm for thoracic vertebra. The maximum error is (5.35 ± 0.93)mm for lumbar vertebra and (4.53 ± 0.82)mm for thoracic vertebra for our 3D reconstruction technique.

The proposed scheme thus constitutes an alternative to CT-scan 3D reconstruction with the advantage of low irradiation and will be of great interest for evaluation of spinal deformities, simulation of orthopaedic treatments, and for reliable geometric models for finite element studies. However, this reconstruction method is not suitable without improvement for surgical navigation applications when compared to CT-scan reconstruction errors of ± 1mm, the gold standard for those applications.

The proposed method remains sufficiently general to be applied to other medical reconstruction problems (i.e., rib cage, pelvis, knee, etc.) for which a database of the anatomical structure is available (with two or more radiographic views).

RECONSTRUCTION 3D BIPLANAIRE NON SUPERVISÉE DE LA CAGE THORACIQUE SCOLIOTIQUE PAR UN MÉLANGE DE MODÈLES A PRIORI PROBABILISTES

Article : Unsupervised 3D biplanar reconstruction of scoliotic rib cage using the estimation of a mixture of probabilistic prior models

Cet article a été soumis au journal *IEEE Transactions on Biomedical Engineering* comme l'indique la référence bibliographique

S. Benameur, M. Mignotte, F. Destrempes and J.A. De Guise. Unsupervised 3D biplanar reconstruction of scoliotic rib cage using the estimation of a mixture of probabilistic prior models. *IEEE Transactions on Biomedical Engineering*, soumis, 2004.

Cet article est présenté ici dans sa version originale.

Résumé

La cage thoracique protège et supporte les organes internes du corps humain. Elle permet aussi la mobilité du tronc lors des mouvements d'inspiration et d'expiration. Les déformations de la cage thoracique sont des conséquences importantes de la scoliose. La reconstruction 3D de la cage thoracique scoliotique à partir d'un ensemble d'images radiographiques n'a pas souvent été étudiée dans la littérature et peu de références existent à ce jour [24][77]. Nous présentons dans cet article une méthode originale et non supervisée de reconstruction 3D des cages thoraciques scoliotiques à partir de deux images radiographiques conventionnelles (postéro-antérieure avec incidence de 0° et latérale) calibrées. Dans la méthode présentée, nous avons supposé que chacune des formes des cages thoraciques est distribuée dans une classe de pathologie scoliotique spécifique, pour laquelle nous avons ensuite défini une réduction de dimensionnalité linéaire d'ACP probabiliste. Dans ce contexte nous avons utilisé un mélange d'ACP probabiliste dont chaque composante représente une classe de déformation particulière de la scoliose. Pour chacune

de ces composantes, un modèle *a priori* paramétrique de forme tridimensionnelle est utilisé pour contraindre notre problème mal-posé de reconstruction 3D. La reconstruction de la cage thoracique relative à chacune des composantes consiste à ajuster les projections (postéro-antérieure et latérale) du modèle *a priori* 3D de la cage thoracique avec les contours préalablement segmentés sur les deux images radiographiques calibrées. Le problème de reconstruction 3D est vu comme un problème d'estimation des paramètres de déformation de ce modèle ou, de façon équivalente, comme un problème de minimisation d'une fonction d'énergie. Cette minimisation est effectuée à l'aide d'un algorithme stochastique d'exploration/sélection [79]. Les paramètres du mélange d'ACP probabiliste sont estimés par une version stochastique de l'algorithme EM (Expectation, Maximization) appelée SEM [33]. La reconstruction 3D optimale correspond à la composante de la déformation et aux paramètres menant à l'énergie minimale. La méthode proposée a été validée sur un échantillon d'une vingtaine de paires d'images radiographiques calibrées n'appartenant pas à la base d'apprentissage et comparée aux reconstructions 3D issues de la méthode stéréo-radiographique [24]. Une erreur moyenne de (1.62 ± 0.50) mm a été obtenue sur les distances point-surface entre le modèle reconstruit avec notre méthode et le modèle issu de la reconstruction stéréo-radiographique [24]. La reconstruction 3D d'une cage thoracique scoliotique nécessite un temps de calcul de l'ordre de 6 minutes (sur un PC/Linux à 2.0 GHz).

CHAPITRE 5

UNSUPERVISED 3D BIPLANAR RECONSTRUCTION OF SCOLIOTIC RIB CAGE USING THE ESTIMATION OF A MIXTURE OF PROBABILISTIC PRIOR MODELS

Abstract In this paper, we present an original method for the automatic 3D reconstruction of the scoliotic rib cage from a planar and a conventional pair of calibrated radiographic images (postero-anterior with normal incidence and lateral). To this end, we first present a robust method for estimating the model parameters in a mixture of Probabilistic Principal Component Analysers (PPCA). This method is based on the Stochastic Expectation Maximization (SEM) algorithm. Parameters of this mixture model are used to constrain the 3D biplanar reconstruction problem of scoliotic rib cage. More precisely, the proposed PPCA mixture model is exploited for dimensionality reduction and to obtain a set of probabilistic prior models associated with each detected class of pathological deformations observed on a representative training scoliotic rib cage population. By using an appropriate likelihood, for each considered class-conditional prior model, the proposed 3D reconstruction is stated as an energy function minimization problem, which is solved with an exploration/selection algorithm. The optimal 3D reconstruction then corresponds to the class of deformation and parameters leading to the minimal energy. This 3D method of reconstruction has been successfully tested and validated on a database of 20 pairs of biplanar radiographic images of scoliotic patients, yielding very promising results. As an alternative to CT-scan 3D reconstruction this scheme has the advantage of low radiation for the patient, and may also be used for diagnosis and evaluation of deformity of a scoliotic rib cage. The proposed method remains sufficiently general to be applied to other reconstruction problems for which a database of objects to be reconstructed is available (with two or more radiographic views).

Key words: *3D reconstruction model, 3D/2D registration, shape model, reduction of dimensionality, mixtures of probabilistic principal component analysers, biplanar radiographies, scoliosis, medical imaging, stochastic optimization.*

5.1 Introduction

Scoliosis is a 3D deformity of the natural curve of the spinal column which can occur at any time during a child's growth. Due to its interaction with the spinal column, the abnormal curvature of the spine will cause a complex deformation of the rib cage including rotation and distortions. If this disease is not treated, a child's heart and lungs will not work properly as the twisted rib cage will not allow them enough space to develop. The rib cage plays also another important role in the protection of several other internal organs and of allowing motion of the trunk in respiration as well as spinal flexion.

In this paper, we are concerned with automatic 3D reconstruction methods of scoliotic rib cage from a pair of planar and conventional calibrated radiographic images (postero-anterior with normal incidence and lateral). This 3D geometrical information is useful for the diagnosis (i.e., to quantify a deformity of a scoliotic rib cage), surgical planing, computer assisted surgery or to quantify the postoperative 3D changes of a scoliotic rib cage [29].

The 3D reconstruction problem of (scoliotic) rib cage from two or several projections has not been widely studied and few references exist in the literature.

One of the first 3D reconstruction technique using two radiographic projections (namely, postero-anterior with normal incidence (I_{PA}) and postero-anterior with 20 ° angled down incidence ($I_{PA-20°}$)) was proposed in [24]. This stereo-radiographic method consists in identifying 11 mid-line points per rib on I_{PA} and $I_{PA-20°}$. 60 points are interpolated on the 2D curve of the rib on I_{PA}. 3D points are obtained by intersection of a projection plane, which is defined using the interpolated points and the 3D position of I_{PA} and $I_{PA-20°}$ X-ray sources, and the 2D curve of the same rib on $I_{PA-20°}$ using a Direct Linear

Transformation (DLT) [71]. This process is repeated for each of the 60 points of all rib defined on I_{PA}. This method is then refined by taking into account patient displacement during stereo-radiography [69]. Nevertheless this technique remains limited due to the inherent inaccuracy produced in identifying 11 points per rib on I_{PA} and $I_{PA-20°}$ (leading to reconstruction errors). Locating these features is widely supervised and, therefore, time-consuming (up to two hours). Moreover, this method does not exploit all information contained in the two X-ray radiographic projections, for instance, the contours of each rib, the geometrical structure or the statistical knowledge of the possible deformation of the rib cage to be reconstructed.

3D reconstruction methods using *a priori* knowledge of the geometric shape of the objects of interest have been recently proposed. For example, a method similar to the one reported by Benameur *et al.* in [8] for the reconstruction of each vertebra of the spinal column was proposed by Mouren [77] to reconstruct the 3D geometry of the rib cage from two radiographic projections (postero-anterior with normal incidence I_{PA} and lateral (I_{LAT})). This method exploits a global *prior* knowledge on the geometrical structure of each rib. To find this geometrical knowledge while reducing the dimensionality of this problem, a Principal Component Analysis (PCA) is applied to each rib extracted from a training scoliotic rib cage database. This PCA allows to obtain a geometric prior model representing a mean shape and containing the typical geometrical deformation modes estimated in the least square sense. Thereafter, the rib model is deformed according to the rays back projected from the contour points of the projections taken a patient. In I_{LAT}, a set of 60 points are manually digitized. This 3D reconstruction is done rib by rib. This method is interesting but may not be very accurate. First, it is significantly supervised and operator-dependent; it requires to identify manually and digitize a set of 60 points in the lateral view. Moreover, the PCA only defines a *linear* dimensionality reduction which is a strong and not necessarily a true assumption in this context.

In order to overcome the problem of supervision and improve the accuracy of the deformation model, we propose herein to use a mixture of Probabilistic PCA [92] (PPCA). In order to estimate the parameters of such a mixture model, the Expectation Maximization (EM) algorithm was already proposed [92]. Nevertheless, the initial parameter values have a significant impact on the convergence of this iterative procedure and on the quality of the final estimation (the EM converges to a *local* and not necessary *global* optimum estimate). In order to make the procedure more robust, we propose a stochastic version of the EM-PPCA relying on the Stochastic version of the EM (SEM) algorithm [33]. This SEM-PPCA is efficiently exploited for dimensionality reduction and to get a set of probabilistic prior models, associated to each detected class of pathological deformations, observed on a representative training scoliotic rib cage population. For each considered class-conditional prior model of pathological deformations, the proposed reconstruction method then consists in fitting the projections of an instance of the deformation model with the segmented contours of the corresponding rib cage on the two radiographic views. This matching problem leads to a set of K optimization problems (one for each detected class of pathological deformations) which is efficiently solved in our application with a exploration/selection algorithm. The optimal 3D reconstruction corresponds to the solution, leading to the minimal energy, amongst these K optimization problems.

Let us note that probabilistic principal component analysis (PPCA) has been already used in shape localization in images [32], object classification [35] and inference of 3D structure [41]. Mixture of PPCA has only been exploited in image compression [92]. To our knowledge, this work is the first to use mixtures of probabilistic PCA for the 3D modeling of a class of complex shapes and to constrain the reconstruction problem in medical imagery.

The remainder of this paper is organized as follows: in Section 5.2, we present the basic concept of a mixture of probabilistic PCA. Section 5.3 is devoted to the stochastic EM algorithm for estimating all of the model parameters in a mixture of probabilistic PCA.

Section 5.4 and 5.5 describe the proposed 3D reconstruction method and the related sequence of energy function to be minimized. Section 5.6 presents the validation protocol of our method. In Section 5.7, we show some 3D reconstruction results and validate the proposed model.

5.2 Probabilistic Model for Dimensionality Reduction

PCA is a well established model for dimensionality reduction. Nevertheless, one limiting disadvantage of this technique is the absence of an associated probability density model or generative model [92]. PPCA overcomes this problem.

5.2.1 Probabilistic PCA

Tipping and Bishop have developed the PPCA model [92, 93] by reformulating PCA as a Maximum Likelihood (ML) solution of a specific form of variable model. Let s and b be two random vectors related by:

$$s = \Phi b + \nu + \varepsilon, \tag{5.1}$$

where Φ is a $d \times m$ matrix that represents the principal subspace of s. The assumption is that $b \sim \mathcal{N}(0, I_m)$ as well as $\varepsilon \sim \mathcal{N}(0, \sigma^2 I_d)$ are zero mean Gaussian distributed random vectors (I_r denotes the $r \times r$ identity matrix and $\mathcal{N}()$ represents the normal distribution). Consequently the random vector s is also normally distributed according to:

$$p_S(s) = \mathcal{N}(s; \nu, \sigma^2 I_d + \Phi\Phi^T). \tag{5.2}$$

The variable s represents the full data, whereas b represents the reduced data (the dimension m of b is significantly smaller than the dimension d of s).

Let $[s_1, s_2, ..., s_u]^T$ be a i.i.d. observation sample issued from s, $\lambda_1, ..., \lambda_d$ be the eigenvalues of the covariance matrix, in decreasing order, of this sample, Λ_m be the diagonal

matrix with entries $\lambda_1, \ldots, \lambda_m$, and U_m be the $d \times m$ matrix with columns equal to the corresponding eigenvectors, normalized so that they have euclidean norm equal to 1. From [92], a ML estimation of (ν, σ^2, Φ) is given by:

$$\begin{aligned} \nu &= \bar{s} = \frac{1}{u}\sum_{i=1}^{u} s_i\,, \\ \sigma^2 &= \frac{1}{d-m}\sum_{i=m+1}^{d} \lambda_i\,, \\ \Phi &= U_m(\Lambda_m - \sigma^2 I_m)^{1/2}. \end{aligned} \tag{5.3}$$

Note that in the PCA, one would take $\Phi = U_m$, but this choice is not optimal in the sense of the ML for the PPCA model (Fig. 32). The diagonal matrix $(\Lambda_m - \sigma^2 I_m)^{1/2}$ gives an appropriate weight to each column vector of the matrix U_m. The conditional probability

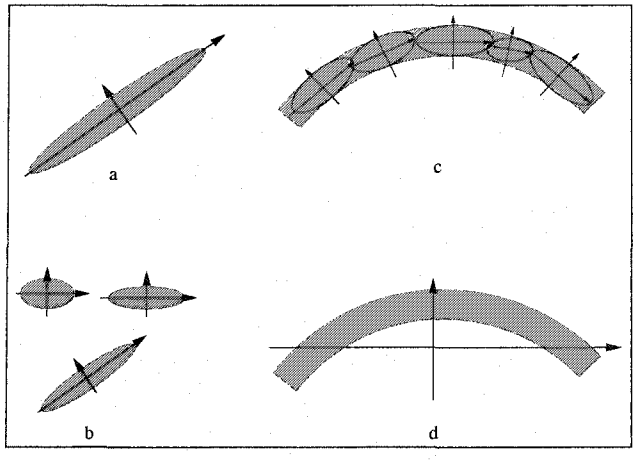

Figure 32 An illustration of adjustment of a distribution. **(a)** and **(d)** adjustment with PCA (not optimal in this latter case), **(b)** and **(c)** adjustment with mixtures of PPCA

distribution of s given b, is expressed by [92]:

$$P_{S/B}(s/b) = (2\pi\sigma^2)^{-1/2}\exp(-\frac{1}{2\sigma^2}\|s - W - \bar{s}\|),$$

where $W = U_m(\Lambda_m - \sigma^2 I_m)^{1/2} b$. Hence, the ML reconstructed data point is taken as:

$$\hat{s} = U_m(\Lambda_m - \sigma^2 I_m)^{1/2}\, b + \bar{s}.$$

In that case, the reduction map is defined by:

$$\hat{b} = (\Lambda_m - \sigma^2 I_m)^{-1/2}\, U_m^t\, (s - \bar{s}),$$

in order to minimize the average reconstruction error (optimal in the least square sens):

$$e = \frac{1}{n} \sum_{i=1}^{n} \|s_i - U_m U_m^t (s_i - \bar{s}) - \bar{s}\|^2,$$

These reconstruction and reduction maps were adopted in [31]. We summarize the PPCA algorithm in Table 13.

5.2.2 Mixtures of Probabilistic Principal Component Analysis

The probabilistic formulation of PCA offers a graceful extension to model complex data structures with a mixture of local PPCA models. A Mixture of PPCA (MPPCA) is a distribution of the form [92]

$$P_S(s) = \sum_{c=1}^{K} \omega_c \mathcal{N}(s; \nu_c, \sigma_c^2 I_d + \Phi_c \Phi_c^T), \tag{5.4}$$

where K designates the number of components of the mixture and ω_c is the c^{th} component's mixing proportion. This mixture depends on a vector of parameters $\Gamma = (\nu_1, \sigma_1, \Phi_1$ $, ..., \nu_K, \sigma_K, \Phi_K)$. In order to reduce dimensionality, the following strategies can be adopted; we compute for each mixture component c, the reconstruction point $\bar{s_c}$ and take the one nearest to s as the one that maximizes the distribution $P_S(s)$ (optimality in the ML sense).

Table 13

PPCA Algorithm

PPCA Algorithm

Estimate in the ML sense the parameters σ^2, ν, and Φ of the PPCA of a sample $[s_1, s_2, \ldots, s_u]^T$ ensuring a reconstruction error $< \epsilon$.

u	Size of $[s_1, s_2, \ldots, s_u]^T$
d	Dimension of the full data
m	Dimension of the reduced data
ϵ	Threshold for reconstruction

begin

Compute the empirical mean shape $\bar{s} = \dfrac{1}{u}\sum_{i=1}^{u} s_i$.

Compute the covariance matrix A^tA, where $A = \frac{1}{\sqrt{u}}[(s_1 - \bar{s}), \cdots, (s_u - \bar{s})]$.

Decompose the matrix A into the form $A = UDV^t$, where U and V are orthogonal matrices, and D is a diagonal matrix ($D = diag(d_1, \ldots, d_r)$, $r = \min(d, u)$, with $d_1 \geq \ldots \geq d_r$).

The eigenvalues of the covariance matrix A^tA are given by $\lambda_j \geq \lambda_{j+1}$ $(1 \leq j \leq d-1)$ where $\lambda_i = d_i^2$ $(1 \leq i \leq \min(d, u))$.

for $j = 1$ ***to*** $d - 1$ **do**

U_j is the matrix of the first j columns of V.

Compute reconstruction error $\varrho = \frac{1}{u}\sum_{i=1}^{u} \|s_i - U_j U_j^t (s_i - \bar{s}) - \bar{s}\|^2$.

if $\varrho < \epsilon$ **then**

$m = j$,

$j = d - 1$.

$\sigma^2 = \frac{1}{d-m}\sum_{i=m+1}^{d} \lambda_i$, $\quad \nu = \bar{s}$, $\quad$ and $\quad \Phi = U_m(\Lambda_m - \sigma^2 I_m)^{1/2}$.

end

5.3 Estimation of a Mixture of PPCA

In order to estimate parameter vector Γ, we resort to the SEM algorithm [33]. This iterative procedure requires initial parameters which can be given by a K-means clustering procedure [45] (in doing so, we assume as first approximation that the considered clusters are spherical with equal volumes). The obtained spherical partitions allow to obtain a rough estimation of the mixture parameters which are then used to initialize the SEM clustering and estimation procedure.

5.3.1 K-means Algorithm

The K-means algorithm consists of the following steps. To initialize K clusters, choose K shapes at random from the training base. For each shape selected in the training base, assign this shape to a class such that the Euclidean distance from this shape to the center of that cluster is minimal. For each cluster, recalculate the means of the cluster based on the shapes that belong to that cluster. This second step is running until the center of each class becomes steady.

5.3.2 Stochastic EM Algorithm

Let K be an upper bound on the number of classes and $\xi \in]0, 1[$ be a chosen threshold. In the context of the estimation of a MPPCA, the SEM algorithm can be outlined as follows, (the superscript denoting the iteration number).

Initialization

We initialize the SEM algorithm by the ML parameters estimated on the complete data obtained by a K-means [45] partition of $[s_1, s_2, \ldots, s_u]^T$ into K classes. For every observation s_i, the probability $P^{[0]}_{S/C}(s_i/c)$ of its belonging to the class c, ($c \in \{1, \ldots, K\}$) can then be defined. This terminates the initialization phase.

An iteration of SEM then consists of three steps.

Step S (Stochastic)

For each s_i, we select from the set of classes an element according to the distributions $[P_{C/S}^{[p]}(1/s_i, \Gamma^{[p]}), \ldots, P_{C/S}^{[p]}(K/s_i, \Gamma^{[p]})]$. This selection defines a partition $[\vartheta_1^{[p]}, \ldots, \vartheta_K^{[p]}]$ of the sample $[s_1, s_2, ..., s_u]^T$.

Step M (Maximization)

The SEM algorithm supposes that every s_i belonging to $\vartheta_c^{[p]}$ for each $c \in [1, K]$, is realized according to the distribution defined by $P_{S/C}(s_i/c, \Gamma)$ (Eq. (5.2)), the density corresponding to class c. Let u be the number of rib cages in the training base. The parameters of the mixture are estimated for the complete data in the ML sense upon setting $\hat{\pi}_c^{[p+1]} = \text{Card}(\vartheta_c^{[p]})/u$ and estimating $\Gamma^{[p+1]}$ on each class according to (Eq. (5.3)). If $\hat{\pi}_c^{[p+1]} < \xi$, we eliminate the class c in the mixture.

Step E (Estimation)

For each s_i, we define the next distribution $[P_{C/S}(1/s_i, \Gamma^{[p+1]}), \ldots, P_{C/S}(K/s_i, \Gamma^{[p+1]})]$ by the posterior distribution based on the current parameter $\Gamma^{[p+1]}$:

$$P_{C/S}(c/s_i, \Gamma^{[p+1]}) = \frac{\pi_c^{[p+1]} P_{S/C}(s_i/c, \Gamma^{[p+1]})}{\sum_{c=1}^{K} \pi_c^{[p+1]} P_{S/C}(s_i/c, \Gamma^{[p+1]})}.$$

Return to step S until the maximum number of iterations has been reached.

5.4 Mixture of Statistical Deformable Models

The shape s of each rib cage of our training database is defined by a set of l control points, or landmarks, which approximate the geometrical shape of the mid-line of each rib in $\mathcal{R}^3$. Each rib cage in the training set is thus represented by the following $3l$ dimensional vector,

$$s = (x_1, y_1, z_1, ..., x_l, y_l, z_l)^t,$$

where $(x_i, y_i, z_i)^t$ are the Cartesian coordinates of the i^{th} control point or landmark of the shape.

5.4.1 Training phase

First, we extend into 3D the method proposed by Cootes in [17] for aligning the set of u 3D shape samples $[s_1, s_2, ..., s_u]$ of our training database to a common scale, rotation, and translation. This step is important and allows to eliminate the variations introduced by affine deformations such as translation, scaling, and rotation.

To this end, an arbitrary shape is selected as the initial average shape estimate. All the other shapes are aligned to this average using a least square minimization. A new average is computed by a simple mean across the corresponding points, and the procedure repeats until convergence. Assuming that 3D translation is represented by a separate translation vector t, a quaternion[3] q representation of scaling and rotation avoids such behavior [51].

Thus, any scaling and rotation in 3D can be expressed as quaternion, where scaling is expressed by the magnitude of the quaternion and the 3D rotation is expressed by the direction of the unit vector u and rotation φ. Quaternion have some advantages amongst which simple derivatives and efficient formulations to find rotation matrices directly for point matching problems [10]. The alignment of two 3D shape instances is accomplished using a well-known procedure given in [10] to optimize for q and t.

We then apply the MPPCA to estimate the parameters of each class and to reduce the dimension to $m_c \ll 3l$ (Fig. 33). Viewing $s_c = (x_1, y_1, z_1, ..., x_l, y_l, z_l)$ as a random vector, we obtain, for each class c ($c \in [1, K]$), an optimal probabilistic deformable model

[3] A quaternion q is defined as the linear combination of a scalar term $q_0 \geq 0$ and three right-handed orthonormal vectors (i, j, and k) $q = q_0 + q_1 i + q_2 j + q_3 k$. The magnitude of the quaternion is defined as, $\mid q \mid = \sqrt{q_0^2 + q_1^2 + q_2^2 + q_3^2}$, and any unit length quaternion can be written as, $q = cos(\varphi) \cdot u + sin(\varphi) \cdot u$, where u is a unit vector and φ represents a rotational twist along the unit vector. The Cartesian rotation matrix is given by,

$$R = \begin{pmatrix} q_0^2 + q_1^2 - q_2^2 - q_3^2 & 2(q_1 q_2 - q_0 q_3) & 2(q_1 q_3 + q_0 q_2) \\ 2(q_1 q_2 + q_0 q_3) & q_0^2 + q_2^2 - q_1^2 - q_3^2 & 2(q_2 q_3 - q_0 q_1) \\ 2(q_1 q_3 - q_0 q_2) & 2(q_2 q_3 + q_0 q_1) & q_0^2 + q_3^2 - q_1^2 - q_2^2 \end{pmatrix}.$$

in the ML sense of the form $S_c = \Phi_c b_c + \nu_c + \varepsilon_c$ with $\varepsilon_c \sim \mathcal{N}(0, \sigma_c^2 I_l)$, Φ_c a $3l \times m_c$ matrix, and $b_c \sim \mathcal{N}(0, I_{m_c})$, by taking $\nu_c = \bar{s}_c$, $\sigma_c^2 = \frac{1}{1-m_c} \sum_{i=m_c+1}^{l} \lambda_i$, and $\Phi_c = U_{m_c}(\Lambda_{m_c} - \sigma_c^2 I_{m_c})^{1/2}$. This gives us non-linear deformations of the mean shape of each pathological deformations detected in our representative learning set, and terminates the training phase (Figs. 34 and 35).

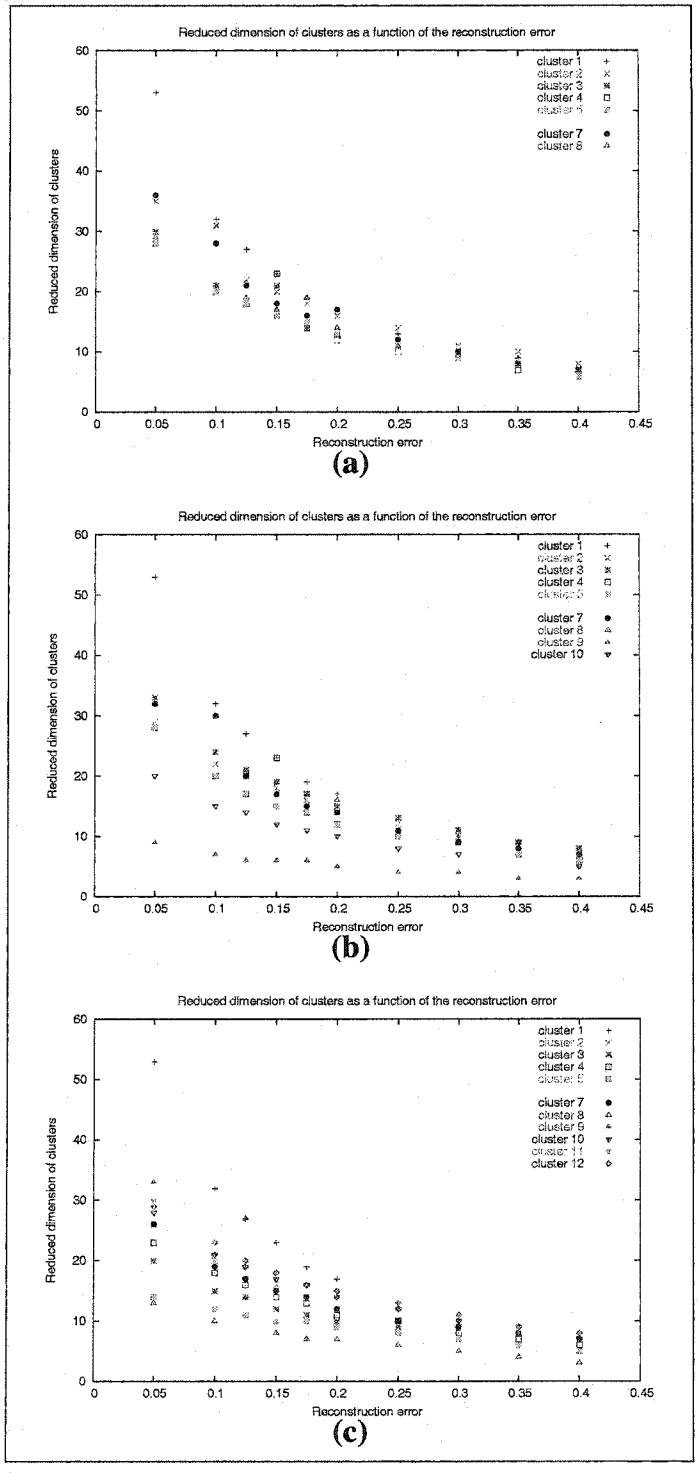

Figure 33 Reduced dimension of clusters as a function of the reconstruction error using different number of clusters **(a)** the rib cage database is partitioned into 8 clusters, **(b)** 10 clusters, **(c)** 12 clusters

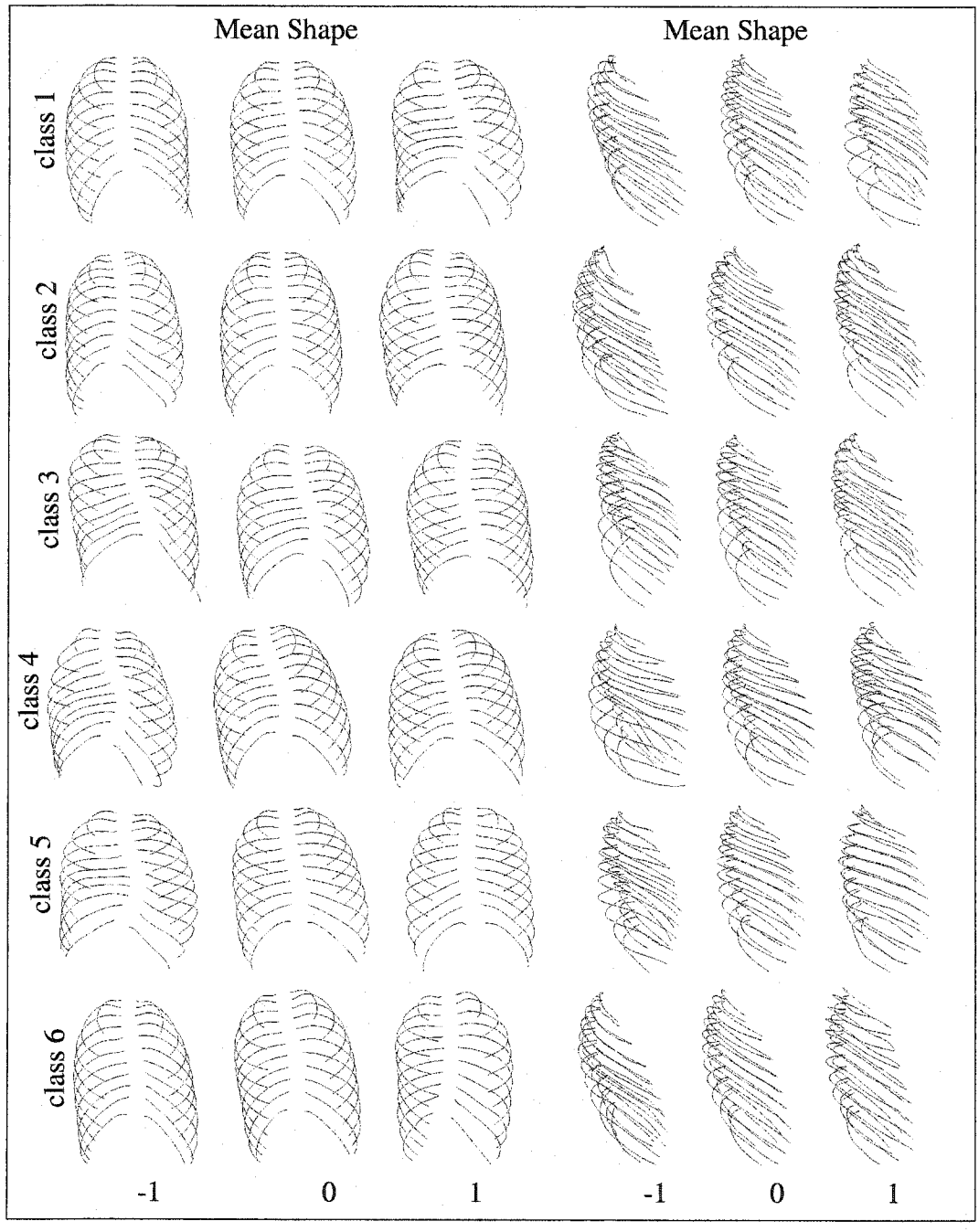

Figure 34 Prior model of each class. Two deformed shapes obtained by applying ± 1 to the mean shape for all deformation modes (sagital and coronal views)

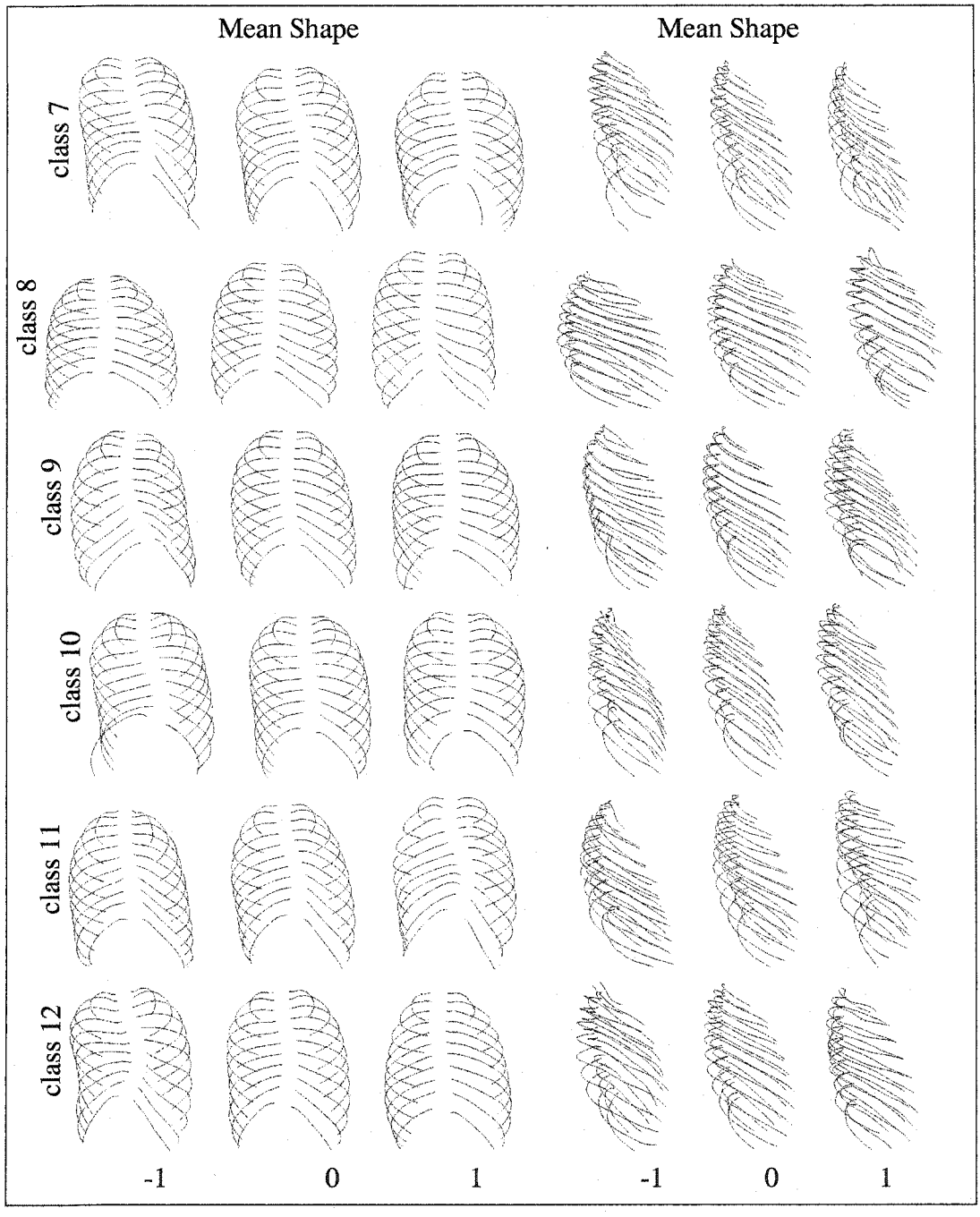

Figure 35 Prior model of each class. Two deformed shapes obtained by applying ± 1 to the mean shape for all deformation modes (sagital and coronal views)

5.4.2 Deformation parameters

From the training phase, we obtain for each class c ($c \in [1, K]$), the mean shape $\overline{s}_c$, and its non-linear deformations $s_c = \Phi_c\, b_c + \overline{s}_c$, where $\Phi_c = [U_1(\Lambda_1 - \sigma_1^2 I_1)^{1/2}, \ldots, U_{m_c}(\Lambda_{m_c} - \sigma_c^2 I_{m_c})^{1/2}]$ is the matrix of the first m_c eigenvectors associated with the m_c largest eigenvalues and $\mathbf{b_c} = (b_{c,1}, \ldots, b_{c,m_c})^t$ is a vector containing the weights for these m_c deformation modes.

In addition, we consider rigid deformations of the template given by global translation $T = (t_x, t_y, t_z)$, scaling $k = (k_x, k_y, k_z)$, and rotation $\alpha = (\alpha_x, \alpha_y, \alpha_z)$ around the x, y and z, axis (applied point-wise to the template). This yields a vector of deformation:

$$\theta = (T, k, \alpha, b_c),$$

of dimension $9 + m_c$. The globally deformed template for class c is then defined by:

$$s_c = M(k, \alpha)[\Phi_c b_c + \overline{s}_c] + T, \tag{5.5}$$

where $M(k, \alpha)$ performs a rotation and a scaling by k.

5.4.3 Prior energy term

Let Θ_c be the random variable corresponding to the vector of $(9 + m_c)$ deformations. We model the distribution of Θ_c by [32],

$$P_{\Theta_c}(s_c(\theta)) = \mathcal{U}(T, k, \alpha) \exp\left(-\frac{1}{2} b^t (I_{m_c} - \sigma_c^2 \Lambda_{m_c}^{-1}) b\right), \tag{5.6}$$

where $\mathcal{U}$ is the uniform distribution. This probability expresses the fact that the shape to be reconstructed is likely close to the mean shape. By considering that,

$$P_{\Theta_c}(s_c(\theta)) = \frac{1}{\zeta_p}\exp(-E_p(s_c)), \tag{5.7}$$

where ζ_p is a normalization constant, a prior energy term can be deduced from this low parametric representation,

$$E_p(s_c(\theta)) = \frac{1}{2}b^t(I_{m_c} - \sigma_c^2\Lambda_{m_c}^{-1})b. \tag{5.8}$$

This energy term, which does not penalize affine transformations, will be used in our energy-based model to rightly constrain our 3D reconstruction model by penalizing the deviation of the deformed template from the mean shape.

5.4.4 Likelihood energy term

In a commonly used energy-based (deformable) model of reconstruction or segmentation, spatial contours (or some spatial gradient measures derived from the input image) are generally exploited in the data likelihood energy term. This term aims at expressing a measure of similarity between the deformed template and the object present in the image by constraining the deformable template to be attracted and aligned to the salient edges of the object to be detected [8]. Due to the low signal-to-noise ratio, low resolution and contrast of the radiographic images used in our application, the sharpness of the contour of each rib is noticeably reduced and our likelihood model cannot rely efficiently solely on this type of gradient measures. Instead, we propose a likelihood energy term exploiting an edge potential field [8] along with a statistical region-based homogeneity criterion. This measure is based on the computation of the grey-level variance inside and outside each rib. In our application, the likelihood energy term is expressed as,

$$E_l(s_c(\theta), I_{\text{PA}}, I_{\text{LAT}}) = E_l(s_c(\theta), I_{\text{PA}}) + E_l(s_c(\theta), I_{\text{LAT}}), \tag{5.9}$$

where $E_l(s_c(\theta), I_{\text{PA}})$ and $E_l(s_c(\theta), I_{\text{LAT}})$ are likelihood energy terms for postero-anterior and lateral images respectively, with, for the postero-anterior image,

$$E_l(s_c(\theta), I_{\text{PA}}) = \frac{1}{n_{\text{PA}}} \sum_{\Gamma_{\text{PA}}} \Psi_{\text{PA}}(x,y) + \\ + \eta\Big(\sum_{i=1}^{n_{rib}} \Big(\text{var}_{\text{Rib}_i^{\text{in}}}(I_{\text{PA}}(x,y)) + \text{var}_{\text{Rib}_i^{\text{out}}}(I_{\text{PA}}(x,y)) \Big) \Big), \tag{5.10}$$

In this expression:

• the first summation of $E_l(s_c(\theta), I_{\text{PA}})$ is overall the n_{PA} points of the external contour of the postero-anterior (I_{PA}) projection of the deformed template (Fig. 36) on a pre-computed edge potential field estimated on I_{PA}.

• the second summation is over the n_{rib} ribs of a rib cage, and $\text{var}_{\text{Rib}_i^{\text{in}}}$ (resp. $\text{var}_{\text{Rib}_i^{\text{out}}}$) designates the variance of the set of grey levels located on the external contour of the I_{PA} projection of the deformed template with a slightly inferior scale $k - \epsilon$ (and resp. slightly superior scale $k + \epsilon$).

η is a factor allowing to control of the balance between the contour-based likelihood energy term and the region-based likelihood energy term.

This energy term is minimal when the external contour of the I_{PA} projection of each rib of the deformed template delineates two homogeneous regions (rib inside and rib outside) separated by a contour (Fig. 37).

To compute the edge potential field Ψ associated with each radiographic projection, we first use a Canny edge detector with the unsupervised technique proposed in [13]. Then, Ψ is defined as in [53] by,

$$\Psi(x,y) = \exp\Big(-\frac{\sqrt{\xi_x^2 + \xi_y^2}}{\tau} \Big) \Big| \cos(\gamma(x,y)) \Big|, \tag{5.11}$$

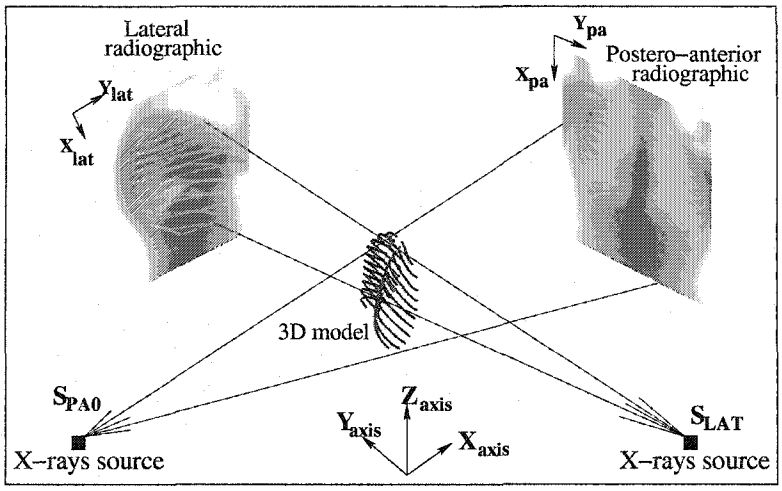

Figure 36 Schematic example of a 3D reconstruction of the scoliotic rib cage

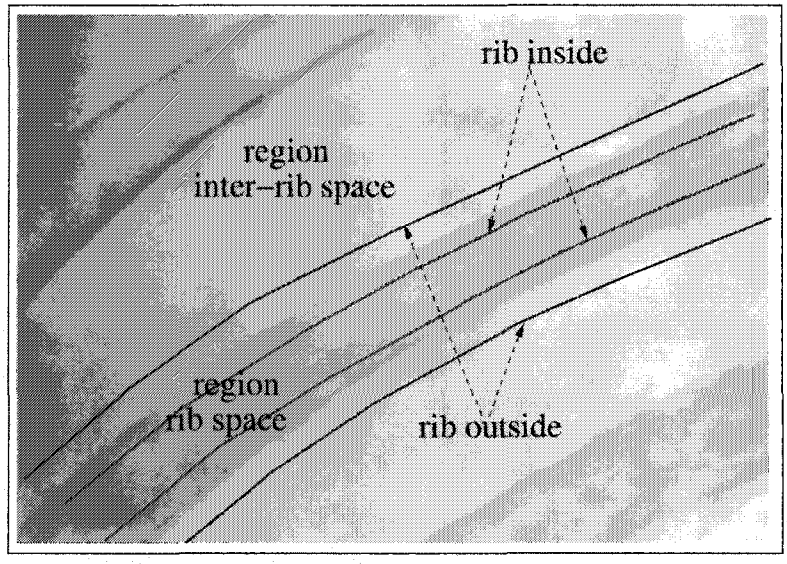

Figure 37 An example demonstrating the use of statistical homogeneity criterion

where $\xi = (\xi_x, \xi_y)$ is the displacement to the nearest edge point in the image, and τ is a smoothing factor which controls the degree of smoothness of this potential field. $\gamma(x, y)$ is the angle between the tangent of the nearest edge and the tangent direction of the contour at (x, y) (Fig. 38). On a lateral radiographic image (I_{LAT}), the ribs are hardly visible and difficult to identify. Moreover, the first rib is occluded by the second rib, and eleventh and

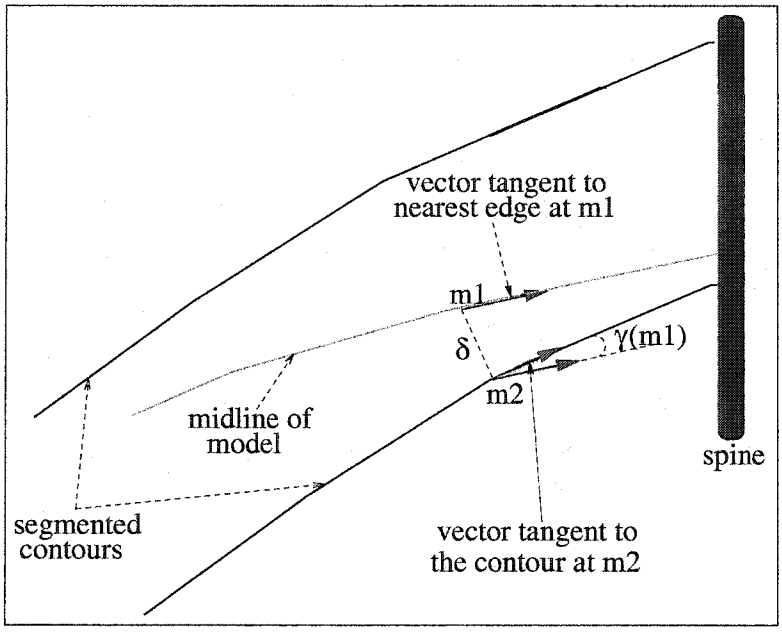

Figure 38 Directional component used in the directional edge potential field Ψ

twelfth ribs are almost completely hidden by the shadow of the abdomen. We cannot rely on the contours or the grey-level homogeneity of each rib as it has been done for I_{PA}.

Instead, we use the likelihood term on I_{LAT} as a kind of constraint and we adopt the following strategy. We use the K-mean clustering procedure to segment I_{LAT} into two homogeneous regions, namely inside and outside the ribcage (with the class label e_{in} and e_{out} for the pixel belonging to the inside and, respectively, outside class). The likelihood energy term for lateral image is then defined by

$$E_l(s_c(\theta), I_{\text{LAT}}) = \frac{1}{n_{\text{LAT}}} \sum_{s \in \Gamma_{\text{LAT}}} \delta(e_s - e_{out}), \tag{5.12}$$

where e_s designates the class label at site s and the summation is overall the n_{LAT} points of the external contour of the lateral projection ($s \in \Gamma_{\text{LAT}}$) of the deformed template on the segmentation of I_{LAT}.

This energy term is minimal when all the points of the external contour of the (laterally) projected deformed template belong to the "inside rib-cage" region.

5.4.5 3D Reconstruction

The only supervision required by our proposed reconstruction method consists in placing manually, using a simple graphical interface, a rectangular bounding box including the whole rib cage for the I_{LAT} and I_{PA0} radiographic images. Using the center of the two rectangular bounding boxes, we estimate the 3D point coordinates corresponding to these two projected centers by the Direct Linear Transformation (DLT) [5]. This estimated center is then considered as the center of the 3D model. We then use the likelihood matching energy defined in Section 5.4.4 in order to fit the two projections of an instance of the deformable model with the two corresponding radiographic images. (Fig. 36). This matching problem leads to a set of K optimization problems (one for each detected class of pathological deformations) which is efficiently solved in our application with an exploration/selection algorithm (see Section 5.5). The optimal 3D reconstruction corresponds to the solution, leading to the minimal energy, amongst these K optimization problems, namely,

$$E_{\text{optimal}}(s_c(\theta)) = \arg\min_{c} \{ \arg\min_{\theta} E(s_c(\theta)) \}.$$

5.5 Optimization strategy

For each considered class-conditional prior model of pathological deformations c ($c \in [1, \ldots, K]$), the unsupervised 3D reconstruction procedure is stated as an energy function minimization problem, namely

$$E(s_c(\theta)) = E_l(s_c(\theta), I_{\text{PA}}) + E_l(s_c(\theta), I_{\text{LAT}}) + \beta E_p(s_c(\theta)), \tag{5.13}$$

where E_l is the likelihood energy term, E_p is the prior energy term (or regularization term) restricting the deformation of the prior model s_c. β is a factor allowing to control the balance between the two energy components and the rigidity of the deformable template.

The energy function to be minimized is a complex function with several local extrema over the deformation parameter space. A global search is usually impossible due to the

size of the configuration space. Instead, we have implemented the exploration/selection algorithm (E/S).

The E/S algorithm belongs to the class of evolutionary algorithms. This class of algorithm has been successfully applied in diverse areas such as medical imaging [74], localization of shapes [32][31], non photorealistic rendering [72], and 3D reconstruction of the scoliotic spine [8].

The E/S algorithm can be summarized as follows (more details are given in [79]). Let F be a finite discrete subset of the Cartesian product of ς compact intervals $[m_i, M_i]$, for $1 \leq i \leq \varsigma$, and $\theta = \{\theta_1, \ldots, \theta_n\}$ be a set of n potential solutions randomly chosen. We define $\hat{\theta}$ as the minimal element θ_i of θ such that $E(s_c(\theta_j)) > E(s_c(\theta_i))$, for $1 \leq j < i$, and $E(s_c(\theta_j)) \geq E(s_c(\theta_i))$, for $1 < j \leq n$. We consider a graph G defined on F called the *exploration graph*. The exploration graph is assumed to be non-oriented and connected. We denote by $\mathcal{N}(a)$ the neighborhood of the element $a \in F$ in the graph G defined by [31] $\{b \in F$: for some j, $|b_j - a_j| \leq r(M_j - m_j)$, $b_i = a_i$, $i \neq j\}$ where r is a real number in interval [0,1] called the radius of exploration.

Each solution of θ is regarded as an individual that attempts a random search on the exploration graph [79]. For $b \in F$, we fix a positive distribution a_b on $\mathcal{N}(b)$. The exploration process acts independently on each individual, and consists of choosing a random N according to the binomial distribution $bin(n, p)$ where n is the size of the population and p is the probability of exploration. We replace θ_i by $\vartheta_i \in \mathcal{N}(\theta_i) \setminus \{\hat{\theta}\}$ according to the uniform distribution, for $i \leq N$ otherwise, we change θ_i by $\hat{\theta}$. This process is running until a criterion is met.

5.6 Validation

The validation of the accuracy of our 3D reconstruction method is a difficult task because a scanned rib cage database is not available.

In our application, our 3D reconstruction technique is validated by visual examination and also by comparing the reconstructed model obtained by our method and by the model resulting from the stereo-radiographic reconstruction technique developed in [24]. The validation procedure consists in fitting the model of our 3D reconstruction method on the model resulting from the stereo-radiographic technique for the same scoliotic patient using quaternion method [51].

5.7 Experimental results

5.7.1 Rib cages database

The training database consists of 532 ($u = 532$) scoliotic rib cages. All rib cages have the same number of ribs (11 right ribs and 11 left ribs). Midline of each rib is composed of 30 points. The 3D coordinates of midline points of each rib cage were recorded in a specific order. The positions of the landmarks of all rib cages within the database are expressed in the same coordinate system.

The 3D geometry of each rib cage within our database is obtained using the 3D reconstruction technique developed in [24]. The accuracy of this technique was evaluated using radio-opaque markers. The mean and standard deviation were 1.01 mm and 0.72 mm [24].

5.7.2 Radiographic images

In our application, we used two radiographic images (i.e., a postero-anterior with normal incidence and a lateral) acquired with a Fuji FCR 7501S radiographic imaging system. The radiographic image illustrates the superposition of the various structures on a same plan and gives place to semi-transparent images. The matrix size of our radiographic images is 2140×880 pixels (coded on 256 gray levels).

5.7.3 Calibration

In our application, the calibration of the radiological environment is done using the 3D coordinates of each steel bead of calibration object previously measured and their corre-

sponding 2D observations on each radiographic views (preliminarily detected) in order to solve the equation

$$(x, y, \mu)^T = D(\vartheta, \kappa) \times (X, Y, Z)^T,$$

for each view. μ is the X-ray tube distance, ϑ and κ being, respectively, the scale and rotation vectors. (x, y) are the image coordinates of a point relative to the principal point. The rotation vector ϑ and the scale κ are regrouped in the 3×3 dimensional matrix $D(\vartheta, \kappa)$. (X, Y, Z) are the object space coordinates. Once the projection equations are calculated, the 3D coordinates of any landmark identified and matched on more than one digital radiography are obtained by finding the intersection between each linear transformation of that particular point.

5.7.4 Comparison protocol

We have validated our 3D reconstruction method on a testing database (disjoint of the training database) of 20 pairs of calibrated radiographic images from scoliotic patients. We use the comparison protocol described in [7]. This comparison uses the distance (mean, and maximum) between a point from the reconstructed rib cage and the surface of the rib cage obtained with the stereo-radiographic reconstruction method [24].

5.7.5 Experimental Results

Figs. 33(a), 33(b), and 33(c) show reduced dimension of clusters as a function of the reconstruction error using different number of clusters when the rib cage training database is partitioned into $K = 8$, 10, and 12 clusters respectively. We note that for a fixed K, the reduced dimension of each cluster decreases when the reconstruction error increases. The

reduced dimensions, associated to each different class (for a reconstruction error ensuring less than $\varrho = 17.5\%$ error[4]) is presented in Table 14.

Table 14

Reduced dimension for each detected class (cluster) of the PPCA mixture

class	1	2	3	4	5	6	7	8	9	10	11	12
reduced dim.	19	14	11	13	10	14	14	7	16	16	16	16

Figs 39 and 42 show two examples of 3D reconstruction of rib cage of two scoliotic patients, for each detected class of pathological deformations. Figs 40 and 43 show the optimal 3D reconstruction corresponding to Figs 39 and 42 respectively.

The 12 deformation classes of the rib cage learned on the training dataset are shown in Fig. 35. For the experiments, we have chosen $\beta = 0.1$ for the weighting factor penalizing the prior energy term with respect to the likelihood energy term, and $\eta = 1$ for the weighting factor allowing to control the balance between the two likelihood energies (contour-based and region-based).

We have used the Canny edge detector to estimate the edge map which is then used for the estimation of the edge *potential fields* on postero-anterior view (used in the likelihood energy term). In our application, $\sigma = 1$, the mask size is 5×5, and the lower and upper thresholds are given by the unsupervised estimation technique proposed in [13]. For the E/S algorithm, we fix the size of population to 100 and the number of iterations to 100.

The 3D reconstruction of a scoliotic rib cage takes about 6 minutes on a 2.0 GHz PC workstation running Linux. We have validated our 3D reconstruction method on a database

[4]Let us clarify that it is not a geometrical reconstruction error. If V_T is the sum of the eigenvalues, then the number m of eigenvalues to be selected is such that,

$$\frac{\sum_{i=1}^{m} \lambda_i}{V_T} \geq (1 - \varrho).$$

of 20 pairs of calibrated radiographic images (postero-anterior and lateral) of scoliotic patients. The mean, and maximum errors between points from the reconstructed rib cage and the surface of the rib cage obtained with stereo-radiographic are, respectively, (1.62 ± 0.50), and (3.62 ± 1.02) mm.

5.8 Discussion and Conclusion

In this paper, we have presented a new technique for the 3D reconstruction of scoliotic rib cage from two radiographic projections I_{PA} and I_{LAT}. This method efficiently exploits the estimation of a mixture of PPCA for both dimensionality reduction and to constrain the 3D reconstruction problem. The proposed 3D reconstruction problem is viewed as a set of optimization problems, each one associated and constrained by a specific class of pathological deformations observed on a representative training scoliotic rib cage population and efficiently detected by the MPPCA method. Our 3D reconstruction method has the advantage of minimizing the X-ray dose (only two radiographic images) and the time needed for digitization and supervision required when compared to that of other reconstruction methods. The results obtained in our experiments are quite encouraging and indicate that accurate unsupervised 3D reconstruction is technically feasible. This is an important improvement compared to the method presented by Mouren [77] or [24].

Let us note that there are several classification systems of spinal deformities [98], but these systems could not be applied for the classification of the rib cage deformities. In our application, the number K of deformation classes (i.e., the number of components in the mixture of PPCA) is chosen empirically, namely $K = 12$, by inspection of the rib cage database and also by the good reconstruction results (in term of accuracy) that we are able to obtain. An extension of this work would be to automatically estimate the number of class of the deformation mixture.

The stereo-radiographic method presented in [24] has been validated on a sample of 7 isolated ribs, by comparing the model obtained from stereo-radiographic method and those

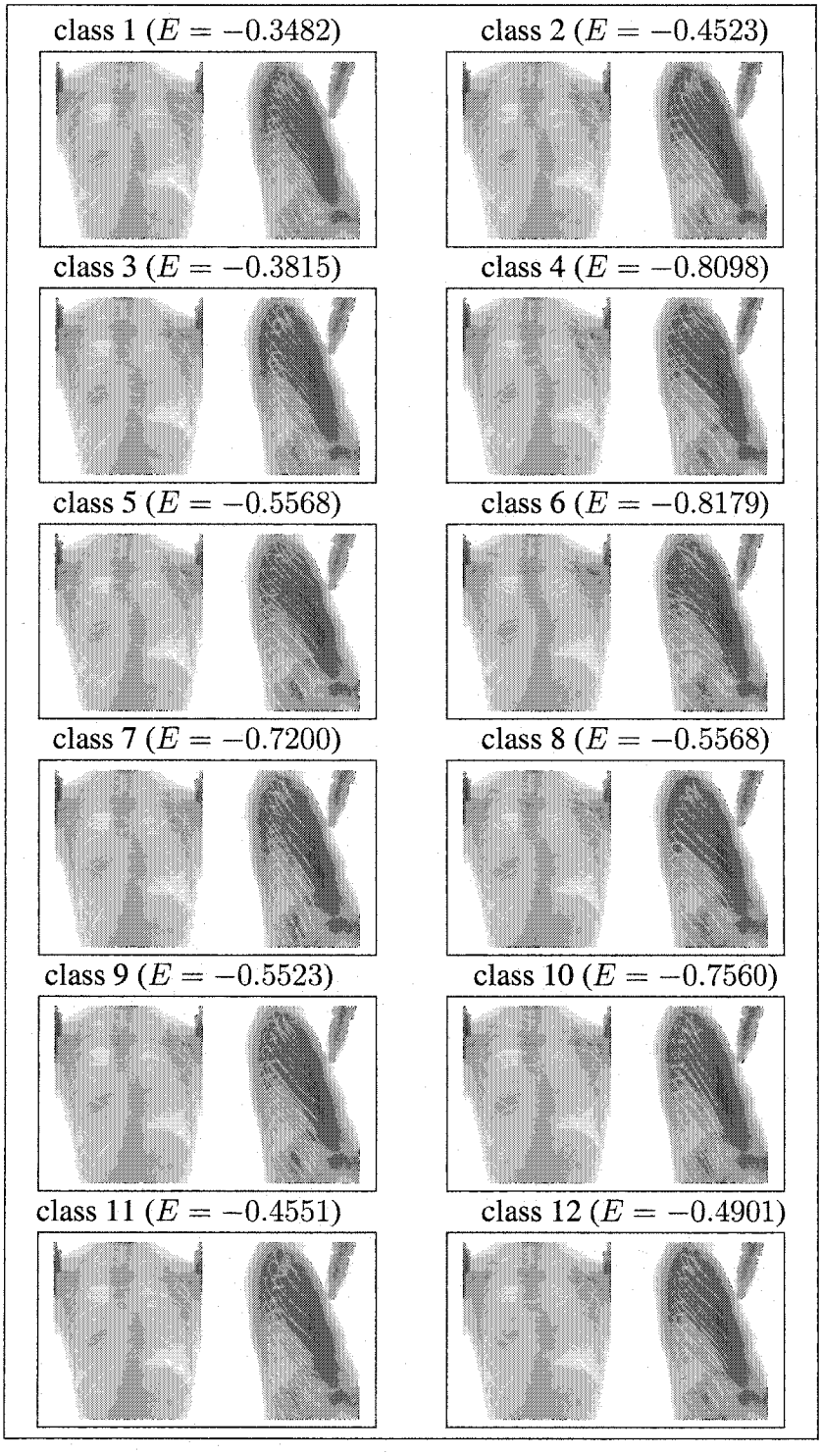

Figure 39 Projections of reconstructed scoliotic rib cage on postero-anterior and lateral images for each detected class of pathological deformations with energy value corresponding. The optimal 3D reconstruction corresponds to the class 6

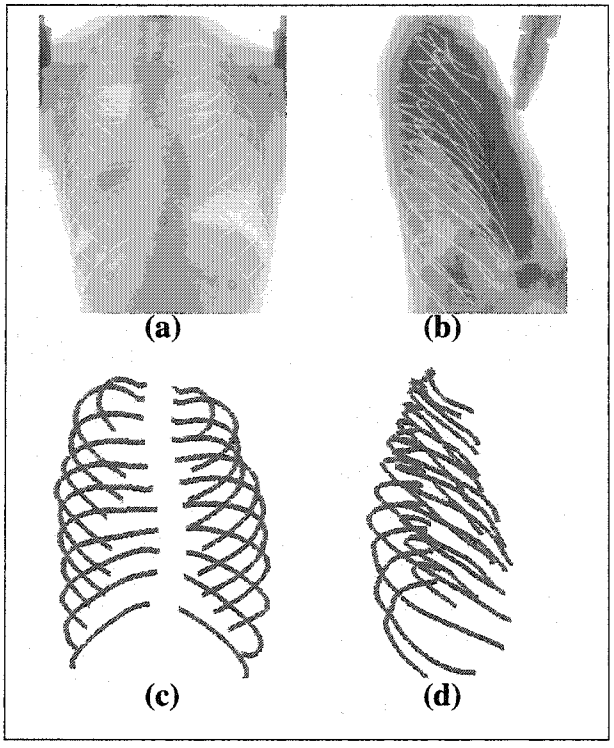

Figure 40 Optimal 3D reconstruction corresponds to the class 6 in Figure 39. **(a)** Projections of reconstructed scoliotic rib cage on postero-anterior image, **(b)** Projections of reconstructed scoliotic rib cage on lateral image, **(c)** and **(d)** Visualization of the reconstructed scoliotic rib cage from the coronal and sagital view

obtained with radio-opaque markers. The mean and standard deviation were 1.01 mm and 0.72 mm. It has also been validated on a sample of 24 ribs by two digitalizations of the different costal lines. The mean difference between the two 3D models obtained was 1.22 mm and standard deviation was 1.04 mm. In our validation, we have used this supervised 3D reconstruction method (whose procedure is summarized in the introduction) as reference for the validation of our reconstruction model. The mean, and maximum errors of our method are, respectively, (1.62 ± 0.50), and (3.62 ± 1.02) mm.

By comparison, the biplanar method proposed in [77] has been only validated on a sample of 20 pairs of synthetic images (in which the authors suppose that poissonian noise in the image is stationary and parameters are known). In their case, the mean and maximum errors are respectively (2.0 ± 0.3) mm, and (18.5 ± 2.3) mm.

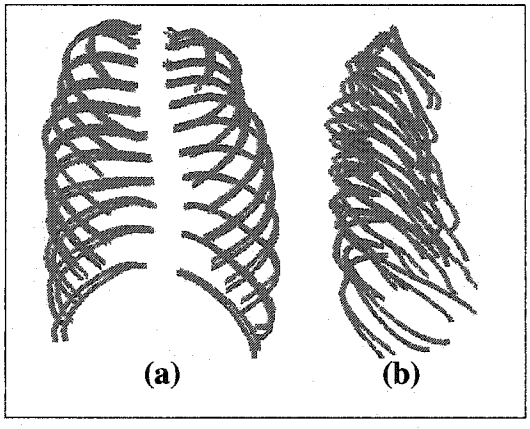

Figure 41 Visual comparison between the 3D reconstruction using our method (red lines) and reference stereo-radiographic (blue lines) corresponds to the class 6 in Figure 39. **(a)** Visualization of the two reconstructed rib cage from the coronal view, **(b)** Visualization of the two reconstructed rib cage from the sagital view

Our proposed scheme thus constitutes an alternative to CT-scan 3D reconstruction with the advantage of low irradiation and will be of great interest for diagnosis of spinal deformities, simulation of orthopedic treatments, and for reliable geometric models for finite element studies. However, this reconstruction method is not suitable without improvement for surgical navigation applications when compared to CT-scan reconstruction errors of ± 1mm, the gold standard for those applications.

The proposed method remains sufficiently general to be applied to other medical reconstruction problems (i.e., pelvis, knee, etc.) for which a database of the anatomical structure is available (with two or more radiographic views).

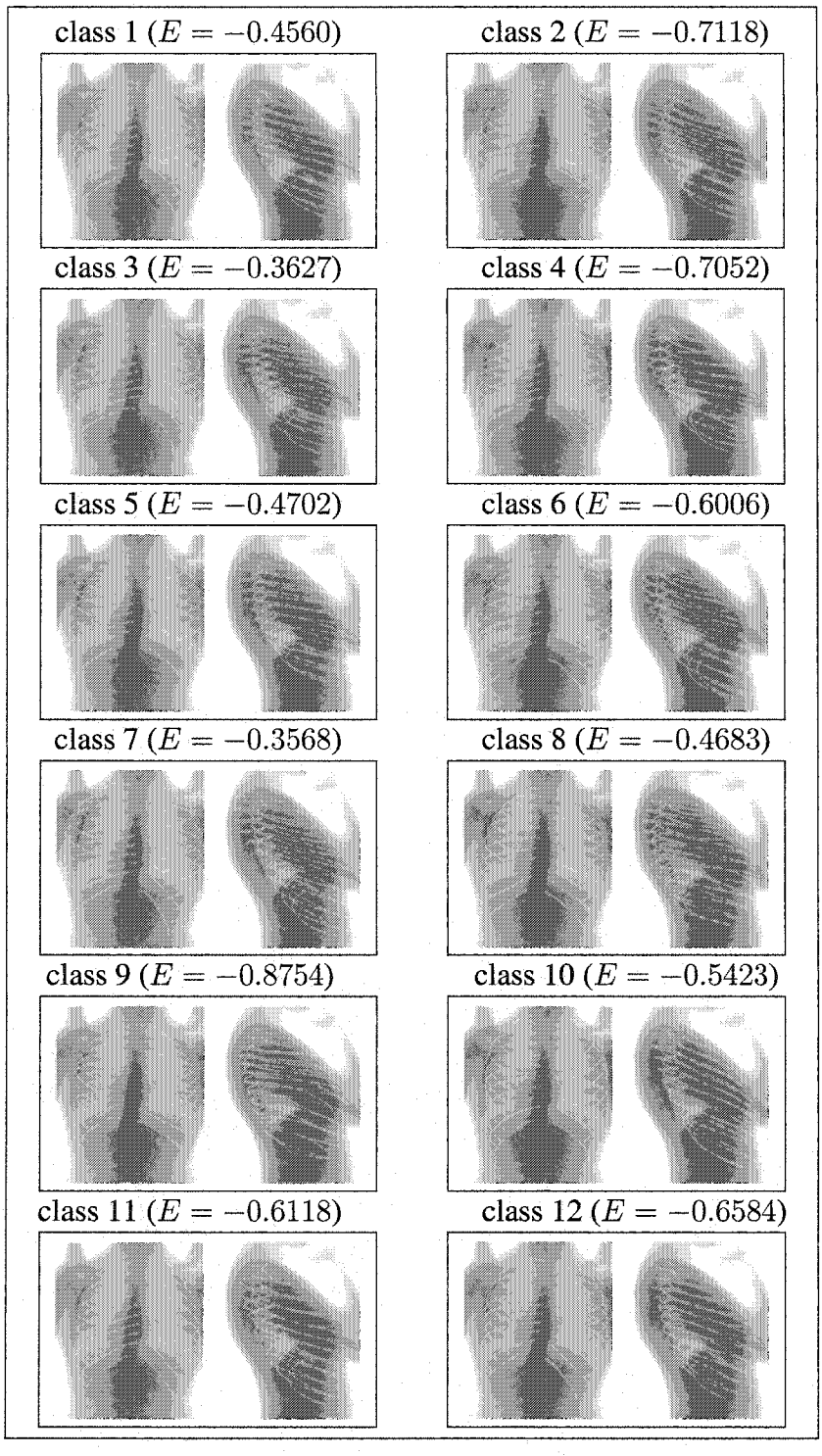

Figure 42 Projections of reconstructed scoliotic rib cage on postero-anterior and lateral images for each detected class of pathological deformations with the corresponding energy value. The optimal 3D reconstruction corresponds to the class 9

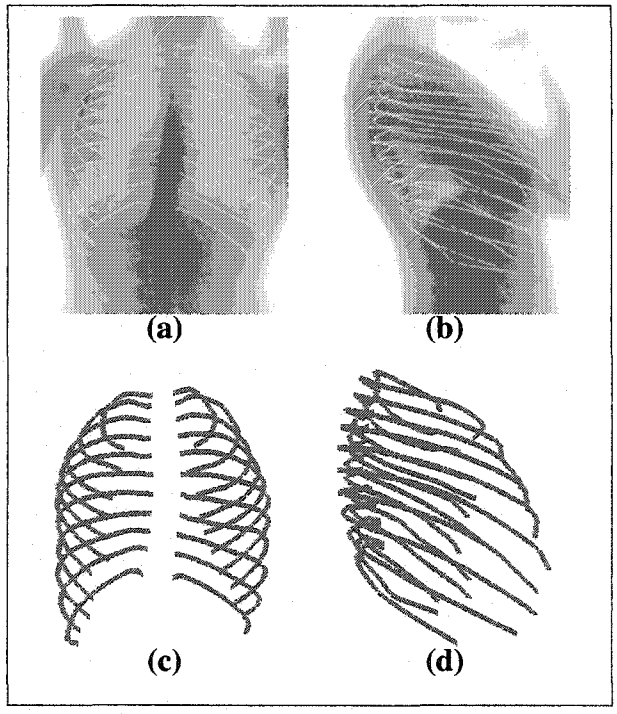

Figure 43 Optimal 3D reconstruction corresponding to the class 9 in Fig. 42. **(a)** Projections of reconstructed scoliotic rib cage on postero-anterior image, **(b)** Projections of reconstructed scoliotic rib cage on lateral image, **(c)** and **(d)** Visualization of the reconstructed scoliotic rib cage from the coronal and sagital view

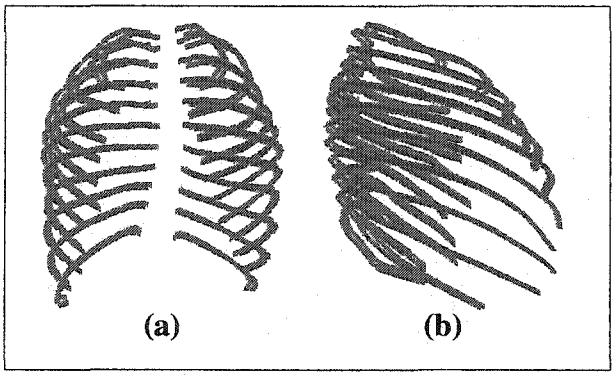

Figure 44 Visual comparison between 3D reconstruction using our method (red lines) and reference stereo-radiographic (blue lines) (corresponding to the class 9 in Fig. 42). **(a)** Visualization of the two reconstructed rib cage from the coronal view, **(b)** Visualization of the two reconstructed rib cage from the sagital view

DISCUSSION GÉNÉRALE

Nous avons présenté dans ce travail de recherche trois approches statistiques pour la reconstruction 3D de la colonne vertébrale et de la cage thoracique scoliotiques à partir de deux images radiographiques conventionnelles (postéro-antérieure avec incidence de $0°$ et latérale). Le problème de reconstruction 3D de la colonne vertébrale scoliotique a tout d'abord été abordé par une méthode supervisée basée sur l'utilisation des contours de vertèbres détectés sur deux images radiographiques conventionnelles et une connaissance géométrique *a priori* de nature statistique de chaque vertèbre. Cette reconstruction 3D est formulée comme un problème de minimisation de fonction d'énergie résolu par un algorithme de descente de gradient. La méthode proposée est validée sur une base de 57 vertèbres lombaires et thoraciques de 13 patients scoliotiques qui ont aussi été reconstruites par la méthode CT-scan pour des fins de comparaison. La méthode s'est avérée performante avec une erreur moyenne de (0.71 ± 0.06) mm pour les vertèbres lombaires et de (1.48 ± 0.27) mm pour les vertèbres thoraciques, ce qui est satisfaisant pour une utilisation en routine clinique. Ces résultats montrent que la reconstruction des vertèbres lombaires obtenues par notre méthode de recalage 3D/2D est plus précise que la méthode non-stéréo-radiographique (NSCP) [75] et la méthode stéréo-radiographique [43] [76]. L'erreur moyenne est de 0.7 mm pour notre méthode, de 1.4 mm pour NSCP, de 2.4 mm pour la méthode stéréo-radiographique [76], et de 2.6 mm pour la méthode stéréo-radiographique [3]. Quelques erreurs maximums obtenues sur des apophyses épineuses sont encore grandes (c'est-à-dire, l'erreur maximum est de 3.9 mm pour les vertèbres lombaires et de 7.9 mm pour les vertèbres thoraciques). Quoique ces erreurs maximums correspondent à des points n'ayant pas de rôle significatif dans la planification de chirurgie, la précision de la reconstruction est relativement acceptable, comparativement aux résultats obtenus avec la méthode CT-scan qui est considérée comme la méthode la plus précise de reconstruction 3D. Nous remarquons que les résultats sont meilleurs pour les vertèbres lombaires. Pour les vertèbres thoraciques, les contours sont plus difficiles à détecter en

raison de la présence des côtes. En plus, la taille de la base de données des vertèbres, sur laquelle nous avons appliqué une analyse en composantes principales (ACP) pour extraire les déformations statistiquement admissibles, reste insuffisante et ne contient pas toutes les déformations scoliotiques. Une grande partie de notre erreur de reconstruction provient de la base d'apprentissage du fait que quelques déformations scoliotiques n'ont pas été modélisées par l'ACP. Une autre partie de notre erreur de reconstruction est due à l'erreur de reconstruction de la méthode CT-scan qui est considérée nulle dans notre protocole de validation. Néanmoins, nous pouvons observer que les résultats obtenus pour des paramètres morphométriques (importants pour la correction chirurgicale de la scoliose) sont presque comparables à ceux obtenus par CT-scan. Contrairement aux méthodes basées sur la numérisation des repères anatomiques [43] [75] où la reconstruction 3D dépend de l'habilité de l'opérateur, notre méthode utilise des contours de vertèbres détectés automatiquement sur deux images radiographiques et l'information *a priori* est issue d'une base d'apprentissage (30 normales et 30 scoliotiques par niveau vertébral) unique et originale établie avec une grande précision. Ceci constitue une contribution non négligeable apportée par notre méthode. Notons que les paramètres de déformations obtenues par la reconstruction 3D peuvent être utilisés pour étudier la scoliose. Notre méthode s'applique à d'autres structures pourvu qu'une base de données de la structure en question soit disponible.

La méthode présentée est supervisée et ne tient pas compte des paramètres de la vertèbre reconstruite à l'étape précédente. Pour pallier à cette limitation, nous avons présenté une autre méthode originale de reconstruction 3D hiérarchique, statistique et non supervisée des colonnes vertébrales scoliotiques basée sur l'utilisation des contours des vertèbres détectés sur deux images radiographiques conventionnelles et une connaissance globale hiérarchique *a priori* comprenant la structure géométrique de la colonne vertébrale et de chaque niveau vertébral. La nouvelle méthode est basée sur la spécification de deux modèles 3D statistiques. Le premier, un modèle géométrique sur lequel des déformations linéaires globales admissibles sont définies, est utilisé pour une reconstruction grossière

de la colonne vertébrale. Une reconstruction 3D précise est alors réalisée pour chaque niveau vertébral par un deuxième modèle de vertèbre sur lequel des déformations non linéaires admissibles (déformations locales) sont définies. Cette reconstruction 3D est formulée comme un double problème de minimisation de fonction d'énergie efficacement résolus par un algorithme stochastique d'exploration/selection. La méthode proposée est validée sur la même base que la première méthode et s'est avérée performante avec une erreur moyenne de (1.45 ± 1.46) mm pour les vertèbres lombaires et de (1.27 ± 1.29) mm pour les vertèbres thoraciques, ce qui est aussi satisfaisant pour une utilisation en routine clinique.

La reconstruction 3D nécessite un temps de calcul de l'ordre de 28 secondes sur une station de travail PC à 2.0 GHz sous Linux pour une vertèbre. En comparant ces résultats à ceux de la méthode précédente [8], nous constatons que la précision de la première est meilleure que celle de la deuxième méthode. Ceci est dû au fait que la méthode précédente [8] est supervisée et exige la connaissance de la position de six repères anatomiques stéréo-correspondants par vertèbre (centroïdes des plateaux vertébraux, sommets des pédicules) sur les deux images radiographiques pour l'initialisation de chaque vertèbre dans l'environnement radiographique en vue d'une reconstruction 3D. Par exemple, la reconstruction 3D du segment de vertèbres (L5/.../T1) nécessite la connaissance de la position de 102 repères anatomiques alors qu'avec cette deuxième méthode, il suffit de connaître la position du centroïde des plateaux vertébraux de la première vertèbre du segment sur les deux images radiographiques. Une contribution importante apportée par cette deuxième méthode est que la reconstruction 3D est non supervisée et permet une reconstruction 3D des segments de la colonne vertébrale. Aussi, cette deuxième méthode s'applique à d'autres structures pourvu qu'une base de données de la structure en question soit disponible.

Finalement, nous avons présenté une méthode originale de reconstruction 3D non supervisée des cages thoraciques scoliotiques à partir de deux images radiographiques con-

ventionnelles (postéro-antérieure avec incidence de 0° et latérale). Dans ce modèle, nous avons posé l'hypothèse que chacune des formes de cage thoracique associée à une pathologie de scoliose possible, et liée à une déformation globale et spécifique de la colonne vertébrale, est distribué dans une classe de déformation spécifique, pour laquelle nous avons ensuite défini une réduction de dimensionnalité linéaire classique telle qu'une technique d'ACP probabiliste. Dans ce contexte, nous avons utilisé un mélange d'ACP probabiliste dont chaque composante de ce mélange représente un type de déformation particulière de scoliose. Les paramètres du mélange d'ACP probabiliste sont estimés par une version stochastique de l'algorithme EM (Expectation, Maximization) appelée SEM. La reconstruction 3D optimale correspond à la classe de la déformation et aux paramètres menant à l'énergie minimale d'une fonction d'énergie heuristiquement définie. Due à l'absence d'une base de cages thoraciques scoliotiques numérisées, la méthode proposée a été validée sur un échantillon de 20 paires d'images radiographiques et comparée aux reconstructions 3D issues de la méthode stéréo-radiographique. Une erreur moyenne de (1.62 ± 0.50) mm a été obtenue sur les distances point-surface entre le modèle reconstruit avec notre méthode et le modèle issu de la reconstruction stéréo-radiographique.

La reconstruction 3D d'une cage thoracique scoliotique nécessite un temps de calcul de l'ordre de 6 minutes sur une station de travail PC à 2.0 GHz sous Linux. Une contribution importante apportée par cette méthode est que d'une part la reconstruction 3D est non supervisée et utilise seulement deux images radiographiques (postéro-antérieure avec incidence de 0° et latérale) ainsi qu'une base d'apprentissage de 532 cages thoraciques scoliotiques, unique dans la littérature. D'autre part, l'utilisation de mélange d'ACP probabiliste, dont les paramètres sont estimés par l'algorithme SEM (Stochastic, Expectation, Maximization), pour la définition d'un mélange de modèle *a priori* de formes 3D pour la régularisation de notre problème de reconstruction 3D n'avait été jusqu'à maintenant jamais été utilisée. En plus de la reconstruction 3D, cette méthode permet un classement implicite et probabiliste de chacune des pathologies scoliotiques existantes dans la base d'apprentissage.

La qualité des contours extraits des deux images radiographiques est la principale limite des approches statistiques proposées dans cette thèse. Ce qui explique les erreurs de reconstruction observées au niveau des vertèbres et des cages thoraciques. Ainsi, le manque de visibilité dans les images radiographiques latérales rend leur segmentation très difficile. Outre cette limite, la taille de la base d'apprentissage par niveau vertébral ne permet pas de représenter toutes les déformations possibles générées par la scoliose.

Principales contributions

Dans le premier article (cf. Chap. 2), nous proposons une méthode statistique de reconstruction 3D des vertèbres scoliotiques à partir de I_{PA} et I_{LAT} [7]. Cette méthode est basée sur une connaissance *a priori* globale de la variabilité géométrique de chaque vertèbre scoliotique apprise sur une base d'apprentissage de vertèbres. Le positionnement initial du modèle déformable statistique dans l'espace radiographique est réalisé par l'utilisation de six repères anatomiques (centroïdes des plateaux vertébraux, sommets des pédicules). La méthode de reconstruction proposée consiste à ajuster les projections (postéro-antérieure et latérale) du contour externe de ce modèle *a priori* 3D de chaque niveau vertébral avec les contours correspondants préalablement segmentés sur les deux vues radiographiques. Cette reconstruction 3D est formulée comme un problème de minimisation de fonction d'énergie résolue par un algorithme de descente de gradient simplifié. Une contribution non négligeable apportée par cette méthode est que, d'une part, l'information utilisée est caractérisée par des contours de vertèbres détectés sur deux images radiographiques et l'information *a priori* est issue d'une base d'apprentissage (30 normales et 30 scoliotiques par niveau vertébral) unique et originale établie avec une grande précision [82]. D'autre part, nous avons adapté l'approche de Cootes pour contraindre le problème mal-posé de recalage des modèles 3D de vertèbres scoliotiques sur des images radiographiques biplanaires.

La méthode présentée dans le premier article est supervisée et ne tient pas compte des paramètres de la vertèbre reconstruite à l'étape précédente. Pour pallier cette limitation,

nous présentons dans le deuxième article (cf. Chap. 3) une nouvelle méthode de reconstruction 3D hiérarchique statistique non supervisée des colonnes vertébrales scoliotiques basée sur l'utilisation I_{PA} et I_{LAT} et une connaissance globale hiérarchique *a priori* comprenant la structure géométrique de la colonne vertébrale et de chaque niveau vertébral [8]. La nouvelle méthode est basée sur les spécifications de deux modèles 3D statistiques. Le premier, un modèle géométrique sur lequel des déformations linéaires globales admissibles sont définies, est utilisé pour une reconstruction grossière de la colonne vertébrale. Une reconstruction 3D précise est alors réalisée pour chaque niveau vertébral par un deuxième modèle de vertèbre sur lequel des déformations non linéaires admissibles (déformations locales) sont définies. Cette deuxième étape consiste à ajuster les projections (postéro-antérieure et latérale) du contour externe de ce modèle *a priori* 3D de chaque niveau vertébral avec les contours du niveau correspondant préalablement segmentés sur les deux vues radiographiques. Cette reconstruction 3D est formulée comme un double problème de minimisation de fonction d'énergie efficacement résolu par un algorithme d'optimisation stochastique. Une contribution importante apportée par cette deuxième méthode est que la reconstruction 3D est obtenue par combinaison de deux modèles 3D statistiques. Un modèle 3D grossier est utilisé pour contraindre un modèle 3D plus précis. Cette méthode est de plus non supervisée et permet une reconstruction 3D precise des segments de vertèbres.

La méthode présentée dans le deuxième article n'est pas applicable directement aux cages thoraciques scoliotiques du fait de leur structure géométrique particulière et surtout, des déformations pathologiques associées à celle-ci, étroitement liée à la déformation globale de la colonne vertébrale elle-même. En plus, les données associées à chacune des cages thoraciques de notre base d'apprentissage ne sont pas linéairement distribuées dans l'espace des formes tridimensionnelles possibles. L'ACP ne peut ainsi être efficacement utilisé. Dans le modèle que nous avons proposé, nous avons supposé moins restrictivement que chacune des formes de cage thoracique est liée à une déformation globale et spécifique de la colonne vertébrale. Ces formes sont distribués dans une classe ou une

pathologie possible, pour lesquelles nous avons ensuite défini une réduction de dimensionnalité linéaire. Dans ce contexte nous avons utilisé un mélange d'ACP. Dans cette stratégie, chaque composante de ce mélange représente concrètement un type de déformation particuliere de scoliose. Parmi les différentes classes de déformation, on choisit ensuite la reconstruction 3D correspondante à la classe de la déformation et aux paramètres menant au minimum d'une fonction d'énergie. Une contribution importante apportée par cette méthode est que d'une part cette méthode de reconstruction 3D est non supervisée et utilise seulement deux images radiographiques (postéro-antérieure avec incidence de 0° et latérale) ainsi qu'une base d'apprentissage de 532 cages thoraciques scoliotiques, ce qui est unique dans la littérature. D'autre part, l'utilisation de mélange d'ACP probabiliste, dont les paramètres sont estimés par l'algorithme SEM (Stochastic, Expectation, Maximization), pour la définition d'un mélange de modèle *a priori* de forme 3D pour la régularisation de notre problème de reconstruction 3D n'avait, à notre connaissance, jamais été utilisé. En plus de la reconstruction 3D, cette méthode permet un classement implicite et probabiliste de chacune des déformations scoliotiques existantes dans la base d'apprentissage.

CONCLUSION GÉNÉRALE ET PERSPECTIVES

Le but de cette thèse a été de développer et valider une méthode de reconstruction 3D de la colonne vertébrale et de la cage thoracique scoliotiques à partir de deux images radiographiques conventionnelles calibrées (postéro-antérieure avec incidence de 0° et latérale).

Nous avons présenté dans cette thèse trois approches statistiques pour la reconstruction 3D de la colonne vertébrale et de la cage thoracique scoliotiques à partir de deux images radiographiques conventionnelles calibrées (postéro-antérieure avec incidence de 0° et latérale).

La première approche est une méthode supervisée basée sur l'utilisation des contours de vertèbres détectés sur deux images radiographiques conventionnelles et une connaissance géométrique *a priori* de nature statistique de chaque vertèbre. La méthode est ensuite validée sur une base de 57 vertèbres scoliotiques reconstruites par la méthode CT-scan. La seconde approche est une méthode originale de reconstruction 3D hiérarchique, statistique et non supervisée des colonnes vertébrales scoliotiques basée sur l'utilisation des contours des vertèbres détectés sur deux images radiographiques conventionnelles et une connaissance globale hiérarchique *a priori* comprenant la structure géométrique de la colonne vertébrale et de chaque niveau vertébral. Elle est basée sur la spécification de deux modèles 3D statistiques. Le premier, un modèle géométrique sur lequel des déformations linéaires globales admissibles sont définies, est utilisé pour une reconstruction grossière de la colonne vertébrale. Une reconstruction 3D précise est alors réalisée pour chaque niveau vertébral par un deuxième modèle de vertèbre sur lequel des déformations non linéaires admissibles (déformations locales) sont définies. La méthode est ensuite validée sur une base de 57 vertèbres scoliotiques reconstruites par la méthode CT-scan. La troisième approche est une méthode originale de reconstruction 3D non supervisée des cages thoraciques scoliotiques à partir de deux images radiographiques conventionnelles (postéro-antérieure avec incidence de 0° et latérale) en utilisant un mélange d'ACP probabiliste. La méthode est

ensuite validée sur un échantillon de 20 paires d'images radiographiques et comparée aux reconstructions 3D issues de la méthode stéréo-radiographique.

Les méthodes de reconstruction 3D présentées offrent une représentation précise de la structure osseuse et utilisent seulement deux images radiographiques conventionnelles (postéro-antérieure avec incidence de 0° et latérale), alors que le système de tomographie scanner à trois dimensions nécessite, quant à lui, entre 300 et 500 images pour obtenir une même image tridimensionnelle infographique. Les méthodes proposées dans cette thèse sont donc moins irradiantes et moins coûteuses.

De ce fait, les risques de cancer liés à une trop grande quantité d'expositions aux rayons X s'en trouvent réduits. Cela constitue un avantage non négligeable pour les personnes qui doivent passer fréquemment des radiographies, comme celles souffrant d'arthrose, de scoliose ou ayant subi des blessures liées à la pratique d'un sport.

De plus, les méthodes de reconstruction 3D proposées peuvent être appliquées à différentes structures osseuses tels que le bassin, le genou, la hanche, etc. pourvu que la base d'apprentissage de la structure osseuse en question soit disponible.

Finalement, les modèles géométriques issues des méthodes de reconstruction 3D pourront être utilisés pour des études morphométriques poussées, la chirurgie assistée par ordinateur et pour la modélisation mécanique de l'effet des traitements orthopédiques et chirurgicaux.

Pour assurer la continuité de ce travail de recherche, on pourrait proposer:

- d'évaluer les méthodes proposées sur des images radiographiques multi-énergie dont la qualité est meilleure;

- de valider la reconstruction 3D des cages thoraciques scoliotiques sur une base de cages thoraciques scoliotiques numérisées en utilisant des mesures d'indices géométriques (gibbosité, angles d'inclinaison, etc.);

- d'augmenter la taille de la base d'apprentissage de chaque niveau vertébral;

- de donner une interprétation médicale au classement implicite et probabiliste des classes de déformation existantes dans la base d'apprentissage;

- d'étudier la possibilité d'estimer le nombre de classes dans le mélange d'ACP probabiliste;

- d'étendre la méthode de reconstruction 3D proposée à des structures osseuses de taille plus importante comme le bassin par une approche hiérarchique tant pour le modèle *a priori* [25] de formes que pour le modèle de vraisemblance;

- d'étudier éventuellement l'intérêt d'un mélange de formes hiérarchiques probabilistes, en combinant un mélange d'ACP probabiliste et une approche hiérarchique [25], pour une technique 3D hiérarchique de recalage.

ANNEXES

ANNEXE 1

GLOSSAIRE DE TERMES

CT-Scan: (abréviation de Computed Tomography scan) Modalité d'imagerie permettant d'acquérir une série d'images détaillées des

régions intérieures du corps pris de différents angles; les images sont créées par un ordinateur lié à une machine de rayon X.

IRM: (abréviation de Imaging Resonance Magnetic) Modalité d'imagerie non invasive dont les ondes radio et un aimant puissant ont lié à un ordinateur sont utilisés pour créer les images détaillées des régions intérieures du corps. Ces images peuvent montrer la différence entre le tissu normal et malade.

Segmentation: Processus de tracer et de marquer des régions d'image en tant que structures distinctes.

Recalage: Détermination d'une transformation géométrique ou d'alignement entre deux espaces quelconques de telle manière que des points dans l'un des espaces soient alignés avec les points (homologues) correspondants dans l'autre espace.

Reconstruction 3D: Consiste à établir une transformation géométrique reliant les plans images d'un objet et sa représentation en 3D.

ANNEXE 2

ANATOMIE

Structure de Base de la Structure Osseuse

Les structures osseuses sont des organes composés de tissu vivant dur. Elles protègent et soutiennent les organes du corps. C'est une matrice des sels de calcium déposés autour des fibres de protéine. Les minéraux rendent la structure osseuse rigide et les protéines fournissent la force et l'élasticité. La couche externe de la structure osseuse s'appelle structure osseuse cortical. 80% de la masse squelettique de la structure osseuse est structure osseuse cortical. La structure spongieuse intérieure représente 20% de la masse de la structure osseuse. Les cavités intérieures de la structure osseuse contiennent la moelle où des globules rouges sont produites.

Colonne Vertébrale

La colonne vertébrale (rachis) constitue avec le crâne le squelette axial postérieur. Elle se divise en quatre segments, de haut en bas : le rachis cervical formé de 7 vertèbres ; le rachis thoracique (ou dorsal) formé de 12 vertèbres sur lesquelles s'appuient les côtes ; le rachis lombaire, formé de 5 vertèbres ; le segment sacro-coccygien constitué du sacrum et du coccyx formé de vertèbres soudées (5 vertèbres pour le sacrum, et 4 ou 5 vertèbres pour le coccyx) (voir Figure 45)[1].

Vertèbre

La vertèbre est formée en avant d'un corps vertébral et d'un arc osseux postérieur. Le corps vertébral est essentiellement constitué de substance spongieuse, délimitant des espaces remplis de tissu hématopoïétique. Les faces supérieures et inférieures du corps constituent les plateaux vertébraux. L'arc postérieur est formé de deux pédicules, de deux lames vertébrales, d'un apophyse épineux, de deux apophyses transverses et de quatre apophyses articulaires (voir Figure 46)[2].

[1] http://www.orthopaedics-scoliosis.com/content/scoliosis_information.html

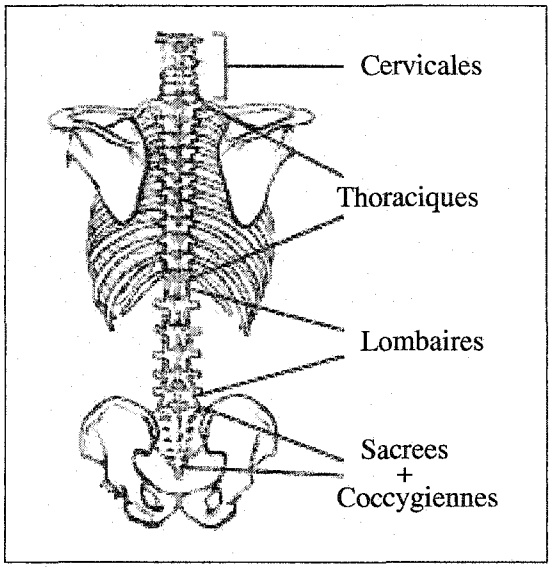

Figure 45 Vue postéro-antérieure de la colonne vertébrale et cage thoracique

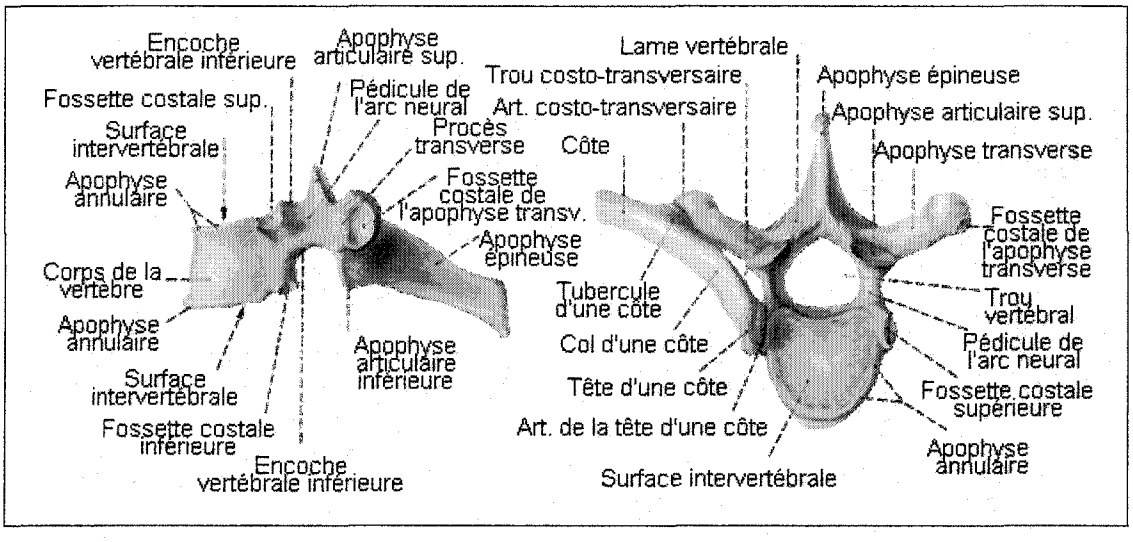

Figure 46 Vues postéro-antérieure et latérale d'une vertèbre

Cage Thoracique

Ensemble du squelette du thorax formé par le sternum en avant, les vertèbres thoraciques en arrière, et les arcs costaux latéralement. On dénombre 12 paires de côtes (gauches et

droites) réparties en trois catégories : les vraies côtes, soit les 7 premières (C1 à C7), chacune s'articulant directement avec le sternum par le biais d'un cartilage; les fausses côtes (C8 à C10), rattachées au sternum par un cartilage commun; les côtes flottantes (C11 et C12) dont l'extrémité antérieure reste libre (voir Figure 47)[2].

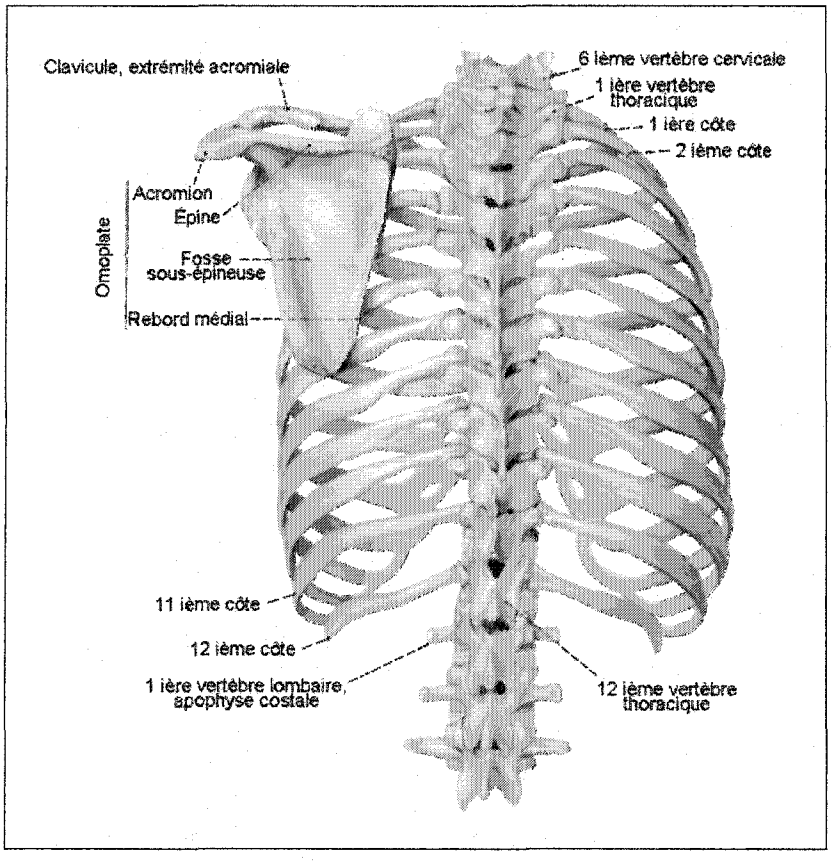

Figure 47 Vue postéro-antérieure de la cage thoracique

[2]http://www.cegep-baie-comeau.qc.ca/bio/Anatomie%20corps%20humain%20cd/dos.html

ANNEXE 3

ALGORITHMES D'ALIGNEMENT DE FORMES

Nous présentons dans cette annexe les algorithmes utilisés dans notre application pour aligner des formes sur une forme moyenne. L'algorithme présenté dans la Table 15 permet d'aligner les formes $s_1, \ldots, s_l$ ayant un même nombre de points 3D sur une forme moyenne. L'algorithme présenté dans la Table 18 permet de trouver les valeurs du facteur d'échelle $\mathbf{k}$, de la matrice de rotation $\mathbf{R}$ (regroupées dans la matrice de transformation $M(\mathbf{k}, \mathbf{R})$) et de vecteur de translation $\mathbf{T}$ qui minimise $|M(\mathbf{k}, \mathbf{R})[s_1] - \mathbf{T} - s_2|$. L'algorithme présenté dans la Table 16 permet de calculer de calculer les quaternions. L'algorithme présenté dans la Table 17 permet de calculer les composantes q_0, q_1, q_2, q_3 du quaternion q. Les formes $s_1, \ldots, s_l$ ont le même nombre n de points 3D et sont représentés par des matrices de dimension $3 \times n$. Les matrices A de dimension 3×3, D de dimension 3×1, M de dimension 3×3, Q de dimension 4×4, R de dimension 3×3 et T de dimension 3×1 sont utilisés dans les trois algorithmes suivants.

Table 15

Algorithme de calcul de forme moyenne.

Algorithme de calcul de forme moyenne

$s_1, \ldots, s_l$ Échantillon de formes ayant un même nombre de points 3D
$\bar{s}$ Forme moyenne

1. Calcul du centre géométrique c_1 de la forme s_1.
2. Translater la forme s_1 vers le point c_1.
3. Poser $\bar{s} = s_1/|s_1|$.

Répéter

1. Aligner chaque forme s_i avec $\bar{s}$; c'est-à-dire, trouver les valeurs du facteur d'échelle $\mathbf{k}$, de la matrice de rotation $\mathbf{R}$ (regroupées dans la matrice de transformation $M(k, R)$) et de vecteur de translation $\mathbf{T}$ qui minimise $|M(\mathbf{k}, \mathbf{R})[s_i] - \mathbf{T} - \bar{s}|$ (voir l'algorithme d'alignement), et remplacer s_i par $M(\mathbf{k}, \mathbf{R})[s_i] - \mathbf{T}$.
2. Calculer la forme moyenne $\bar{s}$ des s_i obtenus.
3. Normaliser la forme moyenne $\bar{s}$.

Jusqu'à *convergence de* $\bar{s}$;

Table 16

Algorithme des quaternions.

Algorithme des quaternions

---

s_1, s_2 Deux formes contenant un même nombre de points 3D

1. Calcul des centres géométriques c_1 et c_2 des formes s_1 et s_2 respectivement.
2. Ajuster les formes s_1 et s_2 pour que les centres géométriques soient c_1 et c_2 respectivement.
3. Calcul de trace $trace(M)$ où $M = s_1 \times s_2^T$.
4. Poser $A = M - M^T$.
5. Poser
   $Q(0,0) = trace(M), Q(0,1) = A(1,2), Q(0,2) = A(2,0), Q(0,3) = A(0,1)$
   $Q(1,0) = A(1,2), Q(2,0) = A(2,0), Q(3,0) = A(0,1)$
   $Q(1,1) = M(0,0) + M(0,0) - 1 \times trace(M)$
   $Q(2,1) = M(1,0) + M(0,1) - 0 \times trace(M)$
   $Q(3,1) = M(2,0) + M(0,2) - 0 \times trace(M)$
   $Q(1,2) = M(0,1) + M(1,0) - 0 \times trace(M)$
   $Q(2,2) = M(1,1) + M(1,1) - 1 \times trace(M)$
   $Q(3,2) = M(2,1) + M(1,2) - 0 \times trace(M)$
   $Q(1,3) = M(0,2) + M(2,0) - 0 \times trace(M)$
   $Q(2,3) = M(1,2) + M(2,1) - 0 \times trace(M)$
   $Q(3,3) = M(2,2) + M(2,2) - 1 \times trace(M)$

Table 17

Algorithme de calcul des composantes du quaternion.

Algorithme de calcul des composantes du quaternion

Q	Matrice de dimension 4×4
q_0, q_1, q_2, q_3	Composantes du quaternion q

1. Algorithme des quaternions pour calculer la matrice Q.
2. Effectuer la décomposition en valeurs singulières de la matrice Q : $Q = UDV^T$, où U est une matrice dont les colonnes sont vecteurs unitaires orthogonaux, tout comme pour la matrice V, et D est une matrice diagonale avec des éléments réels sur la diagonale, d_i, tels que : $d_1 \geq d_2 \geq \ldots \geq d_4 \geq 0$.
3. Poser
   $mini = 4$ ($mini$ est l'indice du plus grand élément de D),
   $q_0 = V(0, mini)$;
   $q_1 = V(1, mini)$;
   $q_2 = V(2, mini)$;
   $q_3 = V(3, mini)$;

Table 18

Algorithme d'alignement.

Algorithme d'alignement de deux formes 3D

s_1, s_2	Deux formes contenant un même nombre de points 3D
k	Facteur d'échelle
R	Matrice de rotation
T	Vecteur de translation

1. Algorithme de calcul des composantes q_0, q_1, q_2, q_3 du quaternion.
2. Calcul des centres géométriques c_1 et c_2 des formes s_1 et s_2 respectivement.
3. Calcul du facteur d'échelle $\mathbf{k} = \sqrt{\sum_{i=1}^{n}(p_{1,i} - c_1)} / \sqrt{\sum_{i=1}^{n}(p_{2,i} - c_2)}$ où $p_{j,i}$ est le i^{ieme} point de la forme s_j.
4. Calcul de la matrice de rotation

$$\mathbf{R} = \begin{pmatrix} q_0^2 + q_1^2 - q_2^2 - q_3^2 & 2(q_1q_2 - q_0q_3) & 2(q_1q_3 + q_0q_2) \\ 2(q_1q_2 + q_0q_3) & q_0^2 + q_2^2 - q_1^2 - q_3^2 & 2(q_2q_3 - q_0q_1) \\ 2(q_1q_3 - q_0q_2) & 2(q_2q_3 + q_0q_1) & q_0^2 + q_3^2 - q_1^2 - q_2^2 \end{pmatrix}$$

5. Calcul du vecteur de translation $\mathbf{T} = c_2 - R \times c_1$.

ANNEXE 4

RÉSULTATS COMPLÉMENTAIRES

Dans cette annexe, nous présentons les résultats complémentaires de la validation de notre méthode de reconstruction 3D des vertèbres scoliotiques. Les figures suivantes montrent la superposition rigide des vertèbres obtenues par notre méthode hiérarchique statistique (en rouge) et celles obtenues par la méthode CT-scan (en bleu). La figure de gauche montre la vue de dessus, la figure du centre montre la vue latérale et la figure de droite montre la vue postéro-antérieure.

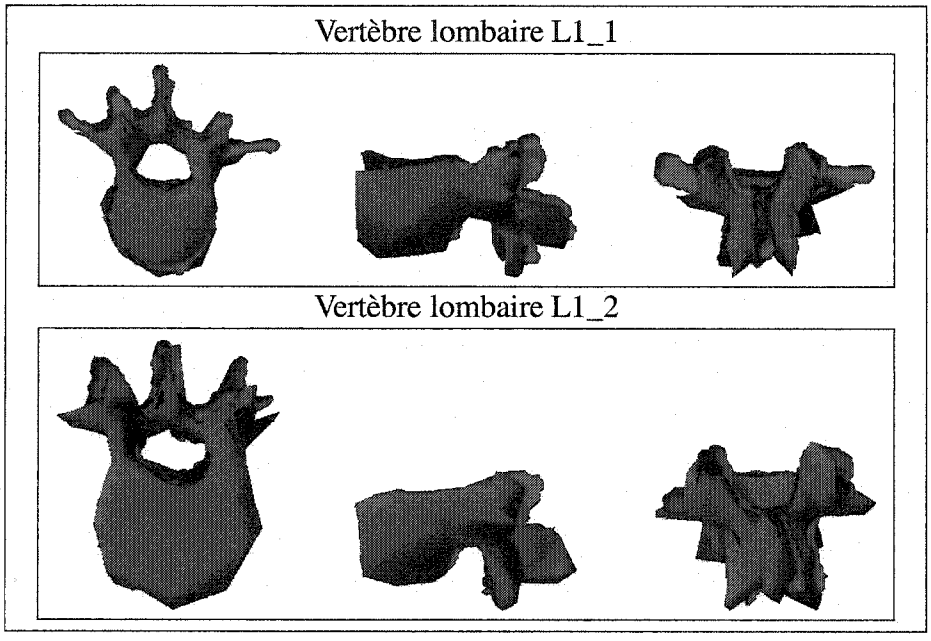

Figure 48 Superposition rigide de la vertèbre L1

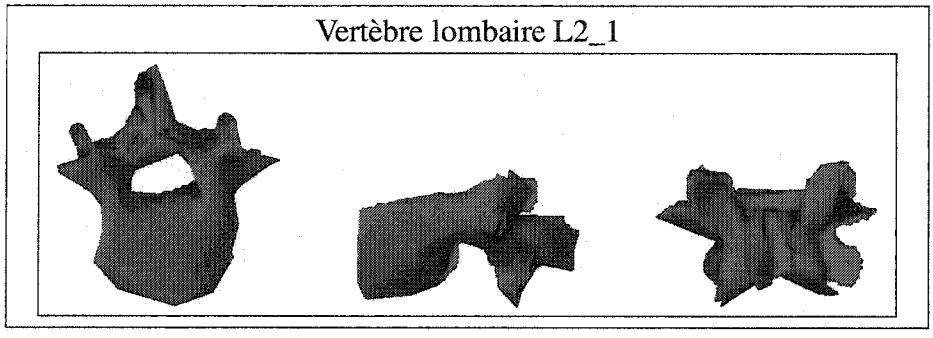

Figure 49 Superposition rigide de la vertèbre L2

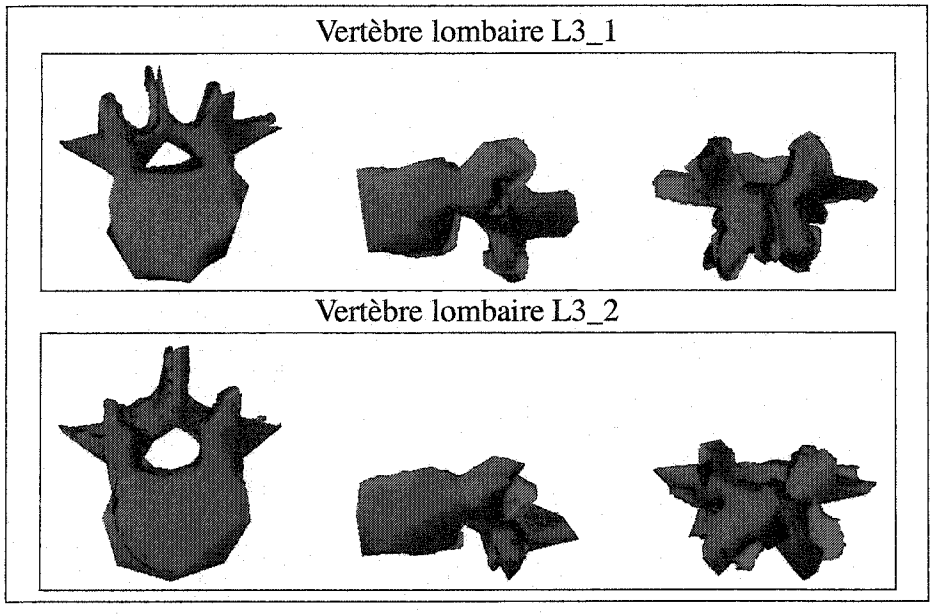

Figure 50 Superposition rigide de la vertèbre L3

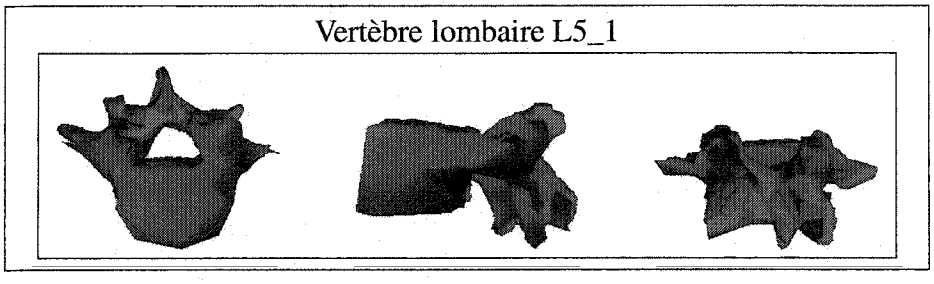

Figure 51 Superposition rigide de la vertèbre L5

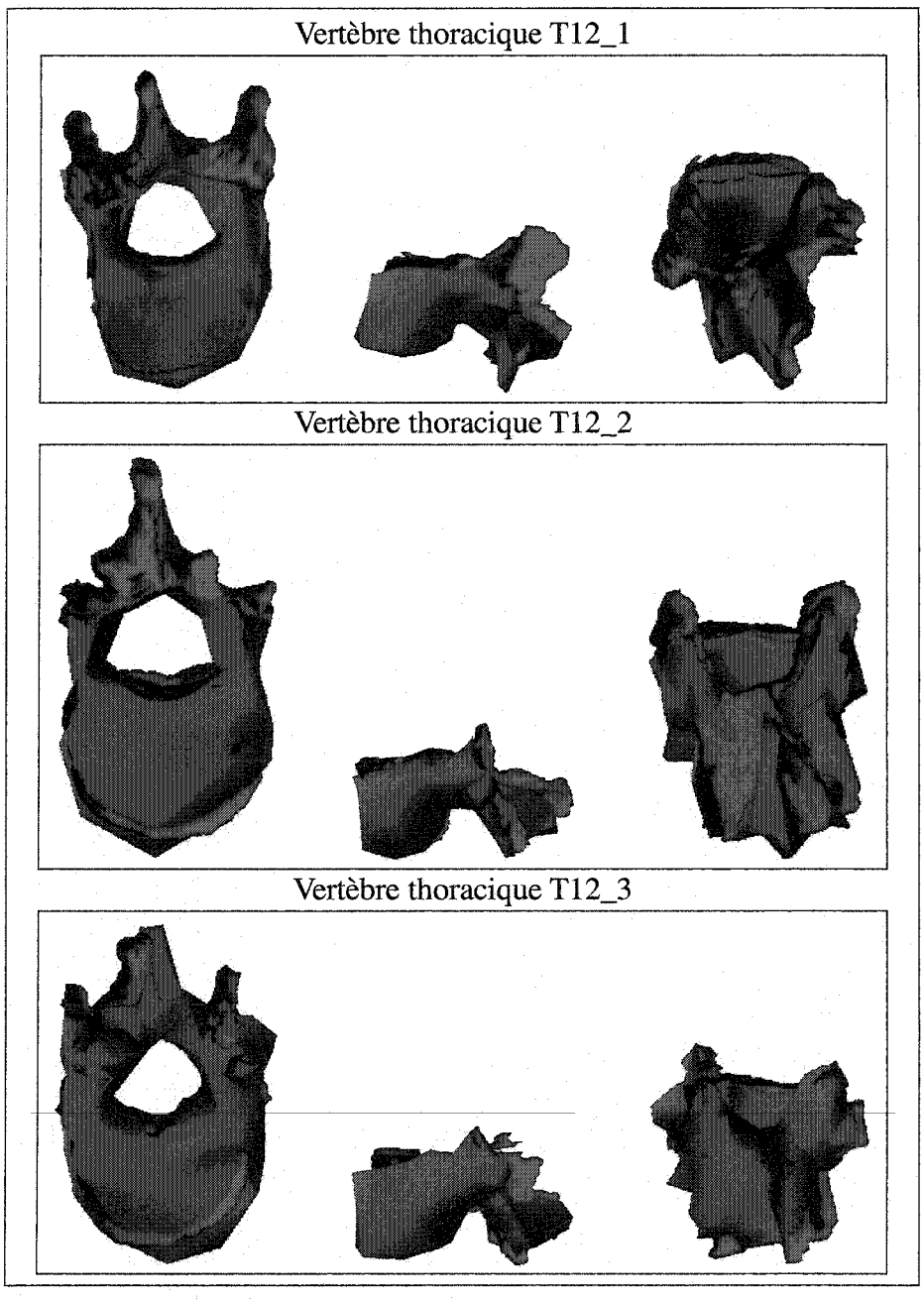

Figure 52 Superposition rigide de la vertèbre T12

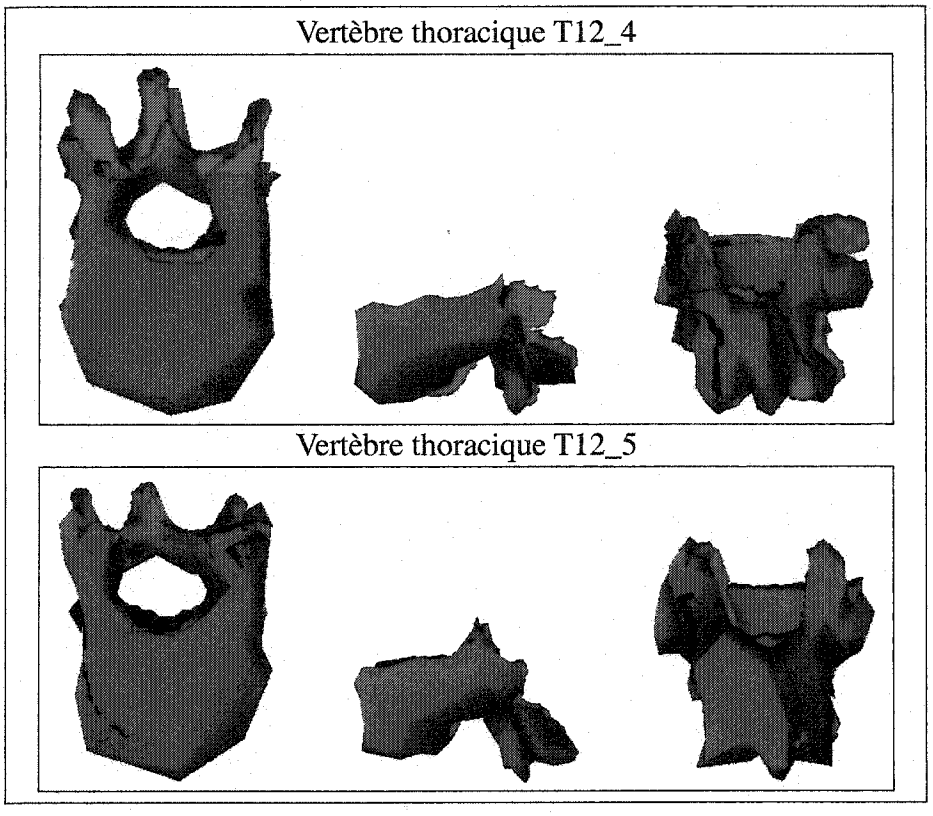

Figure 53 Superposition rigide de la vertèbre T12 (suite)

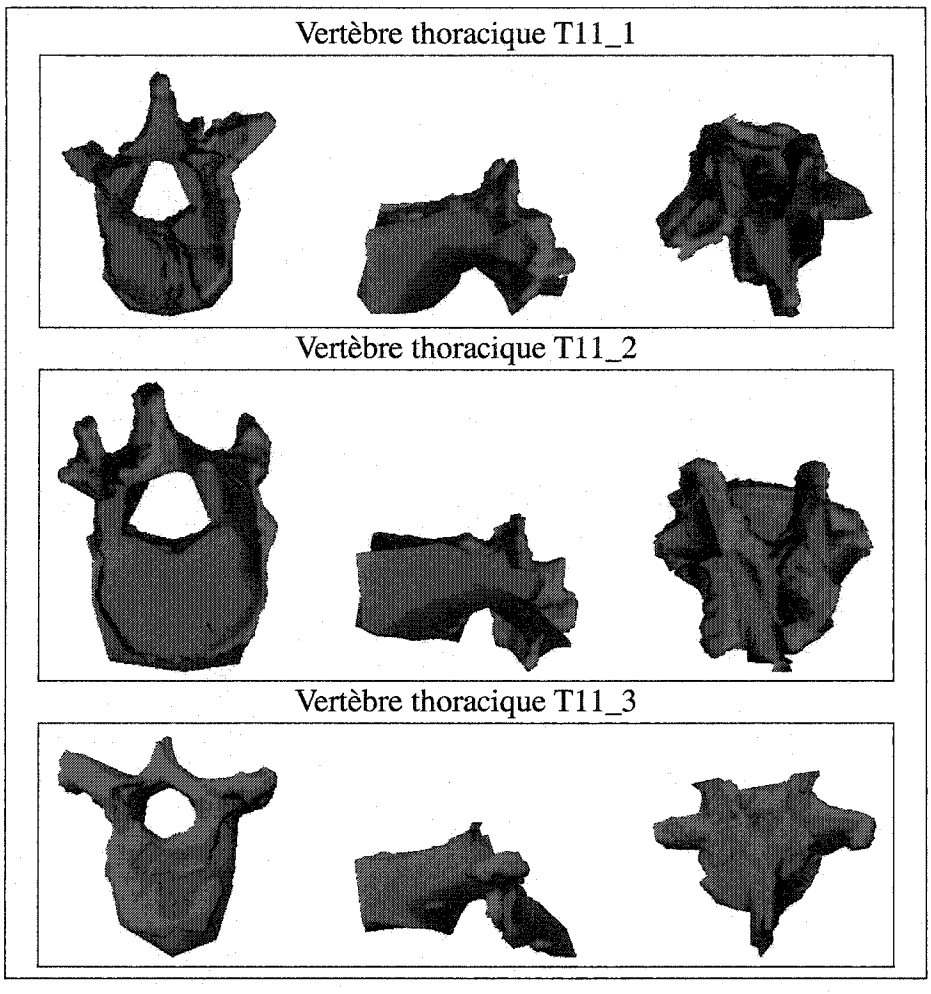

Figure 54 Superposition rigide de la vertèbre T11

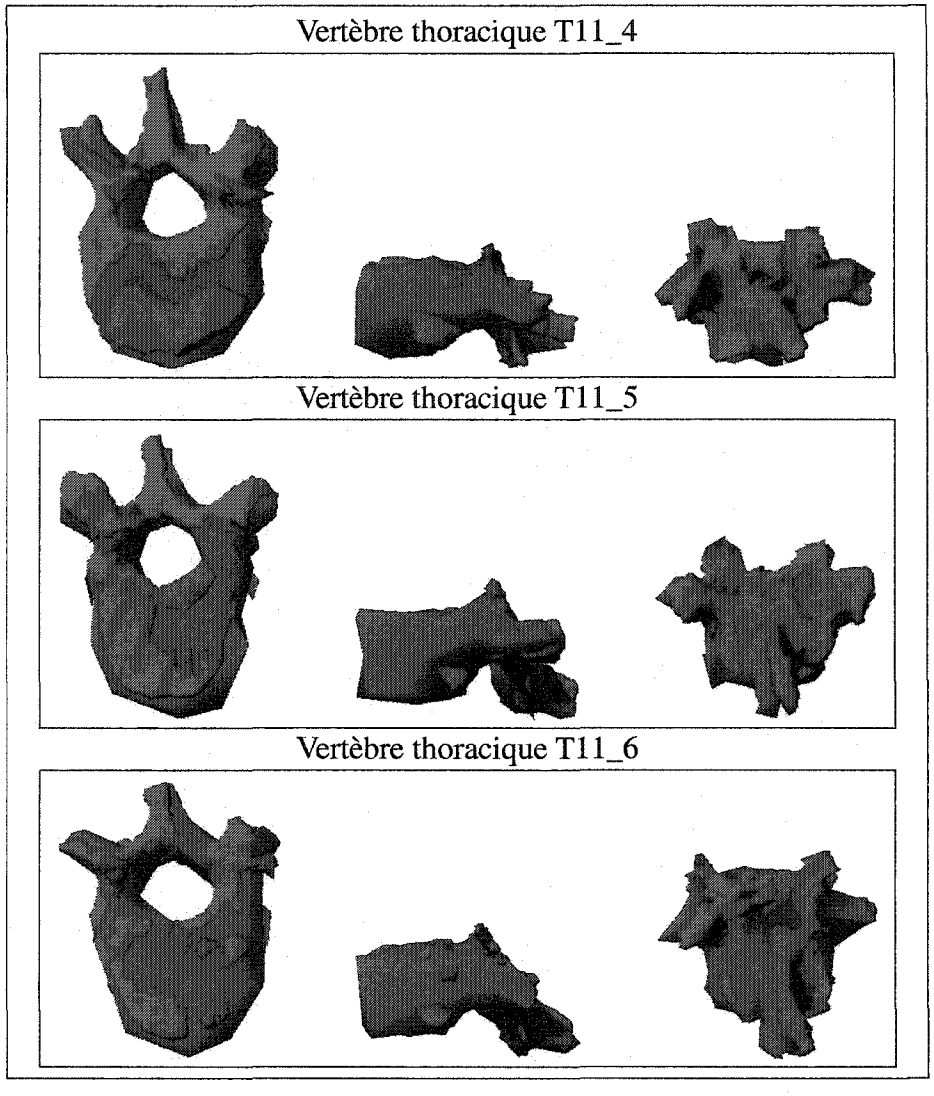

Figure 55 Superposition rigide de la vertèbre T11 (suite)

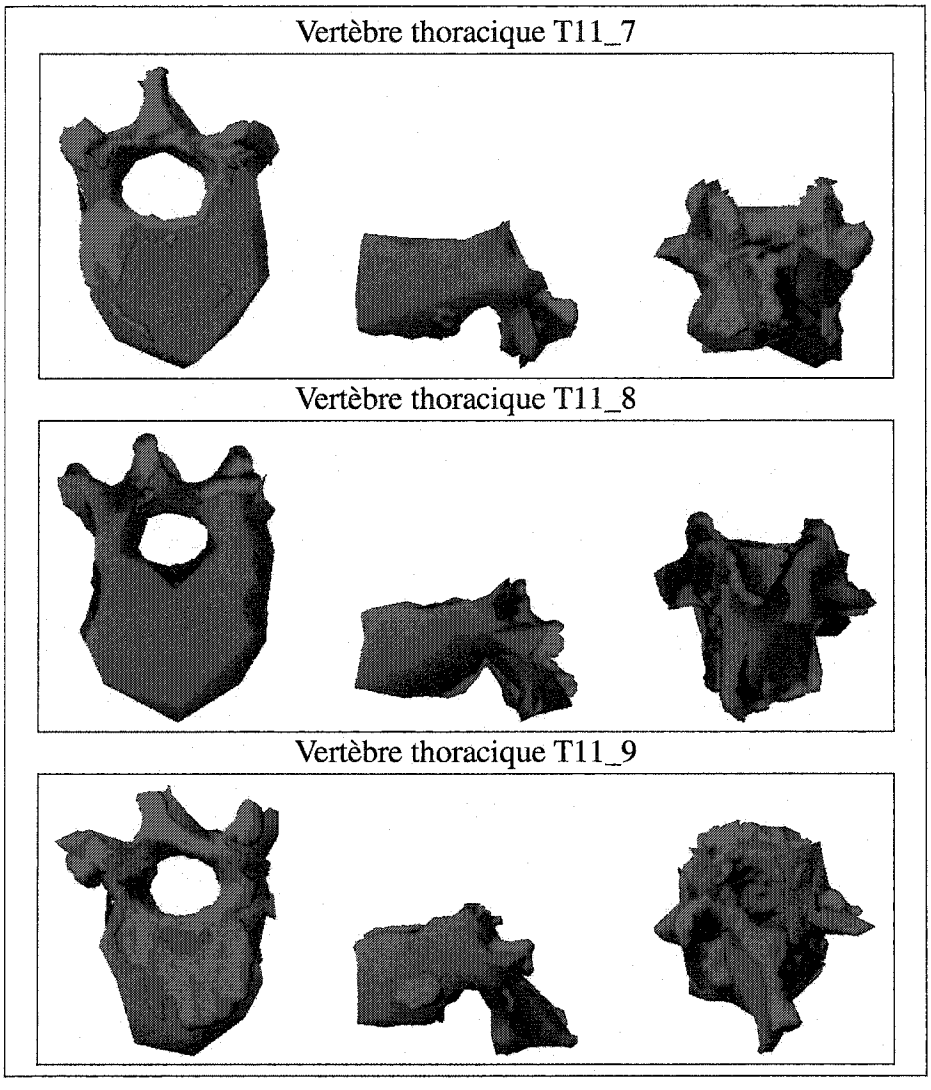

Figure 56 Superposition rigide de la vertèbre T11 (suite)

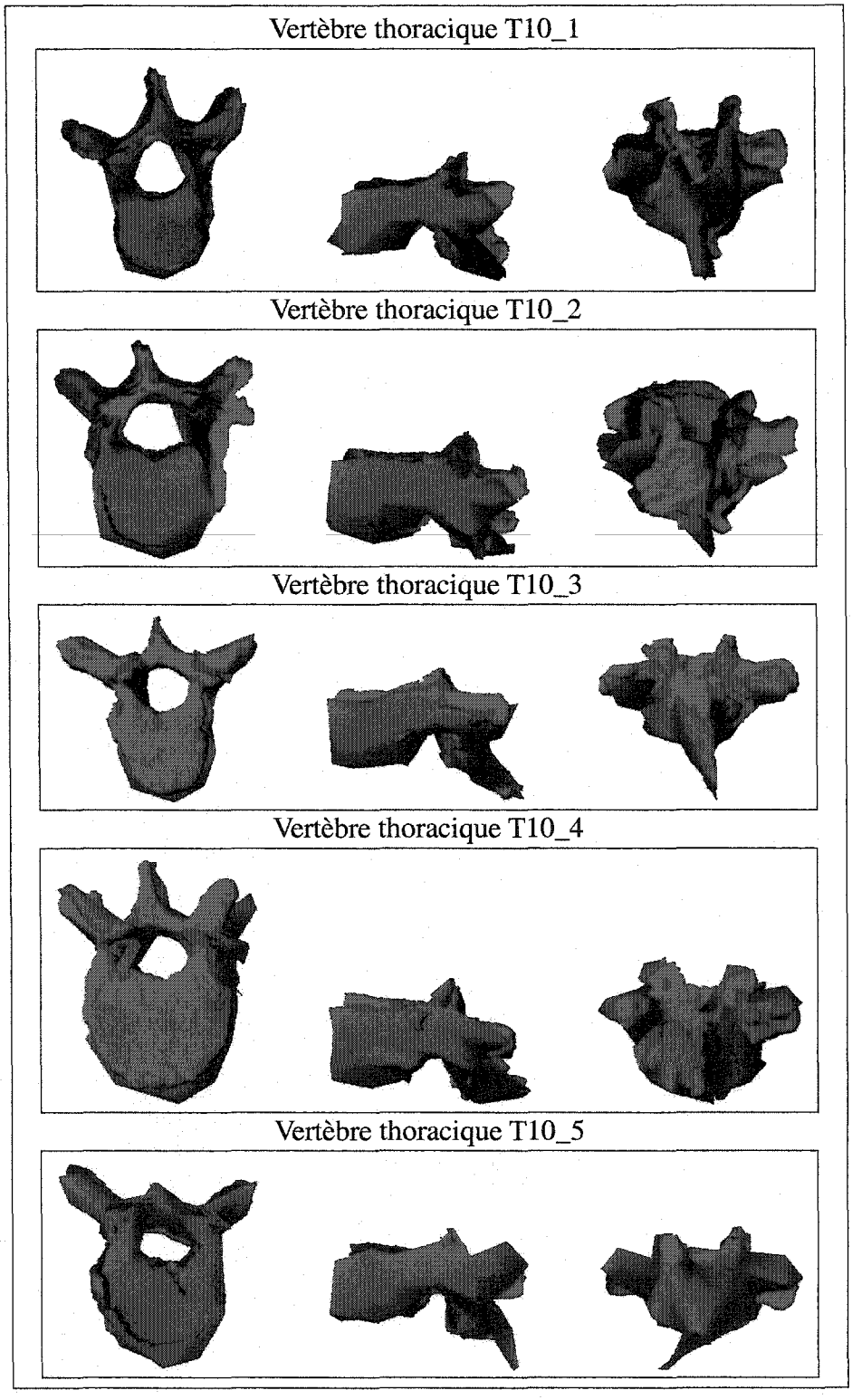

Figure 57 Superposition rigide de la vertèbre T10

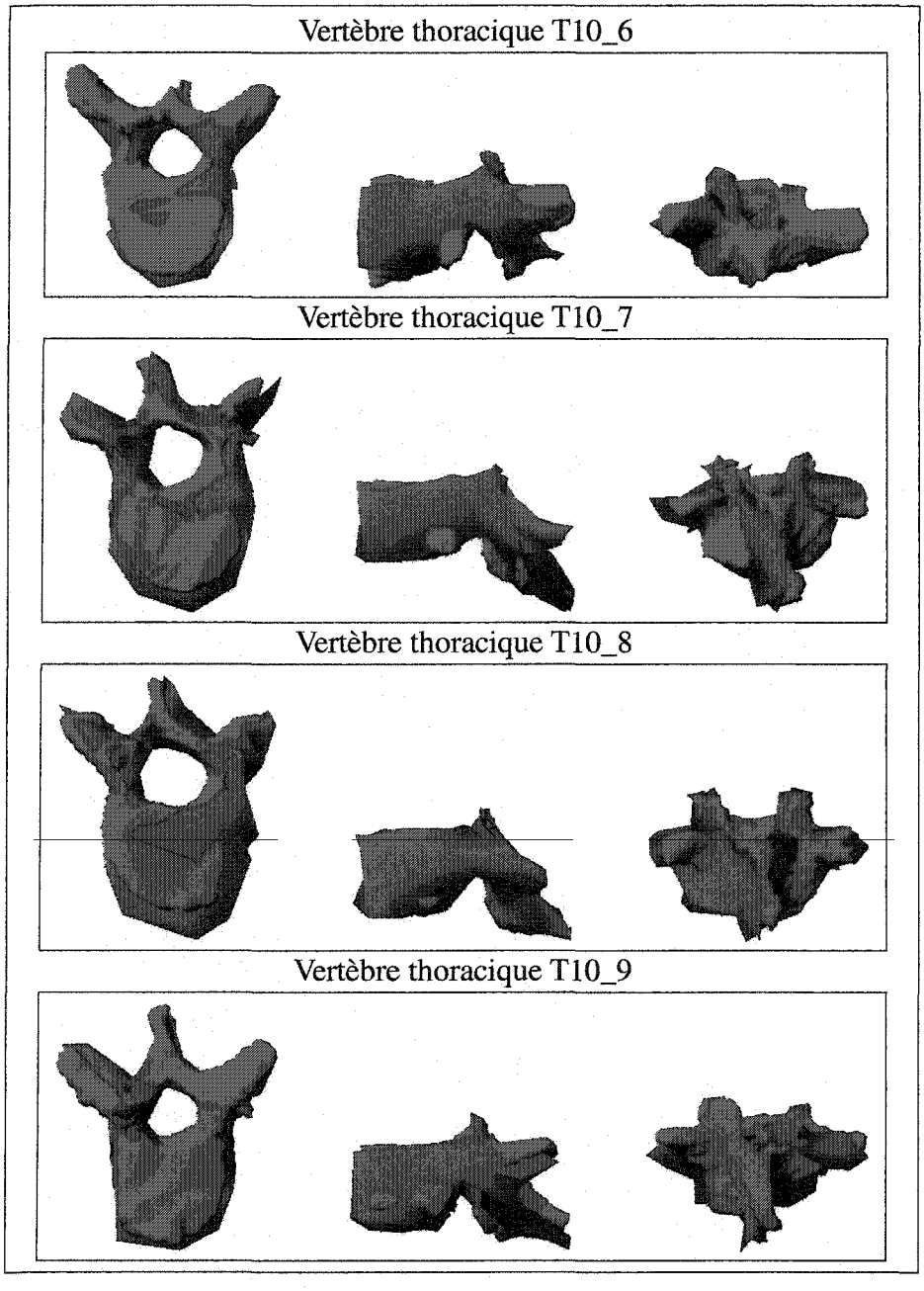

Figure 58 Superposition rigide de la vertèbre T10 (suite)

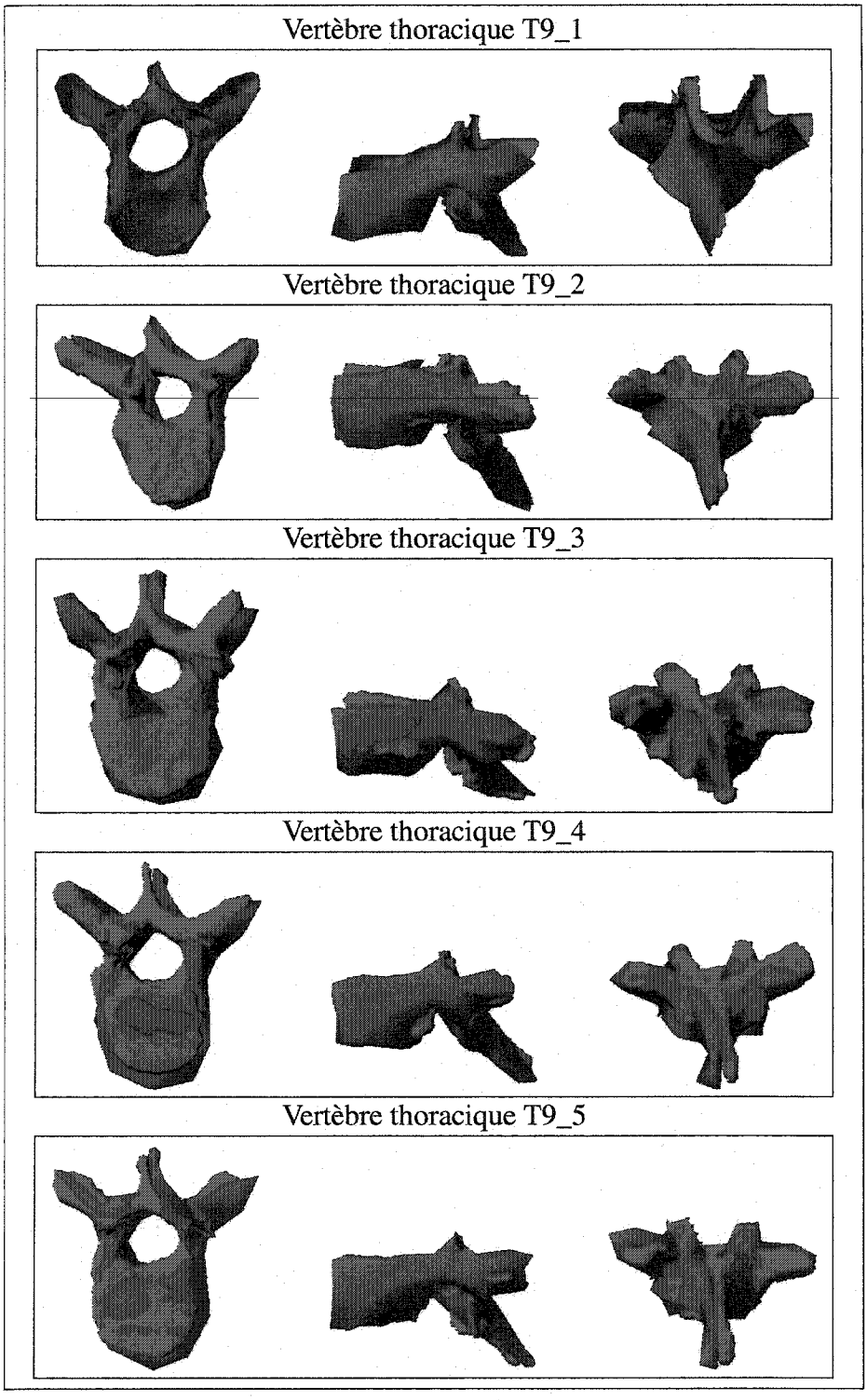

Figure 59 Superposition rigide de la vertèbre T9

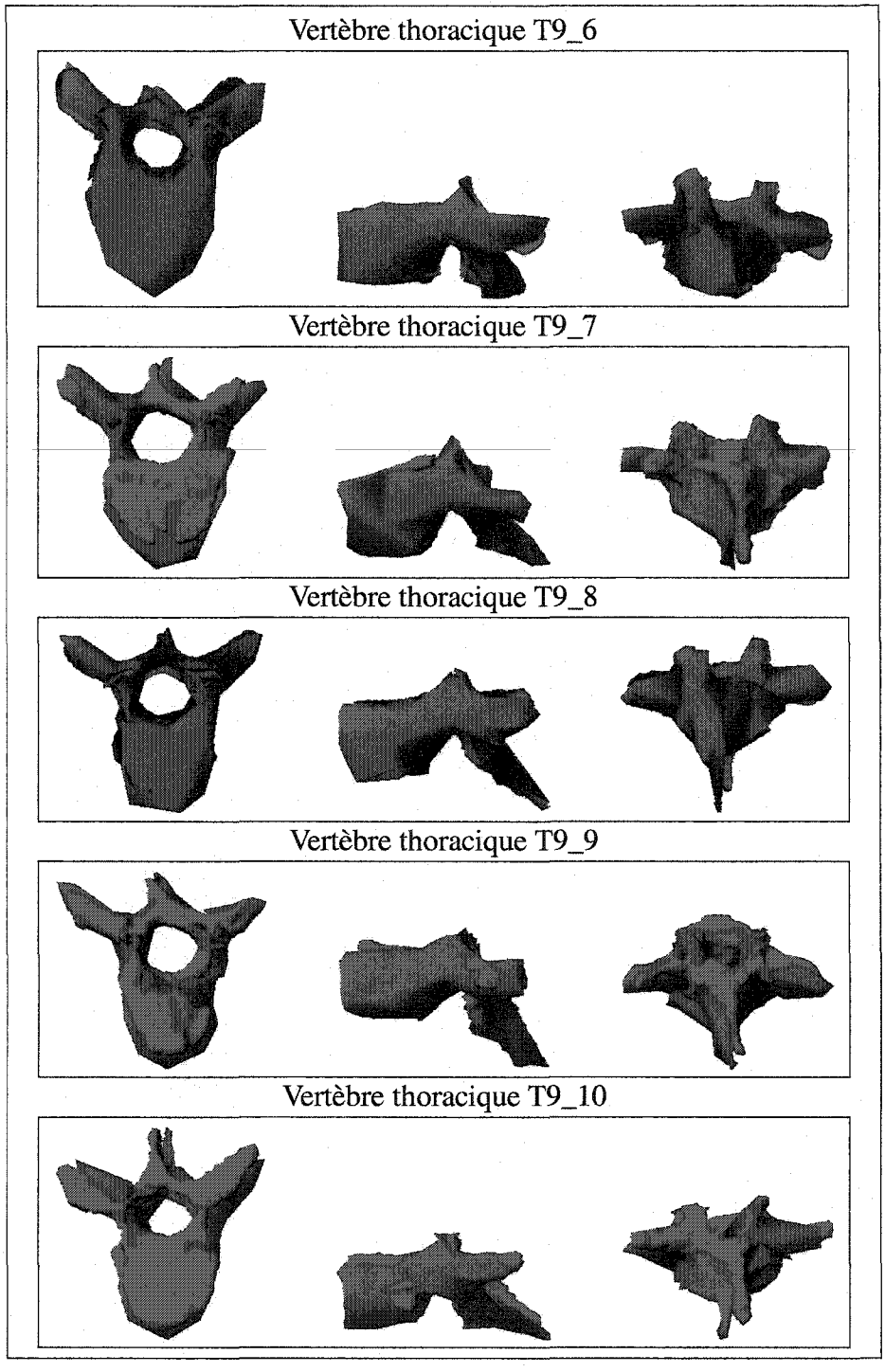

Figure 60 Superposition rigide de la vertèbre T9 (suite)

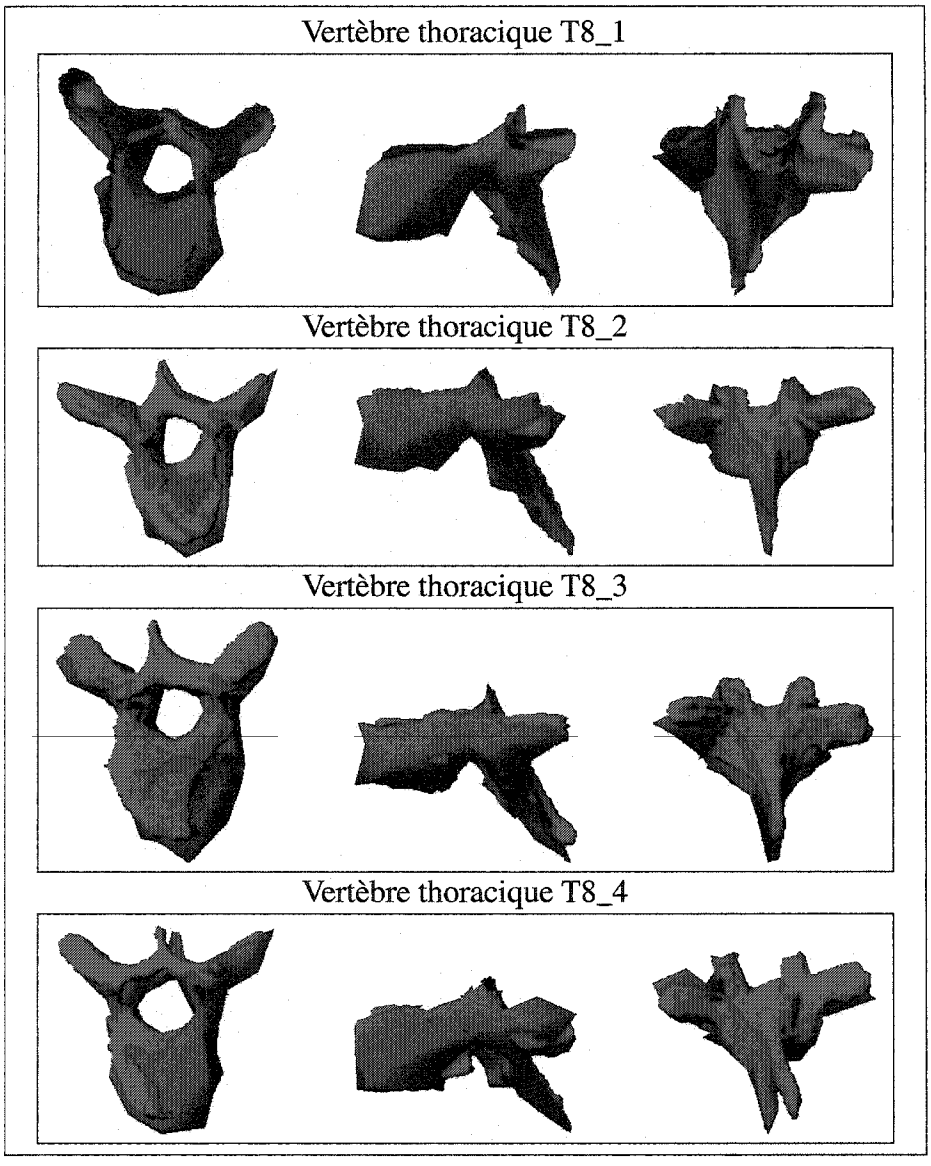

Figure 61 Superposition rigide de la vertèbre T8

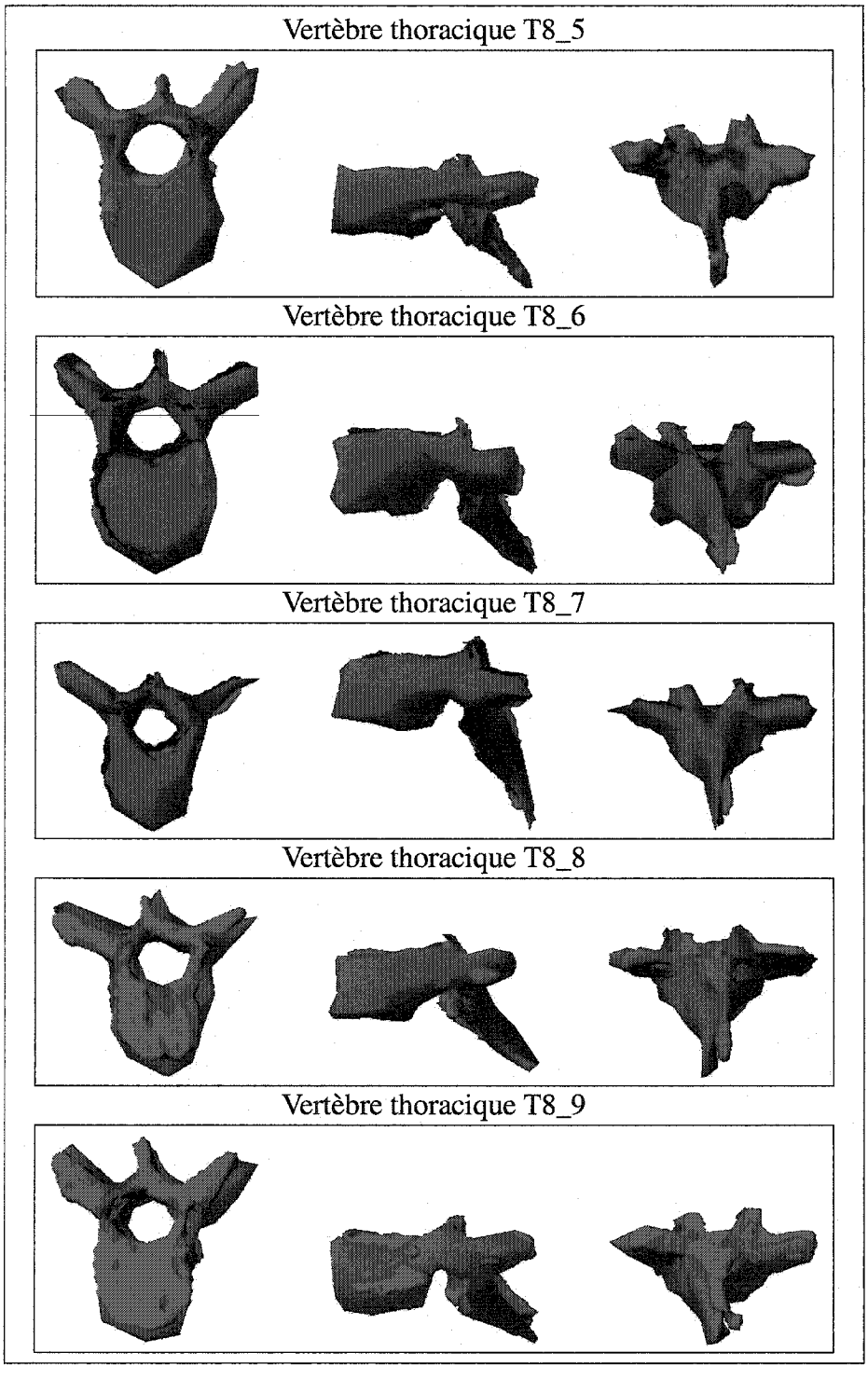

Figure 62 Superposition rigide de la vertèbre T8 (suite)

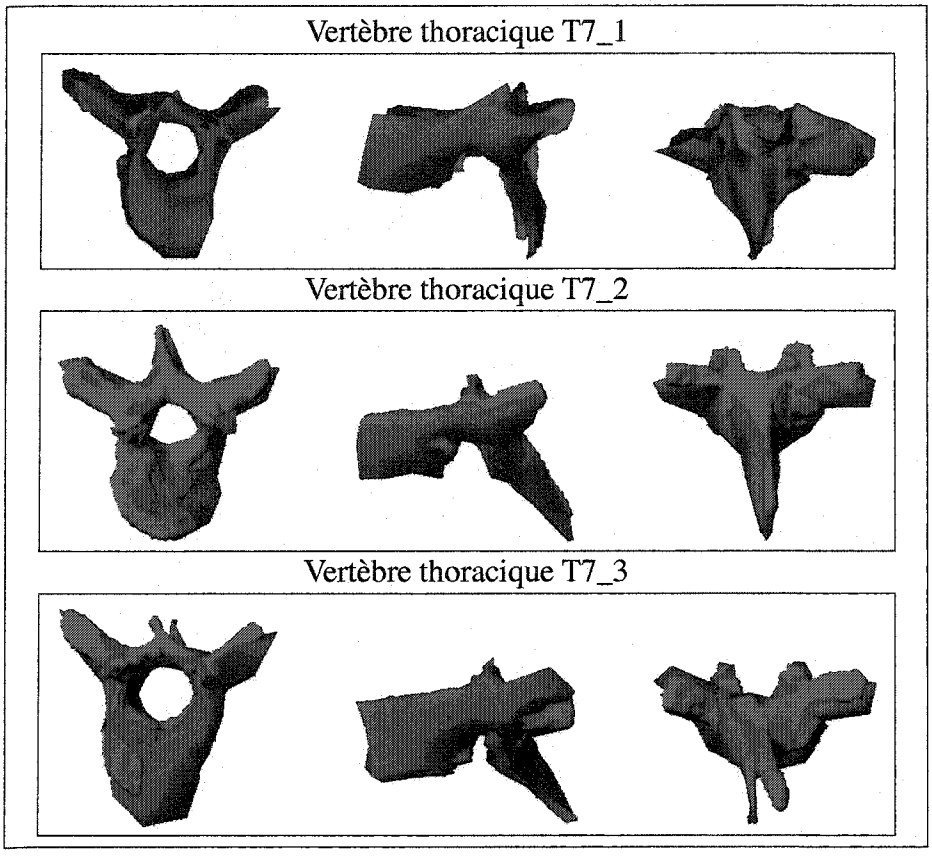

Figure 63 Superposition rigide de la vertèbre T7

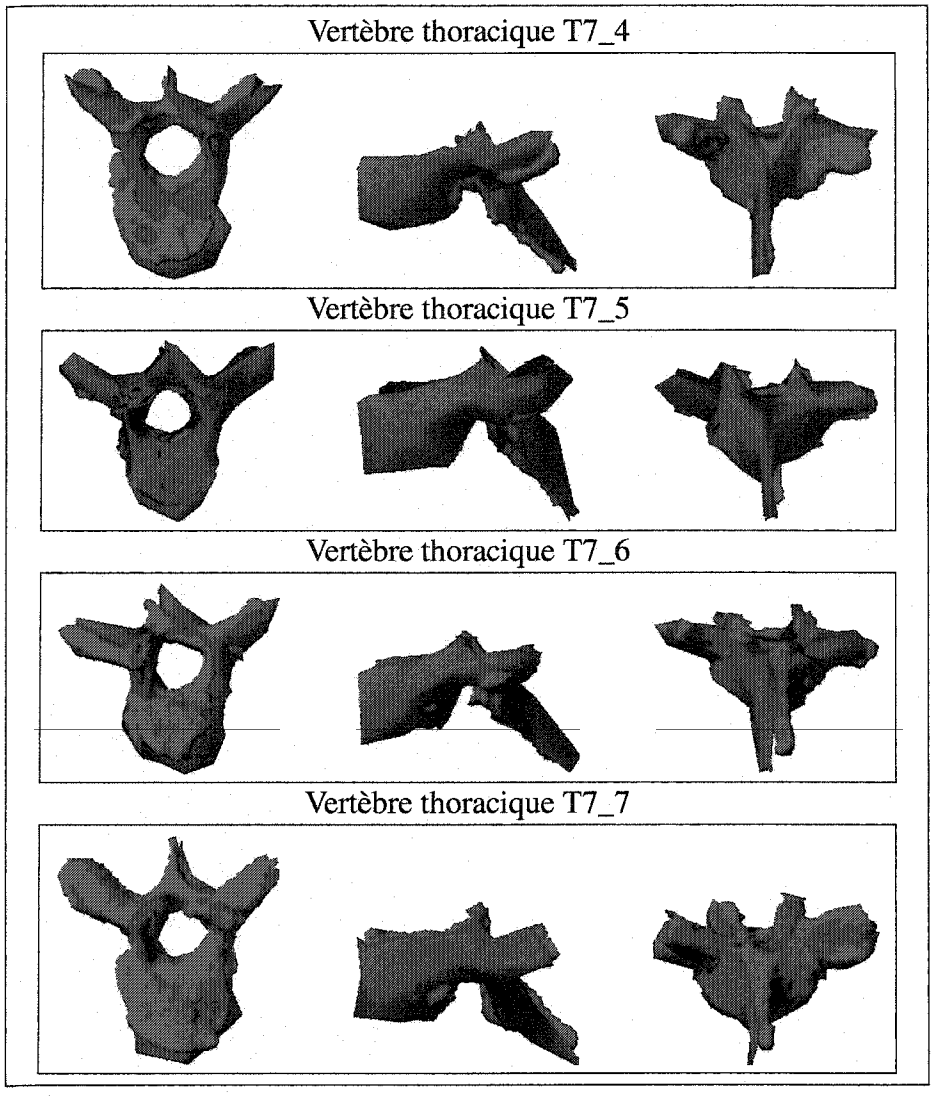

Figure 64 Superposition rigide de la vertèbre T7 (suite)

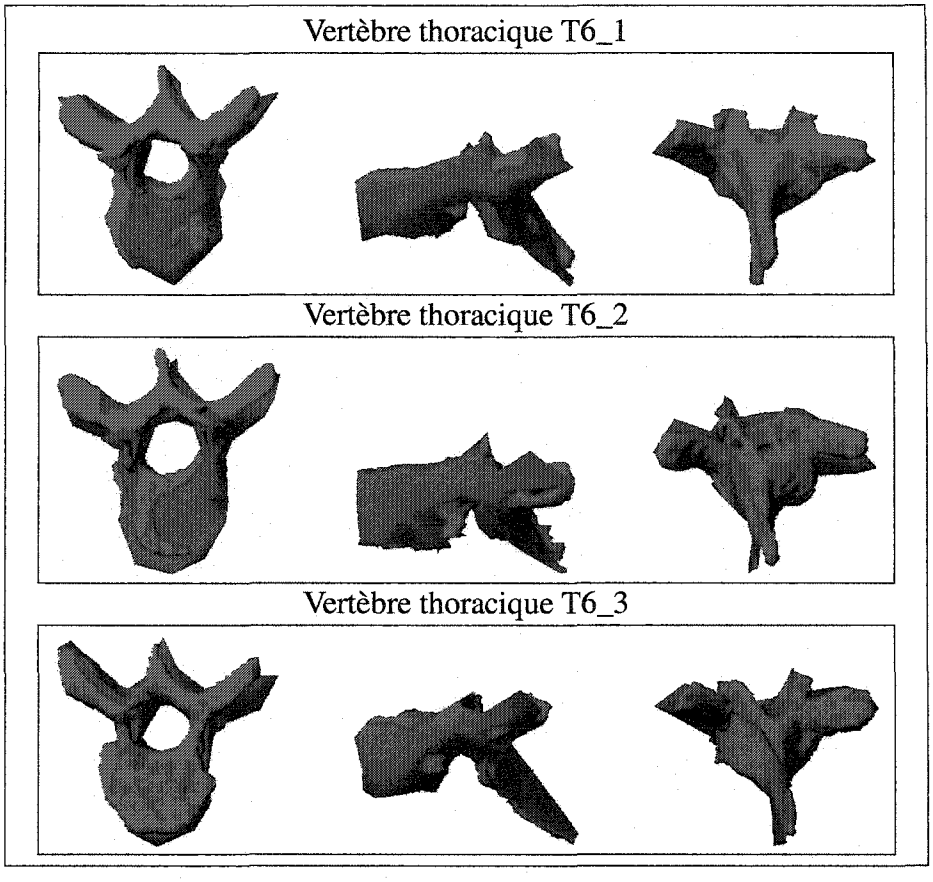

Figure 65 Superposition rigide de la vertèbre T6

BIBLIOGRAPHIE

[1] B. Andre, J. Dansereau, and H. Labelle. Optimized vertical stereo base radiographic setup for the clinical three-dimensional reconstruction of the human spine. *Journal of Biomechanics*, 27(8):1023–1035, 1994.

[2] K.S. Arun, T.S. Huang, and S.D. Blostein. Least-square fitting of two 3D point sets. *IEEE Transactions on Pattern Analysis and Machine Intelligence*, 9(5):698–700, 1987.

[3] C.E. Aubin, J. Dansereau, F. Parent, H. Labelle, and J.A. De Guise. Morphometric evaluations of personalised 3D reconstructions and geometric models of the human spine. *Medical and Biological Engineering and Computing*, 35(6):611–618, 1997.

[4] E. Bardinet, L.D. Cohen, and N. Ayache. A parametric deformable model to fit unstructured 3D data. *Computer Vision and Image Understanding*, 71(1):39–54, 1998.

[5] S. Benameur, M. Mignotte, F. Destrempes, and J.A. De Guise. Estimation of mixture of probabilistic PCA using stochastic EM to the 3D biplanar reconstruction of scoliotic rib cage. In *11th IEEE International Conference on Image Processing*, Singapore, Octobre 2004, Accepté.

[6] S. Benameur, M. Mignotte, S. Parent, H. Labelle, W. Skalli, and J. De Guise. 3D biplanar reconstruction of scoliotic vertebrae using statistical models. In *IEEE Computer Society Conference on Computer Vision and Pattern Recognition*, volume 2, pages 577–582, Kauai Marriott, Hawaii, USA, Décembre 2001.

[7] S. Benameur, M. Mignotte, S. Parent, H. Labelle, W. Skalli, and J. De Guise. 3D/2D registration and segmentation of scoliotic vertebrae using statistical models. *Computerized Medical Imaging and Graphics*, 27(5):321–337, 2003.

[8] S. Benameur, M. Mignotte, S. Parent, H. Labelle, W. Skalli, and J. De Guise. A hierarchical statistical modeling approach for the unsupervised 3D reconstruction of the scoliotic spine. In *10th IEEE International Conference on Image Processing*, volume 1, pages 561–564, Barcelona, Spain, Septembre 2003.

[9] R. Benjamin. Object-based 3D X-ray imaging. In *Computer Vision, Virtual Reality and Robotics in Medicine*, pages 444–448, Paris, France, 1995.

[10] P.J. Besl and N.D. McKay. A method for registration of 3D shapes. *IEEE Transactions on Pattern Recognition and Machine Intelligence*, 14(2):239–256, 1992.

[11] P.L. Borgne, W. Skalli, I.A.F. Stokes, N. Maurel, G. Beaupère, and F. Lavaste. Three-dimensional measurement of a scoliotic spine. In *Three-dimensional analysis of spinal deformities (IOS)*, pages 219–224. 1995.

[12] L.G. Brown. A survey of image registration techniques. *ACM Computing Surveys*, 24(4):325–376, 1992.

[13] J. F. Canny. A computational approach to edge detection. *IEEE Transactions on Pattern Analysis and Machine Intelligence*, 8(6):679–697, 1986.

[14] L. Caponetti and A.M. Fanelli. Computer-aided simulation for bone surgery. *IEEE Computer Graphics and Applications*, 13(6):86–92, 1993.

[15] V. N. Cassar-Pullicino and S. M. Eisenstein. Imaging in scoliosis: What, why and how? *Clinical Radiology*, 57(7):543–562, 2002.

[16] C. H. Chien. *Reconstruction and recognition of 3D objects from occluding contours and silhouettes*. PhD thesis, Department of Electrical Computer Engineering, University of Texas, Austin, USA, 1987.

[17] T.F. Cootes and C.J.Taylor. A mixture model for representing shape variation. In *British Machine Vision Conference*, volume 1, pages 110–119, Essex, England, 1997.

[18] T.F. Cootes, D. Cooper, C.J. Taylor, and J. Graham. Active shape models - their training and application. *Computer Vision and Image Understanding*, 61(1):38–59, 1995.

[19] T.F. Cootes, C.J. Page, C.B. Jackson, and C.J. Taylor. Statistical grey level models for object localization and identication. In *British Machine Vision Conference*, pages 533–542, 1995.

[20] T.F. Cootes and C.J. Taylor. Active shape models - 'smart snakes'. In *British Machine Vision Conferenc*, pages 266–275, 1992.

[21] T.F. Cootes and C.J. Taylor. Active shape model search using local grey-level models: a quantitative evaluation. In *British Machine Vision Conference*, pages 639–648, 1993.

[22] T.F. Cootes, C.J. Taylor, D.H. Cooper, and J. Graham. Training models of shape from sets of examples. In *British Machine Vision Conference*, pages 9–18, 1992.

[23] T.F. Cootes, C.J. Taylor, and J. Haslam. The use of active shape models for locating structures in medical images. *Image and Vision Computing*, 12(6):355–365, 1994.

[24] J. Dansereau and I.A.F. Stokes. Measurements of three dimensional shape of the rib cage. *Journal of Biomechanics*, 21:893–901, 1988.

[25] C. Davatzikos, X. Tao, and D.Shen. Hierarchical active shape models, using the wavelet transform. *IEEE Transactions on Medical Imaging*, 22(3):414 –423, 2003.

[26] M. Defontaine, D. Cenonl, L. Colin, C. Yvon, P. Vince, E. Lacaze, R. Dufait, E. Camus, P. Laugier, and F. Patat. A prototype of 500 khz ultrasonic matricial device: Beam scanner. application to in vivo hell bone quantitative characterization. In *IEEE International Ultrasonics Symposium*, pages 1585–1588, Ceasars Tahoe, Nevada, USA, 1999.

[27] S. Delorme, Y. Petit, J.A. de Guise, C.-E. Aubin, H. Labelle, C. Landry, and J. Dansereau. Three-dimensional modelling and rendering of the human skeletal trunk from 2d radiographic images. In *International Conference on 3D Digital Imaging and Modeling*, pages 497–505, Ottawa, Canada, Octobre 1999.

[28] S. Delorme, Y. Petit, J.A. de Guise, H. Labelle, C-É. Aubin, and J. Dansereau. Assessment of the 3D reconstruction and high-resolution geometrical modeling of the human skeletal trunk from 2D radiographic images. *IEEE Transactions on Biomedical Engineering*, 50(8):989–999, 2003.

[29] S. Delorme, P. Violas, J. Dansereau, J.A. de Guise, C.-É. Aubin, and H. Labelle. Preoperative and early postoperative three-dimensional changes of the rib cage after posterior instrumentation in adolescent idiopathic scoliosis. *European Spine Journal*, 10:101–106, 2000.

[30] P.A. Van den Elsen, J.B.A. Maintz, E.-J.D. Pol, and M.A. Viergever. Medical image matching. a review with classification. *IEEE Engineering in Medicine and Biology*, 12(1):26–39, 1993.

[31] F. Destrempes. Détection non-supervisée de contours et localisation de formes à l'aide de modèles statistiques. Master's thesis, Department of Computer Science and Operations Research, Université de Montréal, Canada, 2002.

[32] F. Destrempes and M. Mignotte. Unsupervised localization of shapes using statistical models. In *International Conference on Signal and Image Processing*, pages 60–65, Kauai Marriott, Hawaii, USA, août 2002.

[33] J. Diebolt and G. Celeux. Asymptotic properties of a stochastic EM algorithm for estimating mixture proportions. *Stochastic Models*, 9:599–613, 1993.

[34] M.M. Doody, J.E. Lonstein, M. Stovall, D.G. Hacker, N. Luckyanov, and C.E. Land. Breast cancer mortality after diagnostic radiography: Findings from the u.s. scoliosis cohort study. *Spine*, 25(16):2052–2063, 2000.

[35] C. Drexler, F. Mattern, and J. Denzler. Hierarchic object models and classification based on probabilistic PCA. In *IAPR Workshop on Machine Vision Applications*, pages 435–438, Nara, Japan, Décembre 2002.

[36] M. Dubuisson-Jolly, S. Lakshmanan, and A.K. Jain. Vehicle segmentation and classification using deformable templates. *IEEE Transactions on Pattern Analysis and Machine Intelligence*, 18(3):293–308, 1996.

[37] J.M. Ferryman, A.D. Worrall, G.D. Sullivan, and K.D. Baker. A generic deformable model for vehicle recognition. In *British Machine Vision Conference*, pages 127–136, The University of Birmingham, Birmingham UK, Septembre 1995.

[38] M. Fleute and S. Lavallée. Building a complete surface model from sparse data using statistical shape models:application to computer assisted knee surgery system. In *Medical Image Computing and computer-assisted intervention*, pages 879–887. 1998.

[39] M. Fleute and S. Lavallée. Nonrigid 3D/2D registration of images using statistical model. In *Medical Image Computing and Computer-Assisted Intervention, Springer-Verlag*, volume 38, pages 138–147. 1999.

[40] B. Godbout, C. Kauffmann, and J.A. de Guise. A simple 2D active contour model to segment non-convex objects in 3D images. In *Vision Interface*, pages 350–358, SFU Harbour Center, Vancouver, British Columbia, Canada, juin 1998.

[41] K. Grauman, G. Shakhnarovich, and T. Darrell. Inferring 3D structure with a statistical image-based shape model. In *IEEE International Conference on Computer Vision*, pages 641– 648, Nice, France, Octobre 2003.

[42] U. Grenander and D.M. Keenan. Towards automated image understanding. *Journal of Applied Statistics*, 16(2):207–221, 1989.

[43] J.A. De Guise, H. Mallouche, J. Dansereau, and H. Labelle. Imaging techniques applied to spinal biomechanics. *Journal of Biomechanics*, 7(3):135–144, 1995.

[44] J. Hadamard. *Lectures on the Cauchy problem in linear partial differential equations*. Yale University Press, New Haven, 1923.

[45] J.A. Hartigan and M.A. Wong. A k-means clustering algorithm. *Applied Statistics*, 28:100–108, 1979.

[46] A. Hill, T.F. Cootes, and C.J. Taylor. A generic system for image interpretation using exible templates. In *British Machine Vision Conference*, pages 1–10, 1992.

[47] A. Hill, T.F. Cootes, and C.J. Taylor. Active shape models and the shape approximation problem. *Image and Vision Computing*, 14:601–607, 1996.

[48] A. Hill, T.F. Cootes, C.J. Taylor, and K. Lindley. Medical image interpretation: a generic approach using deformable templates. In *Journal Medical Informatics*, volume 19, pages 47–59, Janvier - Mars 1994.

[49] A. Hill, A. Thornman, and C.J. Taylor. Model-based interpretation of 3D medical images. In *British Machine Vision Conference*, pages 339–348, 1993.

[50] B.K.P. Horn. Closed-form solution of absolute orientation using unit quaternions. *Journal of the Optical Society of America*, 4(4):629–642, 1987.

[51] B.K.P. Horn and N. Shao. Closed-form solution of absolute orientation using orthonormal matrices. *Journal of the Optical Society of America*, 5(7):1127–1135, 1988.

[52] T.N. Huynh, J. Dansereau, and G. Maurais. Development of a vertebral endplate 3D reconstruction technique. *IEEE Transactions on Medical Imaging*, 16(5):689–696, 1997.

[53] A. K. Jain, Y. Zhong, and S. Lakshmanan. Object matching using deformable templates. *IEEE Transactions on Pattern Analysis and Machine Intelligence*, 18(3):267–278, 1996.

[54] C. Kauffman and J.A. De Guise. Digital radiography segmentation of scoliotic vertebral body using a deformable model. In *Int Soc Optical Engng*, volume 3034, pages 243–251, 1997.

[55] C. Kervrann and F. Heitz. A hierarchical statistical framework for the segmentation of deformable objects in image sequences. In *IEEE Computer Society Conference on Computer Vision and Pattern Recognition*, pages 724–728, Seattle, Washington, USA, Juin 1994.

[56] C. Kervrann and F. Heitz. Statistical deformable model-based segmentation of image motion. *IEEE Transactions on Image Processing*, 8(4):583–588, 1999.

[57] Y. Kita. Elastic-model driven analysis of several views of a deformable cylindrical object. *IEEE Transactions on Pattern Analysis and Machine Intelligence*, 18(12):1150–1162, 1996.

[58] J.-M. Laferte, F. Heitz, P. Perez, and E. Fabre. Hierarchical statistical models for the fusion of multiresolution image data. In *Fifth International Conference on Computer Vision*, pages 908–913, Kauai Marriott, Hawaii, USA, Juin 1995.

[59] S. Lavallée. *Computer integrated surgery*, chapter Registration for computer integrated surgery: methodology, state of the art, pages 77–97. MIT Press, Cambridge, MA, 1995.

[60] J. Liu and P. Moulin. Image denoising based on scale-space mixture modeling of wavelet coefficients. In *IEEE International Conference on Image Processing*, pages 386–390, Kobe, Japan, Octobre 1999.

[61] W.E. Lorensen and H.E. Cline. Marching cubes: a high resolution 3D surface construction algorithm. *Computer Graphics*, 21(4):163–169, 1988.

[62] C. Lorenz and N. Krahnstöver. Generation of point-based 3D statistical shape models for anatomical objects. *Computer Vision and Image Understanding*, 77(2):175–191, 2000.

[63] A. Lorusso, D.W. Eggert, and R.B. Fisher. A comparison of four algorithms for estimating 3D rigid transformations. *Machine Vision Applications*, 9:272–290, 1997.

[64] J. Lötjönen, I.E. Magnin, J. Nenonen, and T. Katila. Reconstruction of 3D geometry using 2D profiles and a geometric prior model. *IEEE Transactions on Medical Imaging*, 18(10):992–1002, 1999.

[65] J. Lötjönen, P-J. Reissman, I.E. Magnin, and T. Katila. Model extraction from magnetic resonance volume data using the deformable pyramid. *Medical Image Analysis*, 3(4):387–406, 1999.

[66] F. Maes, D. Vandermeulen, and P. Suetens. Comparative evaluation of multiresolution optimization strategies for multimodality image registration by maximization of mutual information. *Medical Image Analysis*, 3(4):373–386, 1999.

[67] J.B.A. Maintz and M.A. Viergever. A survey of medical image registration. *Medical Image Analysis*, 2(1):1–36, 1998.

[68] J.A. Marchant and C.M. Onyango. Fitting grey level point distribution models to animals in scenes. *Image and Vision Computing*, 13(1):3–12, 1995.

[69] E. Marcil, J. Dansereau, H. Labelle, and J. De Guise. Incorporation of patient displacement into a trunk reconstruction technique. In *Engineering in Medicine and Biology Society. IEEE 17th Annual Conference*, volume 1, pages 385 –386, Septembre 1995.

[70] W.N. Martin and J.K. Aggarwal. Volumetric descriptions of objects from multiple views. *IEEE Transactions on Pattern Analysis and Machine Intelligence*, 5(2):150–158, 1983.

[71] G. T. Marzan. *Rational design for close-range photogrammetry*. PhD thesis, Department of Civil Engineering, University of Illinois at Urbana-Champaign, USA, 1976.

[72] M. Mignotte. Unsupervised statistical sketching for non-photorealistic rendering models. In *10th IEEE International Conference on Image Processing*, volume 3, pages 573–577, Barcelona, Spain, Septembre 2003.

[73] M. Mignotte, C. Collet, P. Pérez, and P. Bouthemy. Hybrid genetic optimization and statistical model-based approach for the classification of shadow shapes in sonar imagery. *IEEE Transactions on Pattern Analysis and Machine Intelligence*, 22(2):129–141, 2000.

[74] M. Mignotte, J. Meunier, and J.-C. Tardif. Endocardial boundary estimation and tracking in echocardiographic images using deformable templates and markov random fields. *Pattern Analysis and Applications*, 4(4):256–271, 2001.

[75] D. Mitton, C. Landry, S. Veron, W. Skalli, F. Lavaste, and J.A. De Guise. 3D reconstruction method from biplanar radiography using non-stereocorresponding points and elastic deformable meshes. *Medical and Biological Engineering and Computing*, 38(2):133–139, 2000.

[76] A. Mitulescu, I. Semaan, J.A. De Guise, P. Leborgne, C. Adamsbaum, and W. Skalli. Validation of the non-stereocorresponding points stereoradiographic 3D reconstruction technique. *Medical and Biological Engineering and Computing*, 39(2):152–158, 2001.

[77] S. Mouren. Reconstruction 3D biplanaire de cages thoraciques scoliotiques à l'aide de modèles déformables de côtes. Master's thesis, Department of Mechanical Engineering, École Polytechnique at Montréal, Canada, 2003.

[78] B. Nikkhade-Dehkordi, M. Bro-Nielsen, T. Darvann, C. Gramkow, N. Egund, and K. Hermann. 3D reconstruction of the femoral bone using two X-ray images from orthogonal views. In *Computer Assisted Radiology*, page 1015, Juin 26-29 1996.

[79] F. Olivier. Global optimization with exploration/selection algorithms and simulated annealing. *The Annals of Applied Probability*, 12:248–271, 2002.

[80] M.M. Panjabi, V. Goel, T. Oxland, K. Takata, J. Duranceau, M. Krag, and M. Price. Lumbar human vertebrae: quantitative three-dimensional anatomy. *Spine*, 17(3):299–306, 1992.

[81] M.M. Panjabi, K. Takata, V. Goel, D. Frederico, T. Oxland, J. Duranceau, and M. Krag. Thoracic human vertebrae: quantitative three-dimensional anatomy. *Spine*, 16(8):888–901, 1991.

[82] S. Parent, H. Labelle, W. Skalli, B. Latimer, and J.A. De Guise. Morphometric analysis of anatomic scoliotic specimens. *Spine*, 27(21):2305–2311, 2002.

[83] M.J. Pearcy. Stereo radiography of lumbar spine motion. In *Acta Orthopaedica Scandinavica Supplementum*, volume 56, pages 7–37, 1985.

[84] C. Pena-Reyes and M. Sipper. Evolutionary computation in medicine: An overview. *Artificial Intelligence in Medicine*, 19:1–23, 2000.

[85] A. Plamandon, M. Gnon, and G. Maurais. Application of a stereoradiographic method for the study of intervertebral motion. *Spine*, 13:1027–1032, 1988.

[86] J. Ponce and D. Chelberg. Finding the limbs and cusps of generalized cylinders. *International Journal of Computer Vision*, 1(3):195–210, 1987.

[87] S. Sandor and R. Leadhy. Surface-based labeling of cortical anatomy using a deformable atlas. *IEEE Transactions on Medical Imaging*, 16(1):41–54, 1997.

[88] I. Semaan, W. Skalli, S. Veron, A. Templier, J.P. Lasseau, and F. Lavaste. Quantitative three-dimensional anatomy of lumbar spine. *European Journal Orthopaedic Surgery*, 2001.

[89] I.A.F. Stokes, D.G. Wilder, J.W. Frymoyer, and M.H. Pope. Assessment of patients with low-back pain by biplanar radiographic measurement of intervertebral motion. *Spine*, 6:233–240, 1981.

[90] D. Terzopoulos, A. Witkin, and M. Kass. Constraints on deformable models: Recovering 3D shape and nonrigid motion. *Artificial Intelligence*, 36(1):91–123, 1988.

[91] P. Thévenaz and M. Unser. An efficient mutual information optimizer for multiresolution image registration. In *IEEE International Conference on Image Processing*, volume 1, pages 833–837, Chicago, 1998.

[92] M.E. Tipping and C.M. Bishop. Mixtures of probabilistic principal component analysers. *Neural Computation*, 11(2):443–482, 1999.

[93] M.E. Tipping and C.M. Bishop. Probabilistic principal component analysis. *Journal of the Royal Statistical Society: Series B*, 21(3):611–622, 1999.

[94] F. Trochu. A contouring program based on dual kriging interpolation. *Engineering with Computers*, 9:160–177, 1993.

[95] H. Veisterä and J. Lötjönen. Reconstructing 3D boundary element heart models from 2D biplane fluoroscopy. In T. Katila, I.E. Magnin, P. Clarysse, J. Montagnat, and J. Nenonen, editors, *Functional Imaging and Modeling of the Heart, First International Workshop, Helsinki, Finland*, volume 2230 of *Lecture Notes in Computer Science*, pages 17–23. Springer, Novembre 2001.

[96] M.W. Walker, L. Shao, and R.A. Volz. Estimating 3D location parameters using dual number quaternions. *CVGIP: Image Understanding*, 54(3):358–367, 1991.

[97] J. West. Comparison and evaluation of retrospective inter-modality registration techniques. *Computer Assisted Tomography*, 1997; http://cswww.vuse.vanderbilt.edu/ image/registration.

[98] G.C. Wiggins, C.I. Shaffrey, M.F. Abel, and A.H. Menezes. Pediatric spinal deformities. *Journal of Neurosurgery and American Association of Neurological Surgeons*, 14(1):1–14, 2003.

[99] R.P. Woods, S.T. Grafton, C.J. Holmes, S.R. Cherry, and J.C. Mazziotta. Automated image registration: I. general methods and intra-subject, intra-modality validation. *Journal of Computer Assisted Tomography*, 22:141–154, 1998.

[100] R.P. Woods, S.T. Grafton, J. Watson, N.L. Sicotte, and J.C. Mazziotta. Automated image registration: II. intersubject validation of linear and non-linear models. *Journal of Computer Assisted Tomography*, 22(1):153–165, 1998.